Republic of Iraq
Ministry of Higher Education
and Scientific Research
University of Misan
College of Science
Department of Chemistry

Removing of Some Heavy Metals from Cutting Rock and Crude Oil Samples by Using Nano Graphene Oxide

A Thesis Submitted to

the College of Science / University of Misan as Partial Fulfillment
of the Requirements for the Master Degree of Science in Chemistry

By

Ahmed Abd ul-wahid Mohammed Al-Zubadi

B.Sc. Chemistry / Misan University (2012)

Supervisors

Asst. Prof. Safaa Sabri Najim
Lec. Dr. Hawraa Hameed Rady

August – 2021

بسم الله الرحمن الرحيم

(قُلْ هَلْ يَسْتَوِي الَّذِينَ يَعْلَمُونَ وَالَّذِينَ لَا يَعْلَمُونَ
إِنَّمَا يَتَذَكَّرُ أُولُو الْأَلْبَابِ)

صدق الله العلي العظيم

سورة الزمر اية ٩

Dedication

To The Sun and Moon Which Lighting my Life by Pave the Way to my Success…

My Father & My Mother

To My Soul mate Which Stand beside me and Support me all my Life…

My Lovely Wife

To The Happiness Buds Mustafa, Muntadher and my little daughter Jana…

My Children

To Those who have Supported me and are Waiting for my Success…

My Brothers & My Close Friends

To Those who have Given me their Time and Knowledge…

My Supervisors

Ahmed

Acknowledgements

Firstly, very much thanks for Allah the most merciful for his blessings, who gave me health, strength, and facilitated the ways for me to accomplish this work, and the prayer and peace of Allah be upon our Master and prophet Muhammad and his divine good family.

I would like to express my sincere gratitude to my supervisors, **Assistant Professor Safaa S. Najim Al-Omran** and **Dr. Hawraa H. Rady** for highly inspiring guidance, patience, motivation, enthusiasm and immense knowledge, continuous support for completing this thesis.

Much appreciation is offered to the head of The Department of Chemistry, Assistant Professor **Dr.Ahmed M. Abbas** for help to complete my work.

May thanks offered to **Dr. Dhiaa B. Habash** for their help to complete my work.

I would like to express my sincere thanks to **Mr. Salim R. Salman**, Halfaya JMC Chairman in Missan Oil Company for facilitating my work.

Also I express my sincere thanks and gratitude to my family for their help me in providing the appropriate ambiences for study .

Finally, I'd like to thank my post graduate classmates, best friends, my another family Ahmed, Kawther and Sammah for supported me and stand with me, apology to all whom I have not mentioned with my respect. thanks for all.

Ahmed

Contents

List of Figures

List of Tables

List of Abbreviations

Abbreviations	Key
API	American Petroleum Institute
ASTM	American Standard Test and Method
AAS	Atomic Absorption Spectroscopy
^{o}C	Celsius degree
DMF	DiMethyl Formamide
EDX	Energy Dispersion X-ray
FESEM	Field Emission Scanning Electronic Microscopy
FAAS	Flame Atomic Absorption Spectroscopy
FT-IR	Fourier Transform Infra-Red
g	Gram
GO	Graphene Oxide
GFAAS	Graphite Furnace Atomic Absorption Spectroscopy
HR-TEM	High Resolution-Transmission Electronic Microscopy
h	Hour
ICP-OES	Inductively Coupled Plasma- Optical Emission Spectroscopy
LOD	Limit of Detection
NGO	Nano Graphene Oxide
nm	Nano meter
RSD%	Relative Standard Deviation
SPE	Solid Phase Extraction
SPME	Solid Phase Micro Extraction
SD±	Standard Deviation
TEM	Transmission Electronic Microscopy
UV-Vis	Ultraviolet-Visible
XRD	X-Ray Diffraction

Abstract

The thesis consists of three chapters, the first chapter is a general introduction about crude oil, petroleum rocks, nano graphene oxide (NGO), pre-concentration and determination methods of trace elements.

The second chapter describes the experimental which includes, synthesis of nano graphene oxide, digestion of cutting rock and crude oil samples and preparation of stock solutions.

The final chapter explains the results and discussion which includes, characterization of nano graphene oxide, the optimum conditions of adsorption process, using solid phase micro extraction method to separate the trace elements (magnesium, cobalt, nickel, copper, cadmium and lead) from samples by nano graphene oxide as a sorbent at the optimum conditions, pH = 5.5, 6.0, 6.5, 7.0, 7.5 and 8.0 for (Ni, Mg, Cd, Co, Cu and Pb) for each analyte ion respectively, the NGO mass was 0.5 mg, the sample volume was 20 mL , stirring time was 5 min, the sonicating time was 5 min., at the room temperature (30 ºC) with the addition 6.5 mg/mL of NaCl solution. The effect of interfering ions (chromium(III), manganese(IV), iron(II), iron(III), zinc(II), arsine(III), tin(II), lithium(I), potassium(I), calcium(II) and barium(II)) to find the tolerance limit of the coexisting interfering ions with the analytes can decrease or increase the recovery ±5% . Adsorption capacity calculated for Mg, Co, Ni, Cu, Cd and Pb (1 µg/mL) analyte were (34.04, 34.04, 32.88, 28.76, 33.32 and 33.96 µg/mg) respectively. The average concentration of elements in the cutting rock samples (direct determination using FAAS) : Magnesium, Cobalt, Nickel, Copper, Cadmium and Lead (9.72 µg/mL), (1.318 µg/mL), (5.646 µg/mL), (0.616 µg/mL), (0.567 µg/mL) and (9.296 µg/mL) respectively. The average concentrations of elements in crude oil samples : Magnesium, Cobalt, Nickel, Copper, Cadmium and Lead (6.013 µg/mL), (0.654 µg/mL), (23.685 µg/mL), (0.509 µg/mL), (0.317 µg/mL) and (5.665 µg/mL)

respectively. The average concentrations of elements by SPME method have decreased in cutting rock : Magnesium, Cobalt, Nickel, Copper, Cadmium and Lead (2.082 µg/mL), (0.24 µg/mL), (1.066 µg/mL), (0.162 µg/mL), (0.055 µg/mL) and (2.153 µg/mL) respectively. In crude oil samples, Magnesium, Cobalt, Nickel, Copper, Cadmium and Lead (1.044 µg/mL), (0.078 µg/mL), (5.266 µg/mL), (0.091 µg/mL), (0.038 µg/mL) and (1.042 µg/mL) respectively.

CHAPTER ONE

INTRODUCTION

1.1 Crude oil

Crude oil contains three hydrocarbon compounds paraffins, naphthenes, and aromatics. The paraffins are also called methane series and comprises most common hydrocarbons in crude oil, the paraffins are liquid at normal temperature, boiling between 40-200 ºC. The naphthenes are saturated closed ring series and are important as a liquid of refinery products. The aromatics are unsaturated closed ring series, benzene is most common of the series and is present in most of the crude oil . The crude oil also contains nitrogen, sulphur and oxygen in small quantities[1] as shown in Fig. (1-1)[2]. The metals present in the crude oil are mostly V(II) and Ni(II) which are present in large quantity in heavy crude oil, other metals are Al, Mg, Ti, Cr, Mn, Fe, Co, Cu, Zn, Ga, As, Cd, Sn, Pb, Mo, Sb, Ag, Ba and U. Inorganic salts mainly as chloride and sulphate of Na, Mg, K and Ca[3].

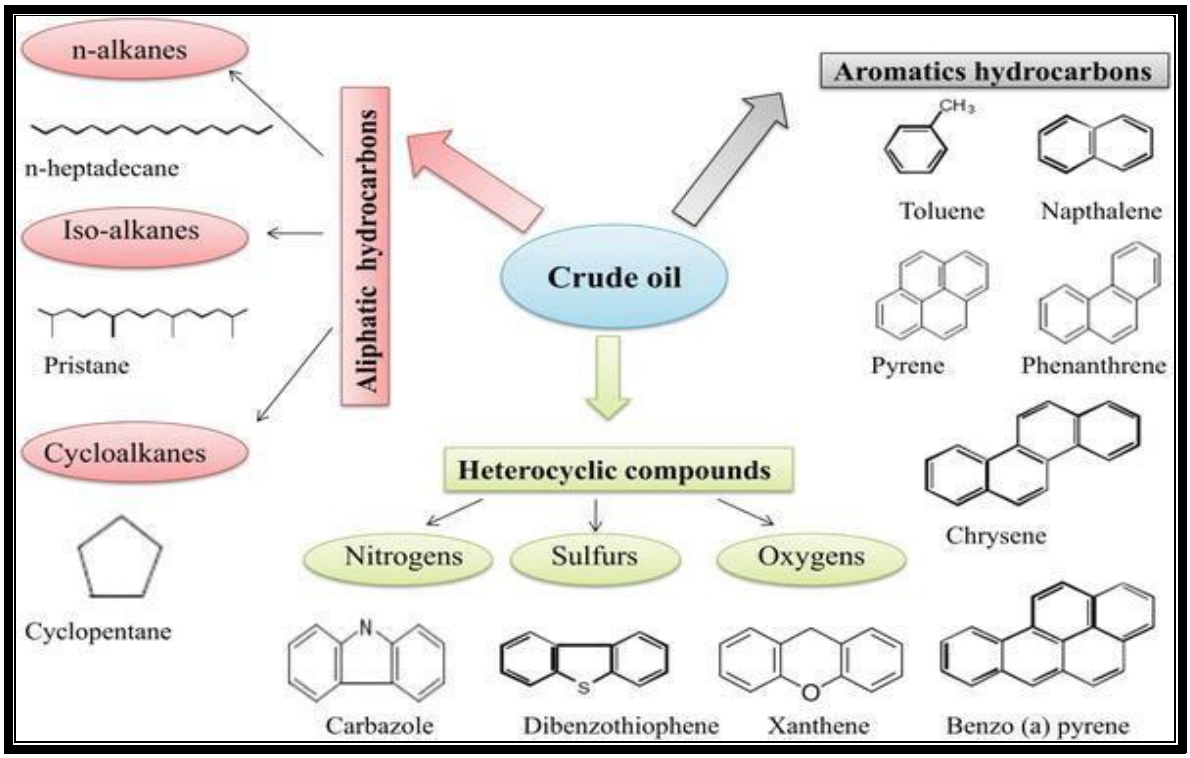

Fig. (1-1): Classes of hydrocarbons in crude oil

1.2 Petroleum rocks

Petroleum physical interpretation is necessary to understand the rocks of the ground reservoir. Detailed under surface requires material measurements made from the well logging. Well logging is a process of recording a details for the geological formations have penetrated by borehole, Well logging represents as an integrated process in the measuring the reservoir. The log depends on the samples taken from the ground or measurements made by physical instruments that have been removed in the hole. Sub-division of oil reservoir depends on many petroleum physical properties (mineralogy, permeability, porosity, water and fluid saturation)[4].The oil fields in Missan province as shown in Fig. (1-2).

Fig. (1-2) Oil fields in Missan province

The locations of oil reservoir in rocks of southern Iraq vary with different depths from one region to another, on this basis it was called the rock formation of the oil reservoir at certain depth, of which: [Mishrif formation , Nahr-Umr formation , Al-Khasib formation, Ahmadi formation, Fatha formation, .. etc.] as shown in Fig. (1-3)[5]

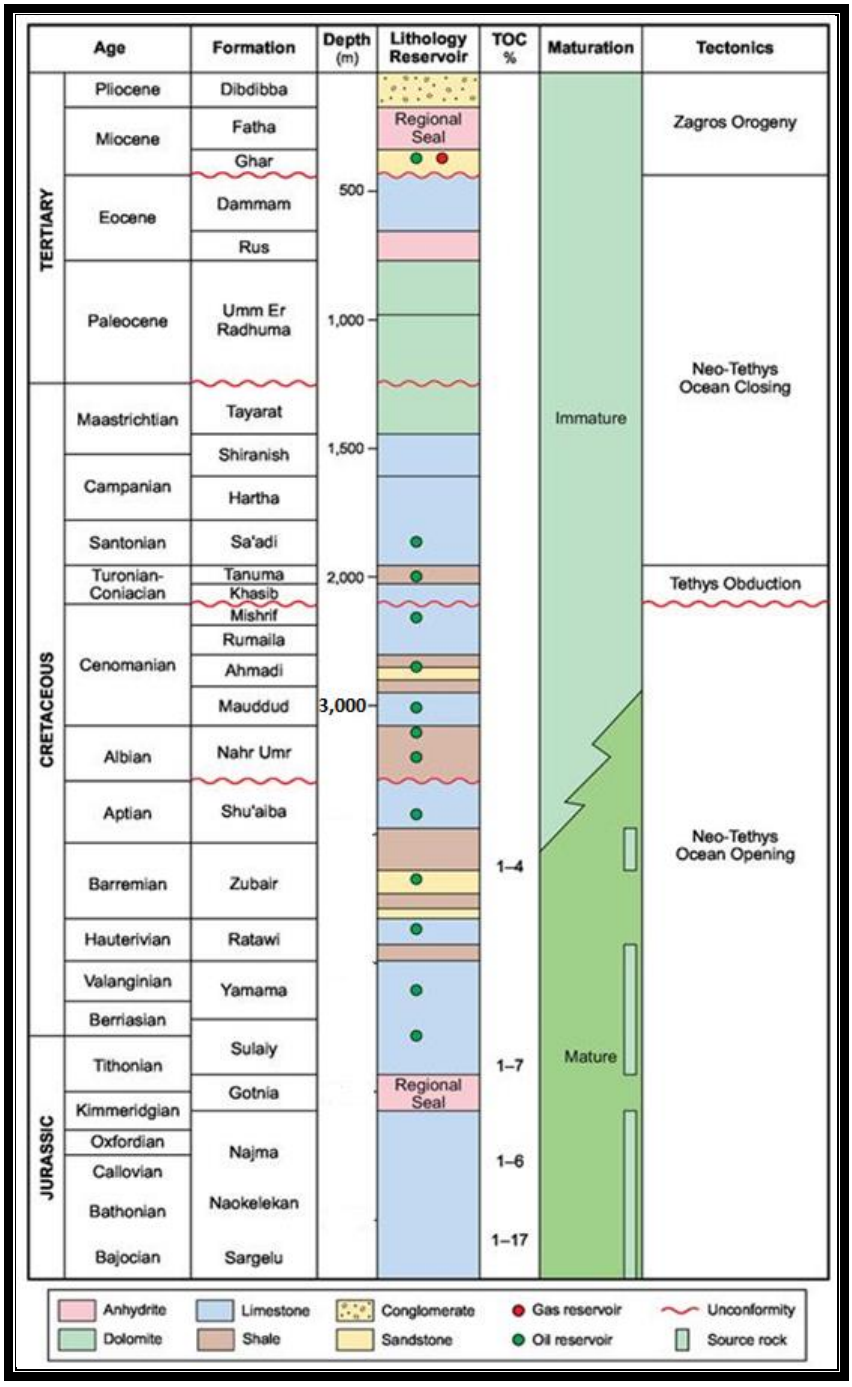

Fig. 1-3: Stratigraphic section of petroleum rock

1.2.1 Geochemistry of elements in petroleum rocks

The sedimentary rocks and sediments which are the product of disintegration and solution of source rocks are subjected to different degrees of roofing and chemical change that are usually reflected in the chemical installation of rock cells and change outputs, and change may also occur during metal fluctuations and also during subsequent transfers. During aluminium silicates hydrolysis one product of their weathering, practically a clay mineral where some of the original silicon and aluminum remain combined. The alkali elements, Na, Mg, K and Ca released during hydrolysis, highly soluble and little of them remain with the alteration product[6]. Geological of petroleum rocks, formed of limestone, anhydrite, dolomite, conglomerate, shale and sandstone[5], while geochemical study included the oxides (SiO_2, Al_2O_3, Fe_2O_3, FeO, TiO_2, MgO, Na_2O, K_2O, MnO and P_2O_5) in the detrital fraction which comprises around (58%) of total mineral phases. Clay minerals (39%), quartz (15%), iron oxides and Ti-minerals (3%) and feldspar (1%). The oxides (CaO, some MgO and CO_2) comprise the chemical fraction, the carbonates (~ 42%)". The trace elements (Co, Ni, Ga, Rb, Zr and Sr) within the detrital fraction are mainly the iron oxides and clay minerals[7]. Used the elements concentration, frequently reported as linked to black shales, i.e. Ni, Co, Cu, Zn, V, Mo, Cr as well as Ba, Cd and P which are usually enriched whilst Mn (and Fe) is usually depleted . These elements may have different behaviors. Ni, Co, Cu and Zn are fixed on organic species. The abundant the reactive organic matter, the more transition metals will form complexes with organic products, the more they will be trapped into the sediment. Differing of the trace elements, V, Cr or Mo are fixed after reduction during oxidation reduction reactions at the expense of organic compounds. Manganese is an element sensitive to redox conditions. When the host sediment is submitted to reducing conditions, Mn may be

solubilized and then migrate upward, back to the water column . Thus, black shales usually, depleted in Mn relative to normal marine shales, Barium with phosphorus and cadmium[8].

1.3 Nano graphene oxide

Nano chemistry has a lot of attention, particularly in the research and industrial communities. It offers many unprecedented opportunities for advancing not only our ability to impact, but the environment in which we live. Ability to design, synthesize and manipulate, specific nano structured materials lie at heart of the future promise of nano chemistry[9]. Graphene is a flat monolayer carbon atoms with 0.142 nm a carbon-carbon distance, the first truly is two-dimensional (2D) crystalline material, without doubt, which is stable at normal conditions and which bonded together in a hexagonal lattice, completely conjugated sp^2 hybridized planar structure, a basic building block for graphitic materials of all other dimensionalities. It can be wrapped up into zero dimension (0D) fullerenes, rolled into one dimension (1D) nanotube or stacked into three dimension (3D) graphite[10]. Since discovered in 2004 , graphene with two-dimensional material comprising a single layer of sp^2-hybridized carbon atoms , has become one of the hottest research topics and gain great attention in material sciences due to its various unique properties . It is reported that graphene possesses a high theoretical specific surface area (2630 m^2g^{-1}) , proposed a high sorption capacity .In addition ,due its large delocalized π-electron system ,graphene can form a strong π–π stacking interaction with the benzene ring[11]. Graphene oxide(GO), traditionally served as a precursor for graphene ,consists of a hexagonal carbon network with hydroxyl and epoxide functional groups on its "basal" plane, whereas the edges are mostly decorated by carboxyl and carbonyl groups[12]. These oxygen-containing functional groups can be bound with metal ions ,especially the

multivalent metal ions ,through both coordinate approaches and electrostatic, which makes GO an ideal adsorbent for metal ions . Recently, the utilization of GO as a sorbent for the removal of heavy metal ions from water has been reported[13].

1.3.1 Importance of nano graphene oxide

Graphene oxide (GO), which is two-dimensional (2D) honeycomb carbon lattice with high specific surface area, remarkable mechanical, structural, thermal, and electrical properties, shows relentless perspectives in nano electronics[14], sensors[15], super capacitors, composite materials[16] and environmental applications[17] and it is considered more propitious than other carbonaceous nano materials. Pure GO with numerous epoxy (−COC), hydroxyl (−OH), carbonyl (−CO), and carboxyl (−COOH) groups can be synthesized by oxidizing graphite in a single step without using metal catalyst . The abundant oxygen containing functional groups at GO surface leads to development of highly active sites for metal ion complexation and hydrophilic character, making it a possibility solid phase extraction (SPE) sorbent and substitute for carbon nano tubes (CNTs)[18].

Graphene oxide (GO), as a novel nanomaterial has been attracting more and more attention in recent decades, resulting its properties and wide range of potential applications including super capacitors , catalysts , drug delivery , fuel cells , biosensors , etc. In some cases, it is necessary to regain desirable characteristics of graphene such as electrical conductivity, magnetic properties or catalytic activity. Therefore, metallic nanoparticles are generally incorporated into GO nano sheets . Some of them cause an increase in electronic and catalytic effects of GO . In addition, the GO combination with iron oxide nanoparticles (Fe_3O_4) leads to magnetic nano composites with interesting properties for a variety of applications, especially solid phase

extraction (SPE). Some of the GO properties such as high surface area, good dispersibility and functionalization are simple due to the presence of the oxygen functionalities which makes it an ideal sorbent [19].

1.3.2 Nano graphene oxide synthesis methods

Graphene oxide can be synthesized through several chemical exfoliation mechanicals. Brodie method, reported in 1859, was pioneering one by using fuming HNO_3 and $KClO_3$ as oxidant . In 1898, Staudenmaier introduced two major changes to improve the method by adding concentrated H_2SO_4 and fuming HNO_3, as well as multiple aliquots of $KClO_3$ solution into the mixture over the course of reaction . These changes resulted in the production of highly oxidized GO in a single reaction vessel, thus greatly simplifying the process[20]. In 1958, Hummers and Offeman reported a method has been widely employed nowadays, known as Hummers method. They used concentration H_2SO_4 and $KMnO_4$ with $NaNO_3$ to graphite oxidation[21], the mechanism of this reaction as shown in Fig. (1-4)[22].

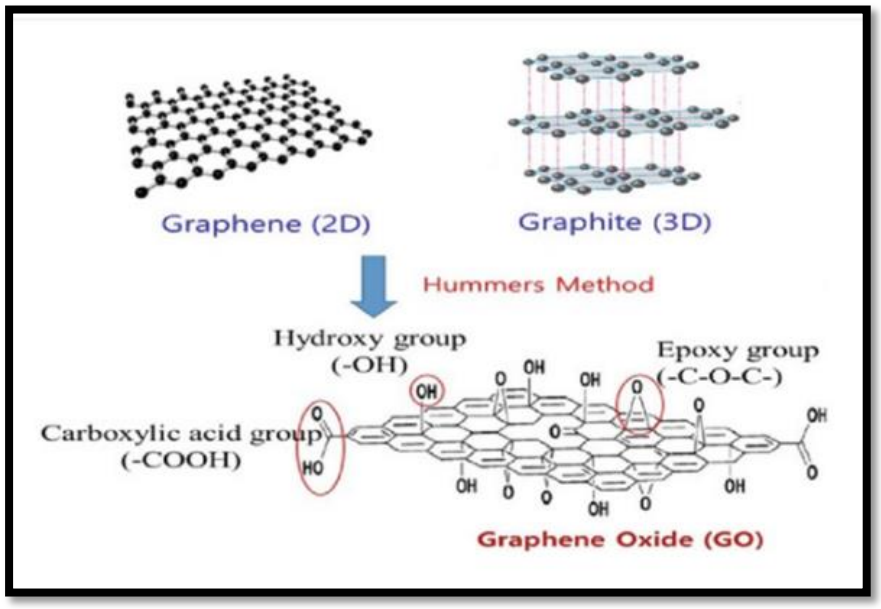

Fig. (1-4) Mechanism of graphene oxide synthesis

So, the main drawbacks of those methods are following, formation of NO_2, N_2O_4 and/or ClO_2 toxic gases, the latter also being explosive, and incomplete oxidation resulting in formation of a graphite/GO mixture[23]. So, several modifications on Hummers method has been made in the last years with different strategies. In 2010, Tour et al. improved the Hummers method by excluding $NaNO_3$, increasing the amount of $KMnO_4$ and performing the reaction in a 9:1 mixture of H_2SO_4/ H_3PO_4[20]. The addition of a protecting agent (H_3PO_4) into the exfoliation reaction produces a GO with more intact graphitic basal planes. In some cases, the protecting agent could be H_3BO_3, H_3PO_4 and $C_2HF_3O_2$[20]. The works by Li et al. and Hu et al. increased the amount of $KMnO_4$ instead of $NaNO_3$[24,25]. However, the oxidation time of graphite to GO with Tour's method is 23 times longer than the Hummers one , consequently, it is not cost-effective for scale-up synthesis of GO[23]. In 2013, Chen et al. developed an ecological Hummers method by removing the $NaNO_3$ which did not affect the yield and oxidation degree of the GO[23]. The same author in 2015 improved his ecological Hummers method with a simple purification process by using small graphite flakes obtaining a high yield and high-quality of GO[26]. Other strategies have adding a step of preoxidation before $KMnO_4$ oxidation (in the absence of $NaNO_3$). In 2015, Sun et al. demonstrated the pre-oxidation of graphite by impure MnO_2 in the mixture of concentrated H_2SO_4 and P_2O_5 which can efficiently improve the production yield of single-layer GO when $KMnO_4$ is employed as the oxidant[27]. Recently, a pre-oxidation approach partially replaces $KMnO_4$ with K_2FeO_4 while $NaNO_3$ is removed has been reported and a single-layer GO has been obtained at room temperature[28,29]. These modifications successfully resolved the two Hammers method problems mentioned above. Unfortunately, the complete conversion of graphite to GO could be achieved[30,24] and the procedure still too long, the shortest one took about 5 hrs. which results in

high cost and poor scalability[29]. On the other hand, the majority of the literature only the weight of the powder is mentioned as the yield of the final product, instead of the number of GO sheets and they did not compare their results with the results obtained by other chemical methods[31].

In 2007, Dmitriy A.Dikin et al. prepared graphene oxide paper and characterized it[32]. In 2011, Guixia Zhao et al. studied few layered graphene oxide (FGO) nanosheets which were synthesized from graphite using the modified Hummers method, and were used as sorbents for the removal of Cd(II) and Co(II) ions from large volumes of aqueous solutions[18], then prepared FGO, used to adsorb Pb(II) ions from aqueous solutions[13]. In 2013, Ji Chen et al. synthesized graphene oxide by Hummer's method as an improved Hummer's method without using $NaNO_3$[23]. In 2014, L. Stobinski et al. studied characterization of graphene oxide and reduced graphene oxide by the X-ray diffraction (XRD), transmission electronic microscopy (TEM) and electron spectroscopy methods[33]. In 2014, Ayrat M. Dimiev and James M. Tour studied mechanism of graphen oxide formation[34]. In 2017, N.I.Zaaba et al. synthesized graphene oxide using modified Hummer's method[35].

1.3.3 Properties of nano graphene oxide

Graphene oxide nano sheets are highly hydrophilic, form stable aqueous dispersions in wide range of concentrations and form stable dispersions in a number of organic solvents like dimethylformamide (DMF), ethylene glycol, n-methyl-2-pyrrolidone **(**NMP) and tetrahydrofuran (THF)[36] attributable to hydrogen bonding between hydroxyl groups on their surface and solvent interface[37]. This property permits making movies on range substrates even the usage of easy drop casting method. Thin movies of GO showcase an excessive optical transparency because of sp^3 hybridization of the maximum a part of

carbon atoms it behaves like wide-band-hole insulator. GO Electric conductivity is decided via way of means of domination of dielectric areas of sp^3 carbon atoms bonded to oxygen containing organizations that separate graphene from every other[38]. As a result the conductance becomes less than 10^{-10} S cm^{-1} . The band structure and GO optical properties depend on the oxygen groups coverage and are harder to predict than for graphene or graphite[39]. Porous structure is identical significance for GO membrane filters. Today membrane technology of filtering wastewater and gases for separation heavy metals and CO_2 play more significant role in environmental protection. The new results show successful application of membranes based on functionalized GO composites with polymers of effective separations of gas mixtures CO_2/CH_4 and CO_2/N_2[40]. The GO membranes ability for ionic and molecular sieving opens the way for radiochemical waste separation[41]. It was also reported the antimicrobial activity of GO[40]. It has been shown that the interlayer spacing of GO-based filter membranes can be tuned by trough intercalation by cations[42]. Besides membranes, chemically modified GO and GO composite are effective adsorbents for removing different contaminants from wastewater.[43] heavy metal ions including[44,45,46]. Moreover, GO-based sorbents can be successfully regenerated for later use[47,48].

In 2010, Yanwa Zhu et al. synthesized graphene and graphene oxide and studied it's properties and applications[49]. In 2019, Artur T.Dideikin and Alexander Y. Vul synthesized graphene oxide and studied it's properties as control optical transparency, electrical and thermal conductance[50]. In 2020, Sumit Yadav et al. studied electro-optical, dielectric and optical properties of graphene oxide dispersed nematic liquid crystal composites[51]. In 2020, Jeevan Jyoti et al. studied mechanical, electrical and thermal properties of graphene oxide-carbon nanotube[52]. In 2020, Ming-Jie Bai et al. studied heat transfer and mechanical friction reduction as properties of graphene oxide nano fluids[53].

1.4 Pre-concentration of trace elements

Environmental pollution with heavy metals occurs due to different reasons, included natural ones such as leaching of rocks, minerals and soils containing different concentration of these elements, industrial reason like mining, discharge of industrial pollutants . Although these useful elements are needed for human body and environment, but some of heavy elements could be toxic or even carcinogenic when consumed or exposure in larger amounts at a long time. So, very important to determination of heavy metals in environmental samples especially in water near industrial area. Common analytical chemistry techniques using the pre-concentration method for heavy metal ions include the membrane filtration, precipitation, sorption, extraction and the ion exchange. Particularly, sorption techniques widely used because it is cost-effective, economical and simple. Some sorbents, such as activated carbon[54], C18[55], polymers[56], silica gel[57], various resins[58], Humic acid[59,60], polyurethane foams[61] and biomass[62] suffer from low sorption capacities, efficiencies or their applicability, which is often restricted only to limited number of analytes .

Nanoparticles plays an important turn to solve this problem due for their high surface area, active sites enhanced, and additionally the presence a lot of functional groups on the surfaces[63]. Graphene oxide (GO) represents a novel type of carbon adsorbents, it has great features which make it an excellent sorbent for the pre-concentration of trace metal ions . The main feature of GO sorbent is large surface area (2630 m^2g^{-1}) which is responsible of the high adsorption capacity, and high chemical activity, due to both sides of graphene oxide planar sheets which are available for adsorption unlike fullerenes and carbon nanotubes (CNTs)[64].

In 2004, Jacobo Otero-Romani et al. studied possibilities of the use of commercial C18 cartridges to separate and pre-concentrate trace elements from sea water, trace elements (Al, Cd, Cu, Fe, Mn, Ni, Pb, Sn, V and Zn) which were previously complexed with 8-hydroxyquinoline, 8-HQ (5×10^{-4} M as final concentration) at alkaline pH (8.0±0.1) and then they were eluted with 2.5 ml of 2.0M nitric acid. Metals eluted from cartridges were measured by inductively coupled plasma-optical emission spectrometry (ICP-OES)[55]. In 2010, Hua Tian et al. studied, activated carbon was chemically modified with 4-(8-hydroxyquinoline-azo) benzamidine, used for separation and pre-concentration of trace amounts of Pb(II) in environmental samples by solid-phase extraction prior to the measurement by inductively coupled plasma atomic emission spectrometry (ICP-AES)[54]. In 2014, Reena Saxena and Prem Lata Meena studied a newly functionalized resin which has been applied in an on-line pre-concentration system for copper and zinc determination. Amberlite XAD-16 functionalized with 8-hydroxyquinoline packed in a minicolumn was used as sorbent material. The retained metals can be quickly eluted from the sorbent material, with the eluent stream consisting of nitric acid solution, directly in the nebulizer burner system of the FAAS[58].

1.4.1 Solid phase extraction method by nano graphene oxide as a sorbent

In last decades, solid phase micro extraction (SPME) played a critical role in the area of separation, not only to separate analyte from a sample matrices, but also to pre-concentrate the analytes before to determination by less sensitive techniques and low-cost[65]. Currently, use of nano materials such as sulfur nanoparticles[66], yeast immobilized TiO_2[67], carbon nanotubes (CNTs) as graphene oxide[68], fullerenes[69], carbon nanohorn[70], activated carbon[71], and carbon nanocones (disks)[72] in SPE has become a research

active area in field separation due to their properties, such as high surface area and high mechanical strength included, CNTs possess high ability to remove the metal ions and the organic pollutants from aqueous solutions, and used as a superior adsorbent for treatment of waste water[65]. Solid phase micro extraction (SPME) is a popular technique for the separation and pre-concentration of metal ions, commonly used before atomic absorption spectrometry (AAS)[73].

Like other nano particles, graphene oxide is usually packed on a substrate or loaded into a column for solid phase extraction/micro extraction (SPE/SPME). Due environmental risk and its toxicity of nano particles[74], a dispersive solid liquid extraction method by graphene oxide direct addition to an aqueous phase applied to solve these problems[75]. The direct dispersion of hydrophobic graphene oxide sheets in water has been considered to be a hard challenge because high surface area and, very strong van der Waals, interactions of layers. This could give to irreversible agglomerates, or even restack, to form graphite and thus decrease the graphene oxide evolution for analytes pre-concentration. In last decade, several efforts have been made to obtain a graphene oxide dispersions stable in water by oxidation chemical[76], using surface-active agents[77] or polar solvents as solubilizing or dispersing agents[78]. The whole pre-concentration process is schematically described as shown in Fig. (1-5).

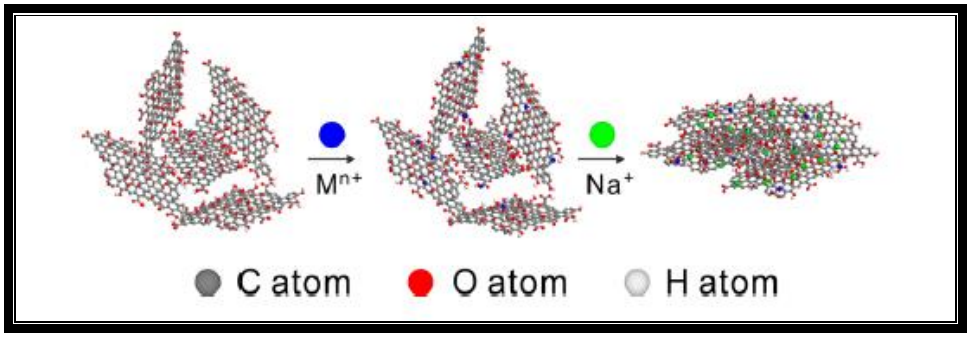

Fig. (1-5): Schematic diagram of the whole pre-concentration process by NGO

In 2011, Yukun Wang et al. studied a new method sorbent by graphene oxide using a column packed with graphene as sorbent was developed for the preconcentration of trace amounts of lead (Pb) using dithizone as chelating reagent prior to its determination by flame atomic absorption spectrometry[74]. In 2011, Zheng-Hong Huang et al. studied adsorb lead ions from an aqueous system by graphen nanosheets (GNSs) that were obtained by vacuum-promoted low-temperature exfoliation[75]. In 2013, Rafal Sitko et al. studied the adsorptive properties of graphene oxide (GO) towards divalent metal ions (copper, zinc, cadmium and lead), the results of batch experiments and measurements by F-AAS were investigated[17]. In 2013, Beata Zawisza et al. studied pre-concentration of trace elements Co(II), Ni(II), Cu(II), Zn(II) and Pb(II) procedure is based on dispersive micro-solid phase extraction (DMSP) using graphene oxide after preparation it[79]. In 2013, Shaowei Su et al. Fe_3O_4-SiO_2-polyaniline–graphene oxide composite (MPANI-GO) was prepared through a simple non covalent method and applied to magnetic solid phase extraction (MSPE) of trace rare earth elements (REEs) in tea leaves and environmental water samples followed by inductively coupled plasma mass spectrometry (ICP-MS) detection[11]. In 2013, Dongyan Deng et al. studied efficient pre-concentration and adsorption of heavy metal ions prior Pb(II), Cd(II), Bi(III) and Sb(III) by graphene oxide[80]. In 2014, Aminul Islam et al. employ solid-phase extractant was synthesized by coupling graphene oxide (GO) on chloro methylated polystyrene through an ethylene diamine spacer unit to develop a column method for the pre-concentration/separation of lead prior to its determination by flame atomic absorption spectrometry[65]. In 2015, Beata Zawisza et al. employ solid phase sorbent by using coupling graphene oxide (GO) to ethylenediamine (EDA). This nanomaterial (referred to as GO-EDA) is capable of adsorbing the ions of iron, cobalt, nickel, copper, zinc and lead[63].

1.5 Determination methods of trace elements

Many optical atomic spectrometric techniques used of which flame atomic absorption spectrometry (FAAS), electro thermal atomic absorption spectrometry (ETAAS), inductively coupled plasma optical emission spectroscopy (ICP-OES)[81], inductively coupled plasma mass spectrometry (ICP-MS) and X-ray fluorescence spectrometry (XFS), are often used to determined heavy metal ions due their accuracy and sensitivity, but the determination is time consuming operation and expensive testing cost, however, cannot be ignored[82,83]. Flame photometer for analytical chemical science experiments for quantitative analysis of lithium, sodium, potassium , calcium and barium alkali and earth alkali metal ions . For the determination of trace elements all across the world, atomic emission spectroscopy is considered as an effective instruments[84]. The electrochemical techniques widely used as a method for obtain metal ions detection under complex environment due the excellent sensitivity, convenient and low cost[85,86]. In addition, analytical instruments used of electrochemical methods are miniaturized, relatively inexpensive and convenient in contrary to those spectroscopic instruments[87,88]. Total reflection X-ray fluorescence (TXRF) instead of XRF where the X-ray beam incident angle is lower than the critical angle for reflection of X-rays at the carrier surface, the detector is placed 90º with respect to incident beam and less than 0.5 mm above the sample surface, TXRF is a reliable and sensitive technique for elemental analysis of environmental samples[89], it offers many advantages compared to other spectrometric techniques such as the elements simultaneous detection , sample low amount (few mL or ng), and short time required for analysis[90]. In case, solid samples mostly, sample pretreatment methods for TXRF analysis are powder suspension, mineralization or direct deposition on the reflector surface[91]. There are several methods to determined heavy metals in soil, among them, laser-induced breakdown

spectroscopy (LIBS) is a spectrochemical analysis method based on analyzing spectra of plasmas that generated by pulsed lasers. Its advantages are easy setup, convenient operation and minimum sample preparation[92,93], In different samples due to its ease of use, low cost and high sample yield. Despite these advantages, it has not sufficient sensitivity for complex matrices and analyte ions have low concentration therefore a separation and pre-concentration step can be necessary just before their determination[94]. Solid phase extraction[95], ion exchange[96], liquid–liquid extraction[97], co-precipitation[98], cloud point extraction[99,100] are considered of the pre-concentration and separation techniques which can solve the problems associated with complex matrices and low concentration of the trace elements then determined by ETAAS , ICP, FAAS or XRF[81,101].

In 1981, the Society et al. studied some heavy elements in the marine sediments of Osaka Bay in Japan at different depths , samples were digested by acids and the elements were determined by Flame Atomic Absorption Spectroscopy (FAAS)[102]. In 2001, Jianrong Chen studied cloud point extraction (CPE) which has been used pre-concentration of Cd, Cu, Pb and Zn after formation of a complex with 1-(2-thiazolylazo)-2-naphthol (TAN) and later analysis by flame atomic absorption spectrometry (FAAS) using (Triton X-114) as surfactant[103]. In 2003, A. Safavi et al. studied Cloud point extraction has been used for the pre-concentration and simultaneous spectrophotometric determination of nickel and cobalt after the formation of a complex with 2-amino-cyclopentene-1-dithiocarboxylic acid (ACDA), and latter analysis by spectrophotometer using Triton X-114 as surfactant[104]. In 2004, Xiashi Zhu et al. studied Cloud point extraction (CPE) separation and electrothermal atomic absorption spectrometry (ETAAS) detection was proposed for the determination of chromium species, when the system temperature is higher than the cloud point extraction temperature (CPT) of

selected surfactant (Triton X-100), the complex of Cr(VI) with dibromo phenyl fluorone (Br-PF) could enter surfactant-rich phase, whereas the Cr(III) remained in aqueous phase[105]. In 2005, Enfeng et al. studied a number of heavy elements at different depths in the Taih Lake sediments in northwestern China, soil samples were digested by acids and the heavy elements were determined by inductive coupled plasma optical emission spectroscopy (ICP-OES)[106]. In 2006, Stefania Gaudino et al. studied comparison between total and partial digestion of soil, sediment and water samples, total digestion a chivied by (microwave aqua regia +HF and HNO_3 +HF) but partial digestion by ($HCl+HNO_3+H_2O_2$) then determined by ICP-MS[107]. In 2009, Harikumar et al. studied the heavy elements in rock crumbs at different depths in five regions of Kerala city, samples were digested by acids and the heavy elements were determined by flame atomic absorption spectroscopy FAAS[108]. In 2010, Seshan et al. studied heavy elements in sediments of southeastern Indian coasts in four regions at different depths. Samples were digested with acids, determined by inductive coupled plasma Atomic emission spectroscopy (ICP-AES)[109]. In 2011, Carreiro et al. in Jefferson County, Colorado, USA, studied the heavy elements in different soils of the province[110]. In 2013 Gayatri et al. studied the heavy elements in the soil and their relationship to the physical properties of the soil where they studied each of the elements Zn, Cd, Cu, Ni, Co, Cr, in 21 study sites in different regions of India[111]. In 2014, Liang et al. studied the elements Zn, Cd, Pb in 9 soil samples[112]. In 2014, Yong Zhang et al. studied rare earth elements (REEs) in intertidal sediments of Bohai Bay in china, the samples digestion by HF, HNO_3 and $HClO_4$ and determined by (ICP-MS) inductively coupled plasma – mass spectrometry[113]. In 2015, Adhikri studied the Cu, Zn, Co, Ni, Cr, and Pb elements in the soil in Bangladesh in 7 sites of the country and was determined using the (AAS) atomic absorption spectroscopy[114]. In 2015, Hussian H. Kharnoob and Ahmed R. Mahmood studied the total concentration of heavy metals (Zn,Cd,Pb,Cu) in contaminated

soil in Baiji oil refinery at Salah -alden province , Iraq, the samples digested by concentration nitric acid and determined by atomic absorption spectroscopy (AAS)[115]. In 2015, Li Jing-Xi et al. studied Rare earth elements (REEs) in sediment in south mid-Atlantic ridge , where digested by HNO_3 + H_2O_2 + HF then determined by ICP-MS[116]. In 2016, G.M.Balak et al. studied the determination of some elements in crude oil samples, digested by dry ashing and measured with atomic absorption spectroscopy (AAS)[117]. In 2017, Martin Makombe et al. studied rare earth elements (REEs) in sediment samples and determined it by (ICP-OAS) inductively coupled plasma- optical atomic spectroscopy[118]. In 2019, Luiza Valli Vieira et al. determined metals in crude oil by inductively coupled plasma optical emission spectrometry (ICP-OES) using nano emulsification as sample preparation[119]. In 2019, M. A. Gab-Allah et al. studied analytical methods for the determination of trace elements in crude oil and sample digestion by ASTM standard[120]. In 2020, Chikaodili E. Chukwuneke et al. determined ash content and trace metal concentration in crude oil samples[121].

The Aims of study

1- Separation the elements (Mg, Co, Ni, Cu, Cd and Pb) by using nano graphene oxide as a sorbent by solid phase micro extraction (SPME) method.
2- Determination of the elements (Cr, Mn, Fe, Co, Ni, Cu, Zn, As, Cd, Sn, Pb, Li, Mg, K, Ca and Ba) in cutting rock and crude oil samples.
3- Studying the optimum conditions of the adsorption process.

CHAPTER TWO

EXPERIMENTAL

2.1 Instruments and Chemicals

The instruments used in the present study and their models, companies and origin are listed in Table (2-1).

Table (2-1) Instruments used in study and their models, companies, origin and laboratory.

Ser.	Devise	Company	Origin	Laboratory
1	Flame atomic absorption spectroscopy, Al 1200	Aurora	UK	Misan University/ College of Science/ Chemistry Dep.
2	UV-Vis spectrophotometer, UV-1800	Shimadzu	Japan	Misan University/ College of Science/ Chemistry Dep.
3	FT-IR spectrophotometer, FTIR-8400S	Shimadzu	Japan	Misan University/ College of Science/ Chemistry Dep.
4	X-ray diffraction (XRD), LabX-XRD-6000	Shimadzu	Japan	Science & Technology Ministry/ Polymers Dep.
5	Transmission electronic microscope (TEM), Techai^{TM} G2 F20	FEI	USA	Tehran University/ Advanced Materials Characterization Institute
6	Field emission scanning electronic microscope (FESEM), 5 KV	Zeiss	Germany	Tehran University/ Advanced Materials Characterization Institute
7	Zeta potential analyzer, Zeta Plus	Brookhaven	USA	The Science & Technology Ministry/ Water & Environment Dep.
8	Flame photometer, PFP7	Jenway	Ireland	Misan University/ College of Science/ Chemistry Dep.

Ser.	Devise	Company	Origin	Laboratory
9	Probe sonicator, FSFJY92-IIN	Sino Sonics	China	Misan University/ College of Science/ Biology Dep.
10	Bath sonicator, WHC-A10H	Daihan Scientific	China	Misan University/ College of Science/ Chemistry Dep.
11	Stirring water bath, KBLEE 2010	Daiki	Japan	Misan University/ College of Science/ Chemistry Dep.
12	pH meter, pH 7110	InoLab	Germany	Misan University/ College of Science/ Chemistry Dep.
13	Muffle furnace, CWF1100	Carbolite	UK	Misan Oil Training Institute

The chemicals used in this study were all analytical reagent grade, Table (2-2) list chemicals, purities, companies and origin.

Table (2-2) Chemicals used and their chemicals formula, purities, companies and origin

Ser.	Chemicals	Chemical Formula	Purity	Company	Origin
1	Sulphuric acid	H_2SO_4	97%	ChemLab.	UK
2	Hydrofluoric acid	HF	40%	CDH	India
3	Per chloric acid	$HClO_4$	70%	GCC	UK
4	Nitric acid	HNO_3	69%	Applichem	USA
5	Hydrochloric acid	HCl	37%	Applichem	USA
6	Ammonia solution	NH_4OH	35%	Fisher chemical	UK
7	Hydrogen peroxide	H_2O_2	50%	Panreac applab.	Spain
8	DMF	$HCON(CH_3)_2$	97%	Thomas beaker	India
9	Graphite	C	99.9%	CDH	India
10	Sodium nitrate	$NaNO_3$	99%	Thomas beaker	India

Ser.	Chemicals	Chemical Formula	Purity	Company	Origin
11	Potassium permanganate	$KMnO_4$	99.5%	GCC	UK
12	Barium chloride	$BaCl_2$	99%	Thomas beaker	India
13	Sodium chloride	NaCl	98%	Thomas beaker	India
14	Magnesium sulphate heptahydrate	$MgSO_4.7H_2O$	99%	Thomas beaker	India
15	Cobalt sulphate heptahydrate	$CoSO_4.7H_2O$	99%	Sigma-Aldrich	UK
16	Nickel sulphate hexahydrate	$NiSO_4.6H_2O$	99%	Sigma-Aldrich	UK
17	Copper sulphate pentahydrate	$CuSO_4.5H_2O$	99.5%	Pubchem	China
18	Cadmium sulphate octahydrate	$CdSO_4.8H_2O$	99.5%	Pubchem	China
19	Lead nitrate	$Pb(NO_3)_2$	99%	Sigma-Aldrich	UK
20	Calcium sulphate	$CaSO_4$	99%	Fine-chem	South Korea
21	Chromium chloride hexahydrate	$CrCl_3.6H_2O$	99%	Aldrich	Germany
22	Ferrous sulphate	$FeSO_4$	99%	Thomas beaker	India
23	Zinc sulphate	$ZnSO_4$	98%	Thomas beaker	India
24	Manganese(IV) oxide	MnO_2	85%	BDH	South Korea
25	Arsenic oxide	As_2O_3	80%	Pub chem	China
26	Ferric chloride	$FeCl_3$	96%	Sigma-Aldrich	UK
27	Potassium chloride	KCl	99%	Thomas beaker	India
28	Tin(II) chloride	$SnCl_2$	95%	GCC	UK
29	Lithium (flame photometry standard 1000 ppm)	Li	99.99%	Jenway	Ireland

2.2 Synthesis of nano graphene oxide

Nano graphene oxide were synthesized by modified Hummer's method[23,35]. This included 0.6 g graphite and 0.5 g sodium nitrate dissolved in 23 mL of cooled (0 ºC) concentrated sulphuric acid in beaker onto ice bath with stirring for 15 min. 3 g Potassium permanganate added gradually to the suspension (black color) , continuous stirring to keep the reaction temperature below 20 ºC onto ice bath for 30 min. The reaction beaker placed in stirring water bath at 35 ºC for 2hrs. (the suspension changed to dark brown). 50 ml Deionized water added gradually (by dropper) into the suspension over a hot plate magnetic stirrer, the temperature kept below 98 ºC, for 15 min, warm deionized water 100 mL added. 10 mL Hydrogen peroxide 30% added gradually (by dropper) to remove the residual $KMnO_4$ and MnO_2 for 15 min. The suspension separated by centrifuge (4000 rpm for 5 min), the precipitate washed with warm hydrochloric acid (HCl) 5% to remove sulphate ions (test by barium chloride $BaCl_2$), the precipitate washed with deionized water until the pH of washing solution became 7. The product (graphene oxide) dried in oven at 60 ºC for 1 hr. 0.5 g of Graphene oxide added to 50 mL of N,N-di methyl formamide and sonicated by probe sonicator for 30 min, the suspension separated by centrifuge (4000 rpm for 10 min), the separated residue dried in oven at 60 ºC for 1 hr.

2.3 Samples Collection

Cutting rock samples have collected from different depths of oil reservoir (Mishrif formation) in Missan province, Amarah oil field depth (2874-3240 m), Noor oil field depth (3301-3668 m) , Halfaya oil field depth (3102-3432 m), north Buzurgan oil field depth (3698-4021 m) and south Buzurgan oil field

depth (3674-4016 m) , while crude oil samples have collected from same oil fields, as shown in Fig. (1-2).

2.4 Sample Digestion

2.4.1 Cutting rock sample digestion

Each sample grinded by grinder , sieved by standard sieve (0.3 mm) portion of the powder, dried by oven at 105 ºC for 1 hour, and cool to room temperature in a desiccator. The samples digested by a modified Totland's method[122,123] , weighed (0.5 g) of each sample into Teflon beaker and moistened with (3 mL) of deionized water, then added (10 mL) concentrated hydrofluoric acid and (4mL) concentrated perchloric acid. The mixture heated at 200 ºC to dryness and crystalline paste appeared after 1.5 hrs. , this step is repeated one time . Concentrated perchloric acid (4mL) added and evaporated to near dryness at 200 ºC (0.5 hrs.). 10 ml of (5M) Nitric acid, heated gently at (65 ºC) until a clear solution appeared, cooling and the solution diluted with deionized water up to the top mark sign of volumetric flask (50 mL). Samples were stored in polypropylene bottles.

2.4.2 Crude oil samples digestion

Digestion of crude oil by dry ash digestion method according to ASTM-D5863-00a[124,120], crude oil 1 g placed in porcelain crucible, 0.5 mL conc. sulfuric acid added, porcelain crucible placed in beaker as on hot plate. Heated gently from the top by the infrared lamp (2 cm above crucible porcelain) while stirring the solution with a glass rod. As decomposition proceeds (indicated by a frothing and foaming) , the temperature increased gradually of the hot plate until the sample is reduced to a carbonaceous ash, the infrared lamp removed. The sample heated in the muffle furnace at 525 °C for 2 hrs. until the carbon is

completely removed. The inorganic residue dissolved with 10 mL of the (1:1 HNO_3) for 15 min., heated gently by a hot plate (100 °C) to dryness, washed with 10 mL of nitric acid (5% V/V), allow to cool and transferred quantitatively to a volumetric flask (50 mL) and diluted with nitric acid (5%) up to the top mark. Samples were stored in polypropylene bottles.

2.5 Solutions

2.5.1 Stock solution of Magnesium(II) (1000 µg/mL)

Magnesium sulphate $MgSO_4.7H_2O$ (1.0143 g) dissolved in a small volume of (5% HCl) into beaker, transferred quantitatively to volumetric flask (100 mL) and filled up to the top mark with deionized water. The working standard solutions were prepared by serial dilution of stock solution.

2.5.2 Stock solution of Cobalt(II) (1000 µg/mL)

Cobalt sulphate $CoSO_4.7H_2O$ (0.4769 g) dissolved in a small volume of (5% HCl) into beaker, transferred quantitatively to volumetric flask (100 mL) and filled up to the top mark with deionized water. The working standard solutions were prepared by serial dilution of stock solution.

2.5.3 Stock solution of Nickel(II) (1000 µg/mL)

Nickel sulphate $NiSO_4.6H_2O$ (0.4476 g) dissolved in a small volume of (5% HCl) into beaker, transferred quantitatively to volumetric flask (100 mL) and filled up to the top mark with deionized water. The working standard solutions were prepared by serial dilution of stock solution.

2.5.4 Stock solution of Copper(II) (1000 µg/mL)

Copper sulphate $CuSO_4.5H_2O$ (0.3927 g) dissolved in a small volume of (5% HCl) into beaker, transferred quantitatively to volumetric flask (100 mL) and filled up to the top mark with deionized water. The working standard solutions were prepared by serial dilution of stock solution.

2.5.5 Stock solution of Cadmium(II) (1000 µg/mL)

Cadmium sulphate $CdSO_4.8H_2O$ (0.3135 g) dissolved in a small volume of (5% HCl) into beaker, transferred quantitatively to volumetric flask (100 mL) and filled up to the top mark with deionized water. The working standard solutions were prepared by serial dilution of stock solution.

2.5.6 Stock solution of Lead(II) (1000 µg/mL)

Lead nitrate $Pb(NO_3)_2$ (0.1598 g) dissolved in a small volume of (5% HCl) into beaker, transferred quantitatively to volumetric flask (100 mL) and filled up to the top mark with deionized water. The working standard solutions were prepared by serial dilution of stock solution.

2.5.7 Stock solution of chromium(III) (1000 µg/mL)

Chromium chloride hexa hydrate $CrCl_3.6H_2O$ (0.5122 g) dissolved in a small volume of (5% HCl) into beaker, transferred quantitatively to volumetric flask (100 mL) and filled up to the top mark with deionized water. The working solutions were prepared by serial dilution of stock solution.

2.5.8 Stock solution of Manganese(IV) (1000 µg/mL)

Manganese dioxide MnO_2 (0.1582 g) dissolved in a small volume of (5% HCl) into beaker, transferred quantitatively to volumetric flask (100 mL) and filled up to the top mark with deionized water. The working solutions were prepared by serial dilution of stock solution.

2.5.9 Stock solution of Iron(II) (1000 µg/mL)

Ferrous sulphate $FeSO_4$ (0.2720 g) dissolved in a small volume of (5% HCl) into beaker, transferred quantitatively to volumetric flask (100 mL) and filled up to the top mark with deionized water. The working solutions were prepared by serial dilution of stock solution.

2.5.10 Stock solution of Iron(III) (1000 µg/mL)

Ferric chloride $FeCl_3$ (0.2904 g) dissolved in a small volume of (5% HCl) into beaker, transferred quantitatively to volumetric flask (100 mL) and filled up to the top mark with deionized water. The working solutions were prepared by serial dilution of stock solution.

2.5.11 Stock solution of Zinc(II) (1000 µg/mL)

Zinc sulphate $ZnSO_4$ (0.2469 g) dissolved in a small volume of (5% HCl) into beaker, transferred quantitatively to volumetric flask (100 mL) and filled up to the top mark with deionized water. The working solutions were prepared by serial dilution of stock solution.

2.5.12 Stock solution of Arsine(III) (1000 µg/mL)

Arsenic oxide As_2O_3 (0.1320 g) dissolved in a small volume of (5% HCl) into beaker, transferred quantitatively to volumetric flask (100 mL) and filled up to the top mark with deionized water. The working solutions were prepared by serial dilution of stock solution.

2.5.13 Stock solution of Tin(II) (1000 µg/mL)

Stannous chloride $SnCl_2$ (0.1597 g) dissolved in a small volume of (5% HCl) into beaker, transferred quantitatively to volumetric flask (100 mL) and filled up to the top mark with deionized water. The working solutions were prepared by serial dilution of stock solution.

2.5.14 Stock solution of Lithium (I)

The working solutions were prepared by serial dilution of lithium flame photometry standard solution 1000 µg/mL (Jenway company).

2.5.15 Stock solution of Potassium(I) (1000 µg/mL)

Potassium chloride KCl (0.1911 g) dissolved in a small volume of (5% HCl) into beaker, transferred quantitatively to volumetric flask (100 mL) and filled up to the top mark with deionized water. The working solutions were prepared by serial dilution of stock solution.

2.5.16 Stock solution of Calcium(II) (1000 µg/mL)

Calcium sulphate dihydrate $CaSO_4.2H_2O$ (0.4303 g) dissolved in a small volume of (5% HCl) into beaker, transferred quantitatively to volumetric flask (100 mL) and filled up to the top mark with deionized water. The working solutions were prepared by serial dilution of stock solution.

2.5.17 Stock solution of Barium (1000 µg/mL)

Barium chloride dihydrate $BaCl_2.2H_2O$ (0.1779 g) dissolved in a small volume of (5% HCl) into beaker, transferred quantitatively to volumetric flask (100 mL) and filled up to the top mark with deionized water. The working solutions were prepared by serial dilution of stock solution.

2.6 Optimum conditions of sorption by NGO

2.6.1 Effect of solution pH[17]

Serial dilution of the stock solution (1 µg/mL) of each analyte (Mg, Co, Ni, Cu, Cd and Pb) prepared in beaker. Deionized water added less than 50 mL, few drops of HNO_3 (0.1M) or NH_4OH (0.1M) added to set the pH (2,4, 4.5,5.0,5.5,6.0,6.5,7.0,7.5 and 8.0) by the pH meter. The solution filled in volumetric flask (50 mL) up to the top mark. Nano graphene oxide 0.5 mg placed in each beaker, analyte solutions (at different pH 2-8) added to each beaker, the solutions sonicated by bath sonicator for 2 min. , and stirred by magnetic stirrer for 5 min. at room temperature. Three drops of (5.75 mg/mL NaCl) added and centrifuged for 5 min (5000 rpm) to each solution. The analyte concentration determined by flame atomic absorption spectroscopy.

2.6.2 Effect of Mass of nano graphene oxide[125]

Prepared four solutions of each analyte (1 μg/mL) in (50 mL) volumetric flask at the optimum pH for each analyte ion. Nano graphene oxide (0.25, 0.5, 0.75 and 1.0 mg) placed in each beaker, each analyte solution poured in the beaker, sonicated by bath sonicator for 2 min. , and stirred for 5 min. at room temperature . Three drops of (5.75 mg/mL NaCl) added and centrifuged for 5 min (5000 rpm) to each solution. The analyte concentration determined by flame atomic absorption spectroscopy**.**

2.6.3 Effect of Sample volume[125]

Prepared five solutions of each analyte (1 μg/mL) in volumetric flasks (5, 10, 20, 25 and 50 mL) at the optimum pH for each analyte ion. Nano graphene oxide 0.5 mg placed in each beaker, each analyte solution poured in the beaker, sonicated by bath sonicator for 2 min. , and stirred the solutions for 5 min. at room temperature . Three drops of (5.75 mg/mL NaCl) added and centrifuged for 5 min (5000 rpm) to each solution. The analyte concentration determined by flame atomic absorption spectroscopy**.**

2.6.4 Effect of Sonicating time

Prepared six solutions of each analyte (1 μg/mL) in (20 mL) volumetric flask at the optimum pH for each analyte ion. Nano graphene oxide 0.5 mg placed in each beaker, each analyte solution poured in the beaker and each single solution sonicated for (0, 2, 4, 6, 8 and 10) min. respectively by bath sonicator , stirred for 5 min. at room temperature. Three drops (5.75 mg/mL

NaCl) and centrifuged for 5 min (5000 rpm) to each solution. The analyte concentration determined by flame atomic absorption spectroscopy.

2.6.5 Effect of Stirring time[125]

Prepared six solutions of each analyte (1 µg/mL) in (20 mL) volumetric flask at the optimum pH for each analyte ion. Nano graphene oxide 0.5 mg placed in each beaker, each analyte solution poured in the beaker, sonicated by bath sonicator for 2 min. , and each single solution stirred for (5, 15, 30, 60, 90 and 120) min respectively at room temperature. Three drops (5.75 mg/mL NaCl) added and centrifuged for 5 min. (5000 rpm) to each solution. The analyte concentration determined by flame atomic absorption spectroscopy.

2.6.6 Effect of Temperature[80]

Prepared six solutions of each analyte (1 µg/mL) in (20 mL) volumetric flask at the optimum pH for each analyte ion. Nano graphene oxide 0.5 mg placed in each beaker, each analyte solution poured in the beaker, sonicated by bath sonicator for 2 min. , and stirred for 5 min. at different temperature (20, 30, 40, 50, 60 and 70) ºC by stirring water bath. Three drops of (5.75 mg/mL NaCl) added and centrifuged for 5 min (5000 rpm) to each solution. The analyte concentration determined by flame atomic absorption spectroscopy.

2.6.7 Effect of NaCl concentration[80]

Prepared six solutions of each analyte (1 µg/mL) in (20 mL) volumetric flask at the optimum pH for each analyte ion. Nano graphene oxide 0.5 mg placed in each beaker, each analyte solution poured in the beaker, sonicated by bath sonicator for 2 min. , and stirred for 5 min. at room temperature. Three

drops to each solution added of (2, 4, 6, 6.5, 7 and 8) mg/mL NaCl respectively and centrifuged for 5 min (5000 rpm) to each solution. The analyte concentration determined by flame atomic absorption spectroscopy.

2.6.8 Tolerance limit[63]

To each single analyte solution (1 μg/mL) at the optimum conditions interfering ions added as Cr^{+3}, Mn^{+2}, As^{+3}, Sn^{+2} ions (0.2-1 μg/mL), Fe^{+2}, Fe^{+3}, Zn^{+2},Li^{+} ions (1- 5 μg/mL), K^{+}, Ca^{+2} ions (10-40 μg/mL) and Ba^{+2} ions (20-80 μg/mL) respectively by serial dilution of the stock solutions. The analyte concentration determined by flame atomic absorption spectroscopy.

2.7 Determination of analytes in the samples

2.7.1 Blank solution

2.7.1.1 Blank solution for cutting rock sample

5 mL conc. HF , 4 mL conc. $HClO_4$, 10 mL HNO_3 (5M) and deionized water mixed in Teflon beaker .

2.7.1.2 Blank solution for crude oil sample

0.5 mL conc. H_2SO_4, 10 mL HNO_3 (1:1) mixed in beaker, transferred quantitatively to volumetric flask (50 mL) and filled to the top mark with deionized water.

2.7.1.3 Blank solution for standard solutions

5 mL conc. HCl added to volumetric flask and filled to the top mark with deionized water.

2.7.2 Direct determination of the analytes in samples

The analytes concentrations determined by flame atomic absorption spectroscopy (without NGO) before separation them by using solid phase micro extraction (SPME) method by nano graphene oxide.

2.7.3 Solid phase micro extraction (SPME) method to separate analytes from samples by nano graphene oxide (NGO)

According to the following optimum conditions of SPME by nano graphene oxide, 20 mL of the digested sample, at the optimum pH for each analyte ion, added 0.5 mg of nano graphene oxide, sonicated by bath sonicator for 2 min., stirring for 5 min. at room temperature, added (6.5 mg/mL NaCl) and centrifuged for 5min (5000 rpm) to separate the solid phase of NGO from the solution. Analytes concentration determined in the residual solutions by flame atomic absorption spectroscopy (FAAS).

CHAPTER THREE

RESULTS AND DISCUSSION

3.1 Spectral characterization of nano graphene oxide

Nano graphene oxide was characterized spectrally by Fourier transform infrared (FTIR) spectroscopy , UV-Vis spectrophotometer, zeta potential analyzer and X-ray diffraction (XRD).

3.1.1 Fourier transform infrared spectrophotometry

The FT-IR spectrum of synthesized NGO as shown in Fig. (3-1), band at 1626 cm^{-1} for C=C bond , the broad band of O−H bond appeared at 3000-3700 cm^{-1}, the C=O band stretching vibrations of carbonyl and carboxylic groups appeared at around 1709 cm^{-1}, the bands around 1217 cm^{-1} to C−OH and 1035 cm^{-1} are attributed C−O of epoxy group stretching vibrations. The FT-IR spectrum of graphite shows no peaks for functional groups except C=C at 1550 cm^{-1} stretching vibration and bending vibration of C-C bond at 700 cm^{-1} as shown in Fig. (3-2)[126].

3.1.2 Ultraviolet - visible spectrophotometry

The UV−vis spectrum of the NGO dispersion (0.1 mg/mL) as shown in Fig. (3-3) , the maximum of absorption peak λ_{max}= 239.5 nm and a shoulder peak 289.5 nm which were the absorption bands corresponding to π→π* electron transitions of poly aromatic C=C bonds and n→π* electron transitions of C=O bonds respectively[126] shows a good agreement with the previous studies[127,80].

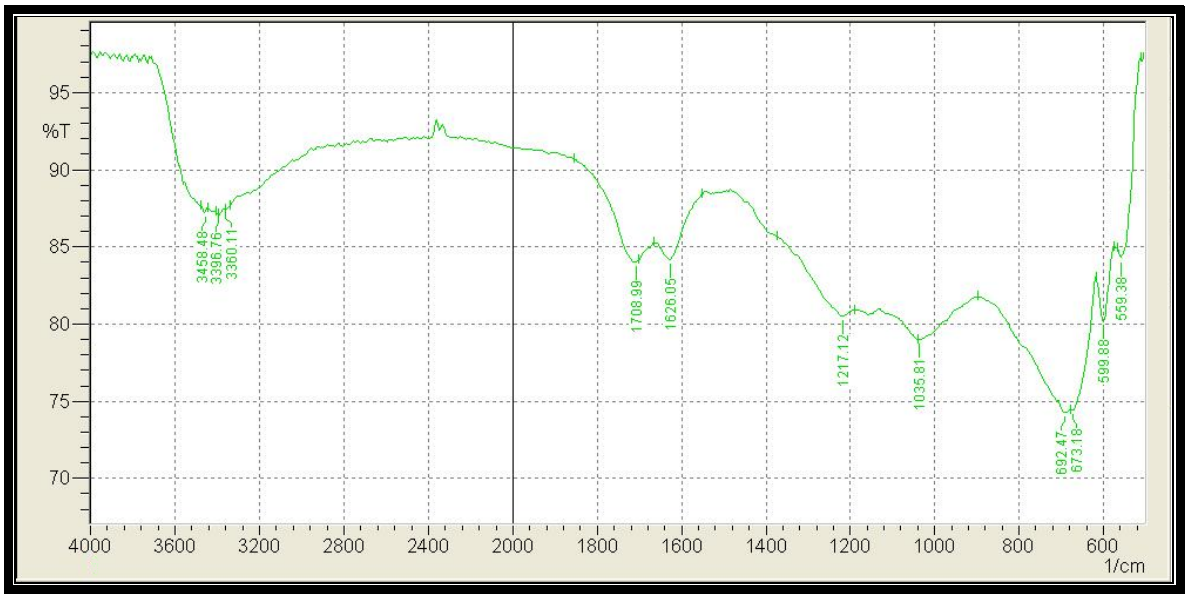

Fig. (3-1) FT-IR spectrum of NGO

Fig. (3-2) FT-IR spectrum of graphite

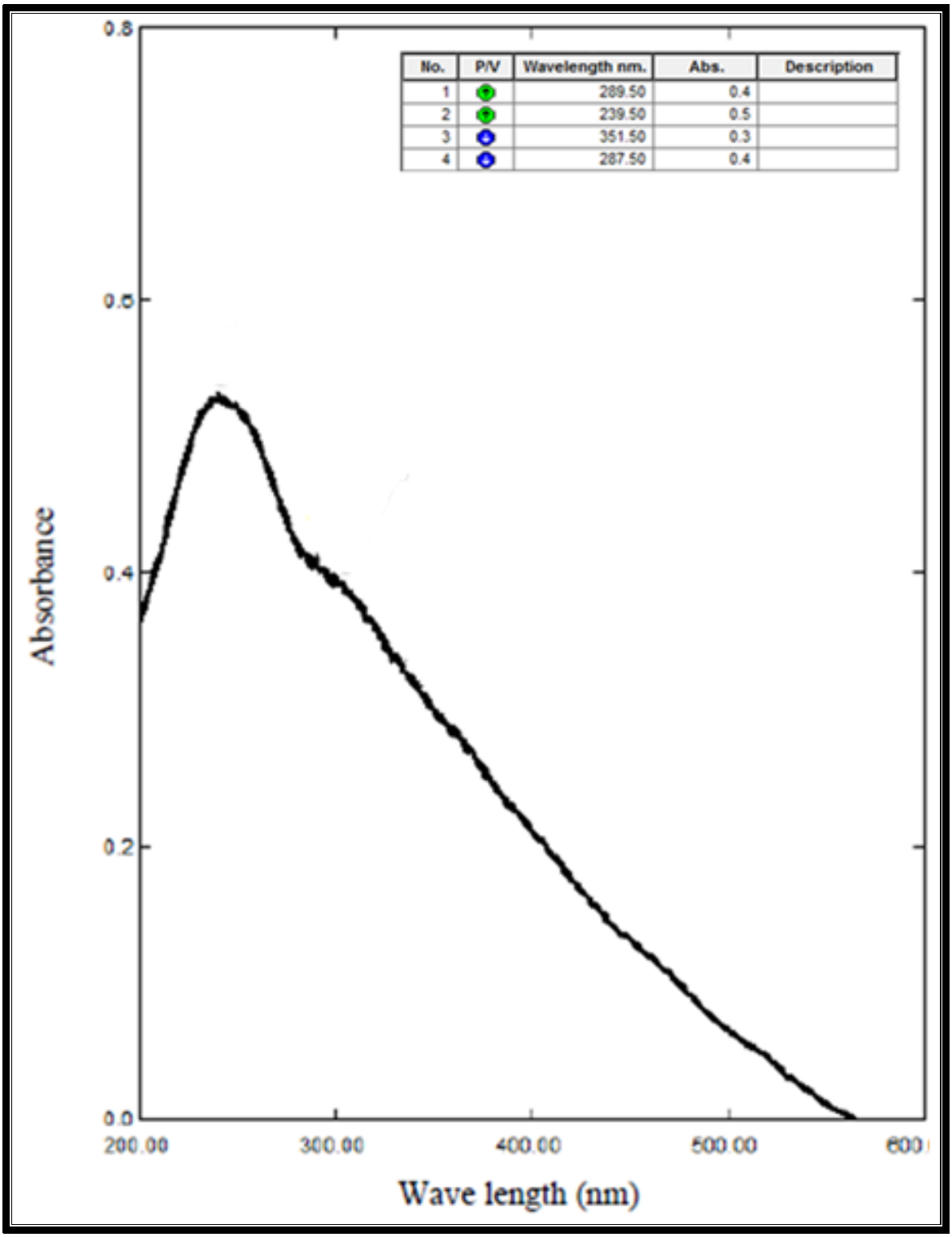

Fig. (3-3) UV-Vis spectrum of NGO (0.1 mg/mL)

FT-IR and UV−Vis spectra proved the presence of large amounts of oxygen functional groups (hydroxyl, carboxyl, carbonyl, and epoxy groups) on the surface of the synthesized GO.

3.1.3 Zeta potential analysis

Zeta potentials study the surface charge of a particle which affects the nanomaterial agglomeration and adsorption of ions onto nano surface[128]. So the electrical mobility of the particle is defined as the ratio of the drift velocity to the magnitude of the electric field , the charged particle in a liquid acted upon by a uniform electric field, it will be accelerated until it reaches a constant drift velocity according to the formula $\mu = V_d/E$, where: V_d is the drift velocity (SI units: m/s), E is the magnitude of the applied electric field (V/m), μ is the mobility ($m^2/(V \cdot s)$)[129].

Mobility and zeta potential analyzed for synthesized NGO (1 mg/mL) by electrophoresis light scattering (ELS) method (-1.34 cm^2/V.S) and (-17.17 mV) as shown in (Fig. 3-4) and (Fig. 3-5) respectively which confirm the negative electrical

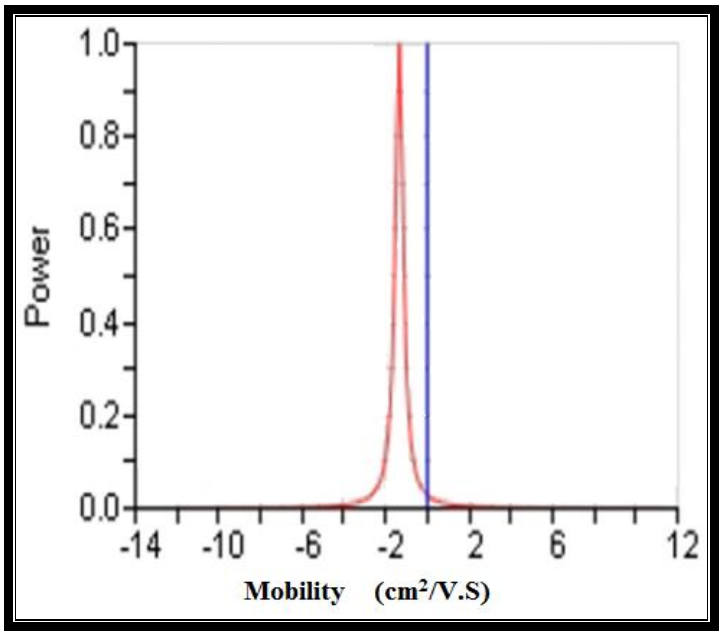

Fig. (3-4) Mobility ELS graph of NGO (1 mg/mL)

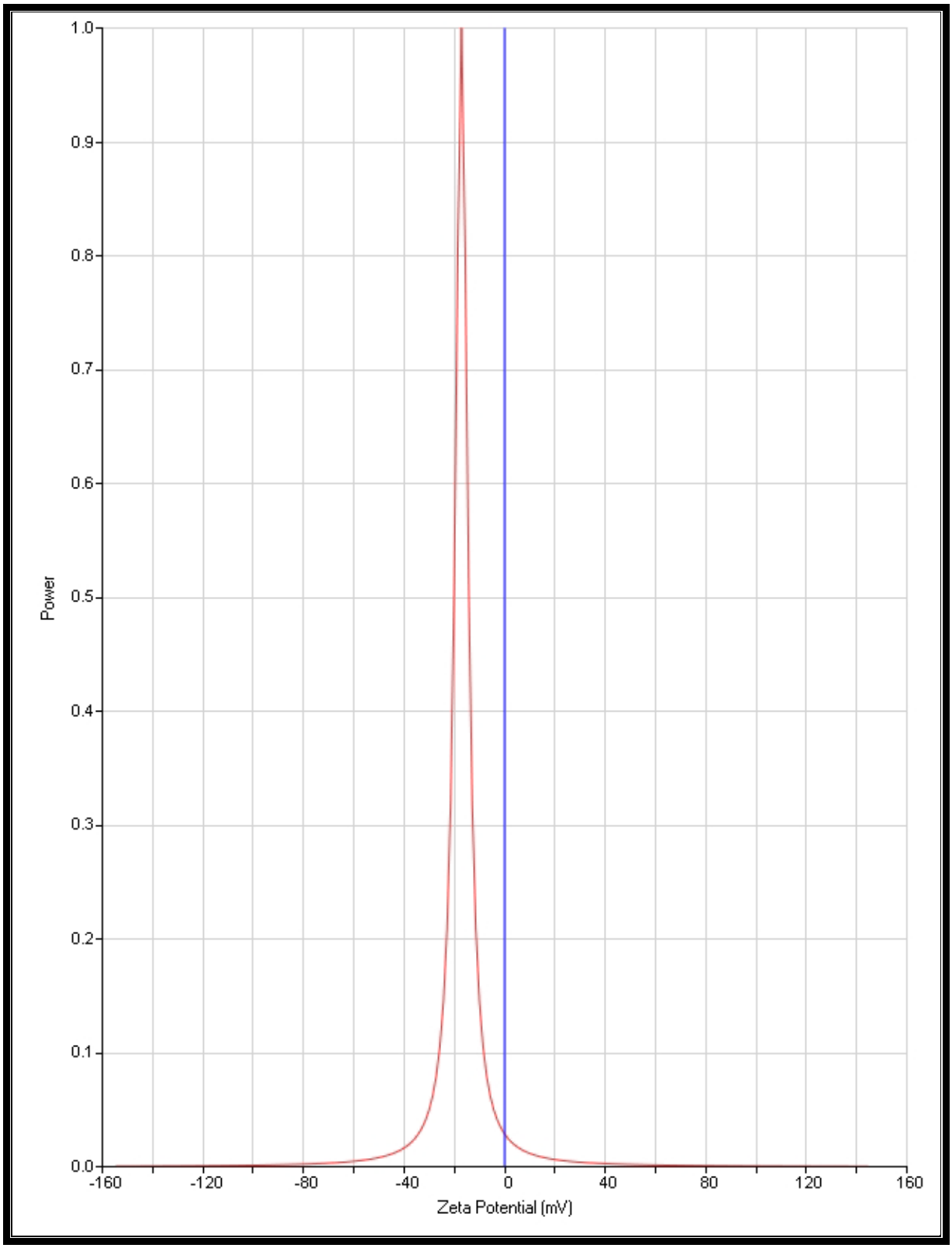

Fig. (3-5) Zeta potential ELS graph of NGO (1 mg/mL)

3.1.4 X-ray diffraction spectroscopy

The XRD spectrum measured in a range (5° - 60°) of 2θ at 0.154 nm, voltage 40 KV and current 30 mA as shown in Fig. (3-6), diffraction peaks at (2θ= 11.1297°) high intensity corresponding to interlayer spacing of (d=7.94350 A°), (2θ= 42.4972°) low intensity with interlayer spacing of (d=2.12546 A°) and (2θ= 9.1074°) low intensity with interlayer spacing of (d=9.70232 A°), The obtained results agree with the previous studies[33,130]. The XRD spectrum of graphite as shown in Fig. (3-7), 2θ = 26.7° [131], the peak disappeared by the oxidation process where a new peak appeared at a lower angle (2θ ≈11°) provided the presence of the synthesized NGO.

The crystal size of NGO calculated by Debye-Scherrer equation[132] $D = \frac{K\lambda}{\beta \cos \theta}$

where D: crystal size, K: Scherrer's constant equal 0.9 , λ: wave length of x-ray radiation source , β: full width at half maximum (FWHM) and θ :X-ray diffraction angle in radians. The average crystal size of synthesized NGO is (7.4 nm) as shown in Table (3-1).

Table (3-1) Debye- Scherrer equation values

2 theta (2θ) (degree)	FWHM (β) (degree)	Theta (θ) (radians)	β (radians)	D (nm)	$D_{average}$ (nm)
11.1297	1.23	0.097	0.0214	6.45	7.4
42.4972	0.93	0.37	0.0162	8.55	
9.1074	1.1	0.079	0.0192	7.22	

Note: rad = (π/180) * degree

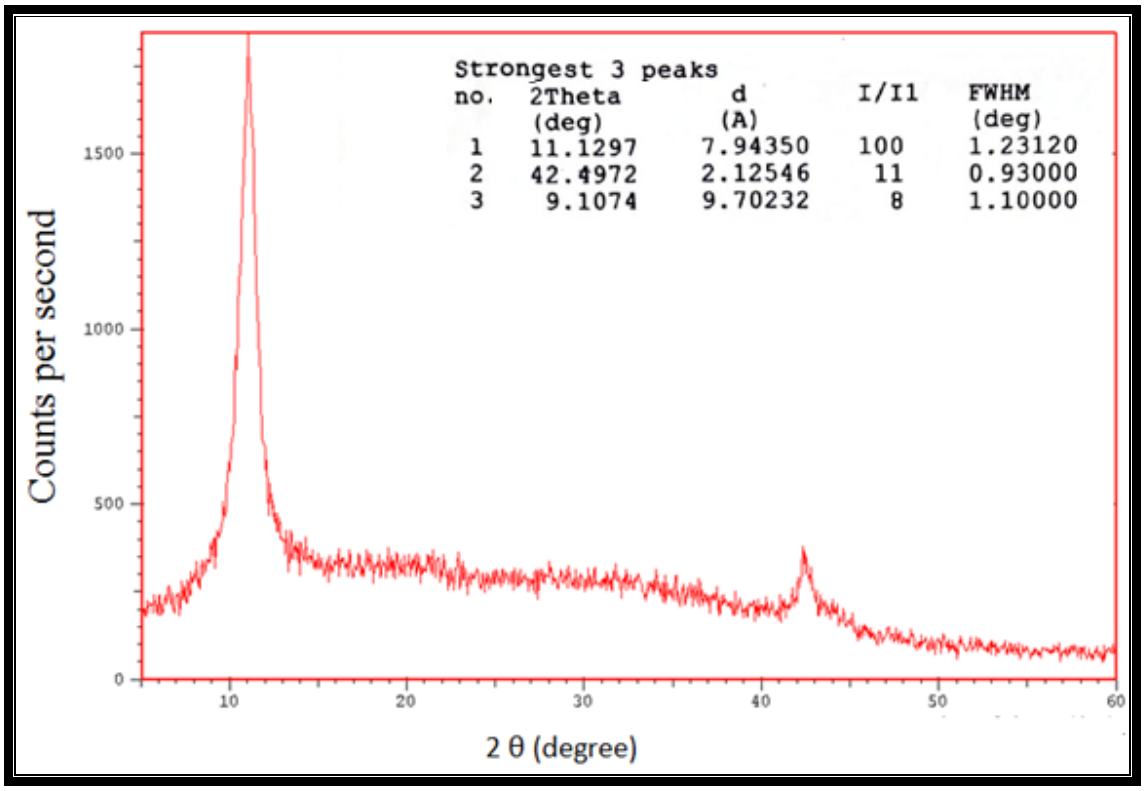

Fig. (3-6): The XRD spectrum of NGO

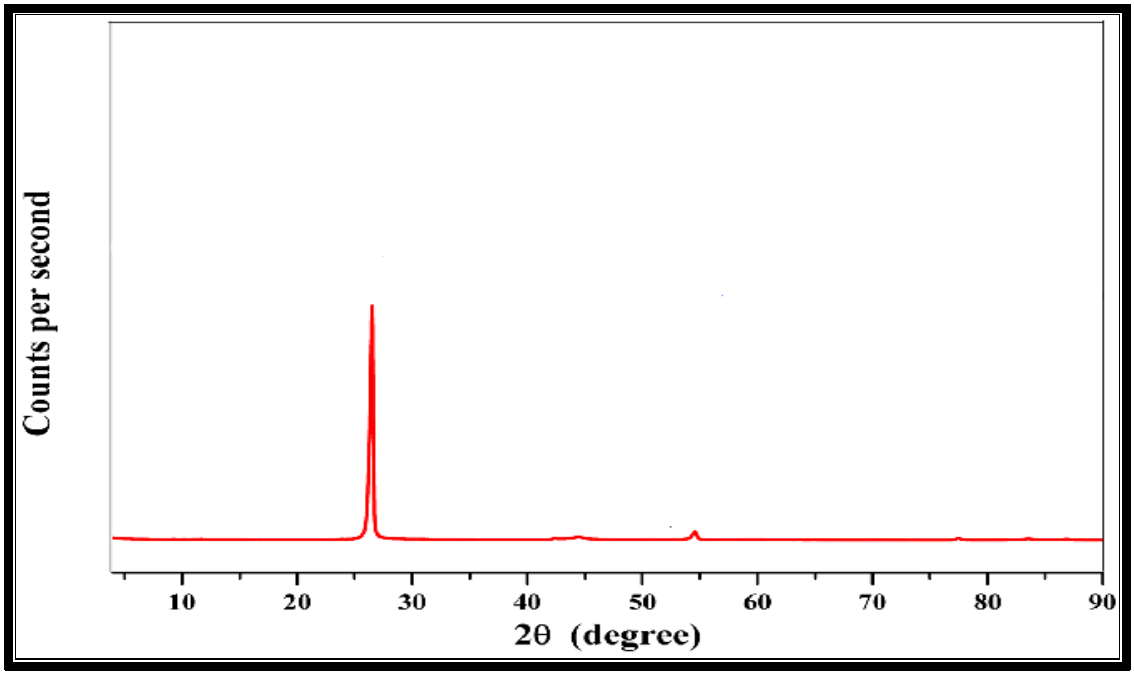

Fig. (3-7): The XRD spectrum of graphite

3.2 Morphologic characterization of nano graphene oxide

3.2.1 Transmission electron microscopy TEM

The TEM and HRTEM (high resolution TEM) images indicating intensity of electrons attenuated by NGO platelets of different thickness show a sheet like morphology with different transparencies as shown in Fig. (3-8). Dark areas indicate the thick stacking nanostructure of several graphene oxide layers with some amount of oxygen functional groups. The higher transparency areas indicate much thinner films of a few layers graphene oxide resulting from stacking nanostructure exfoliation. The obtained results agree with the previous studies[33,133].

3.2.2 Field emission scanning electron microscopy FESEM

The FESEM used to study the surface morphology of NGO as shown in Fig. (3-9) the corrugation shape observed, crystal size was (13.94 – 38.86 nm) at scale 100 nm as it was clear. Low wrinkled on NGO surface are more sensitive and show better recovery ability[134].

The energy dispersive X-ray (EDX) (attached with the FESEM), used to identify the elements involved in the NGO formation as shown in Fig. (3-10), the appearance of a peak at energy (0.18 keV) to carbon atoms, and another peak at energy (0.5 keV) to oxygen atoms, this evidence proved the presence carbon and oxygen atoms only in pure NGO synthesized. The obtained results agree well with the previous studies[135, 35].

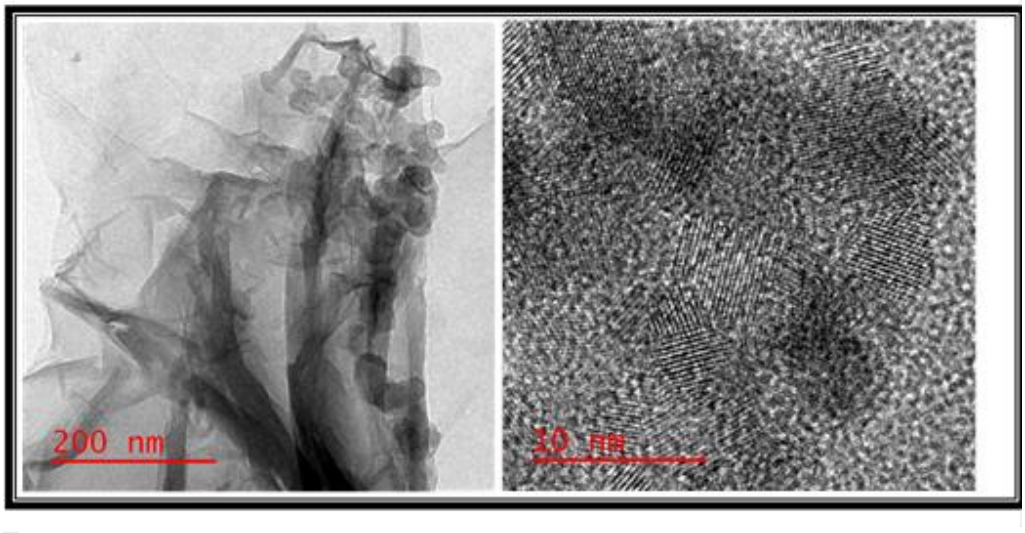

Fig. (3-8): TEM and HR-TEM images of NGO

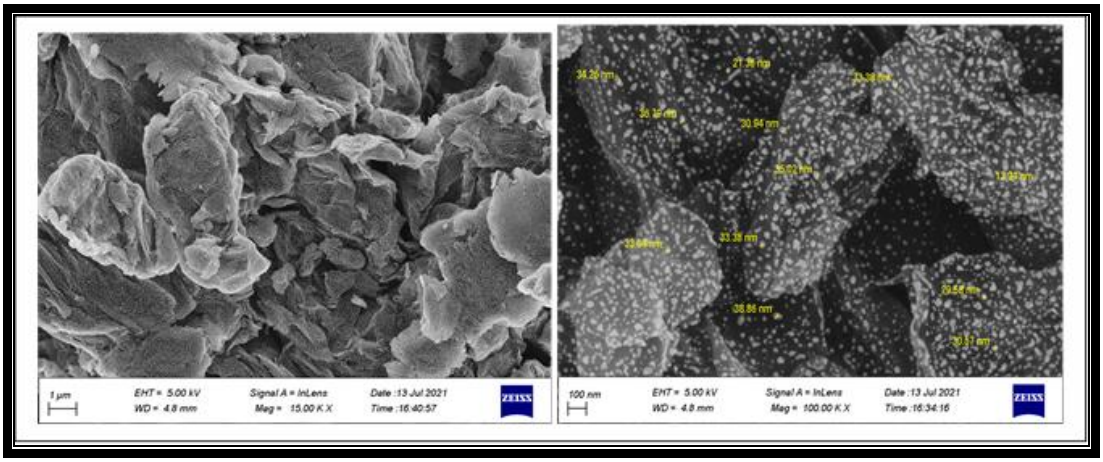

Fig. (3-9): FESEM images of NGO

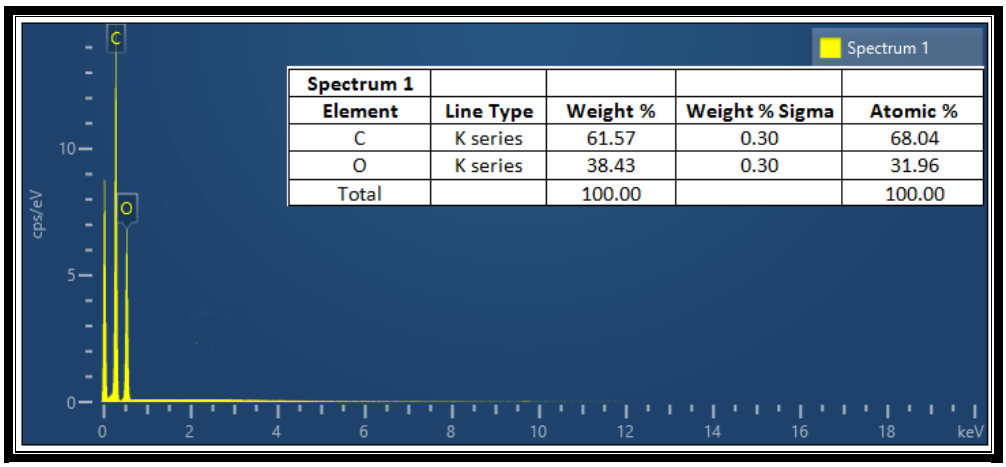

Spectrum 1				
Element	Line Type	Weight %	Weight % Sigma	Atomic %
C	K series	61.57	0.30	68.04
O	K series	38.43	0.30	31.96
Total		100.00		100.00

Fig. (3-10) EDX of NGO

3.3 Adsorption of metal ions on NGO

Wallace found that NGO sheets were highly negatively charged because of the ionization of carboxylic acid and phenolic hydroxyl groups[136]. On the basis of this information, we speculate that adsorption of analyte ions , dispersion and aggregation of NGO may also depend on the degree of the ionization of its carboxylic acid and phenolic hydroxyl groups. It is well-known that aqueous dispersions of NGO are stabilized via electrostatic repulsions which are pH dependent[137], as shown in Fig. (3-11)[138]. In this work, the adsorption process was carried out for (Mg^{+2}, Co^{+2}, Ni^{+2}, Cu^{+2}, Cd^{+2} and Pb^{+2}) ions by solid phase micro extraction (SPME) method by using nano graphene oxide, the recovery determinate for the solution with SPME method, analyzed by flame atomic absorption spectroscopy (FAAS). The recovery was evaluated by using the following equation: $R\%= [(C_{added}–C_{after})/C_{added}]*100\%$, where C_{added} the direct concentration of analytes (without NGO), and C_{after} the concentration of analytes by the SMPE method[125].

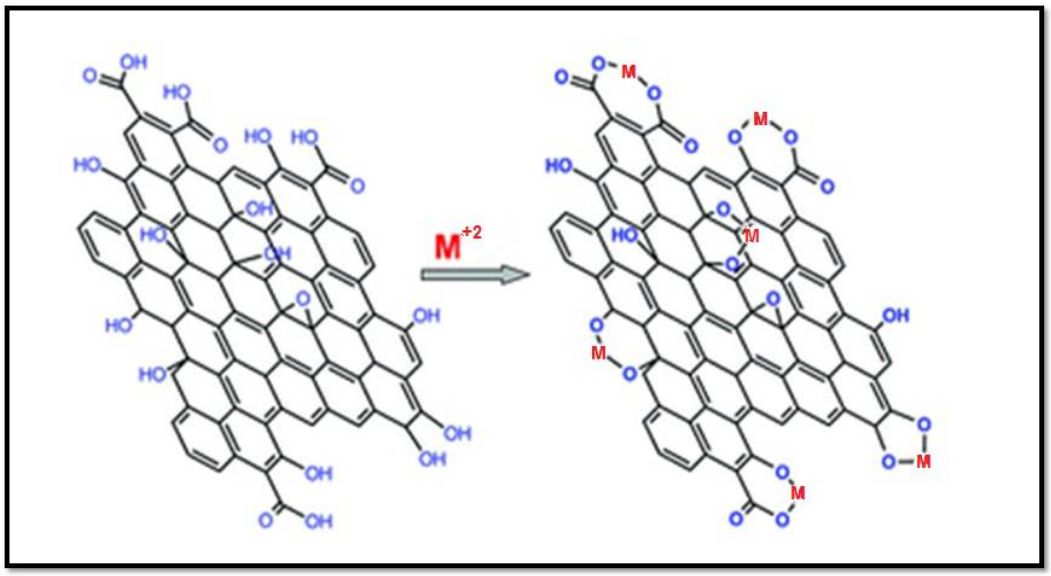

Fig. (3-11) Mechanism of metal ions adsorption on nano sheets of graphene oxide surface

3.3.1 Optimum conditions of SPME method

3.3.1.1 Effect of pH

The pH of the standard solution (1 μg/mL) of each analyte were arranged from (2-8). The effect of pH on the recovery percentage, The pH > 8 was not taken under consideration because of the risk of the precipitation of metal hydroxide. The presence of hydroxyl and carboxyl groups in NGO can enhance the retention of analyte ions to be pre-concentrated process of analyte ions. These functional groups are responsible for increasing cation exchange capacity because of the electrostatic attraction between the cations and the negative charge on NGO surface as well as the oxygen atoms in functional groups donate single pair of electrons to metal ions[139]. The relationship between recovery percentage values and the pH as shown in Table (3-2) and Fig. (3-12), the optimum pH = 5.5, 6.0, 6.5, 7.0, 7.5 and 8.0 for (Ni, Mg, Cd, Co, Cu and Pb) for each analyte ion respectively.

Table (3-2) Effect of pH on the recovery% of metal ions

pH	Recovery %					
	Mg	Co	Ni	Cu	Cd	Pb
2.0	6.8	9.9	10.4	2.4	1.2	0.8
4.0	58.9	47.9	52.7	8.9	35.7	9.8
4.5	60.7	51.2	70.4	38.6	41.2	24.7
5.0	73.6	61.3	76.3	43.4	56.6	30.2
5.5	79.5	69.9	81.7	48.3	77.7	39.4
6.0	83.6	77.5	78.0	47.5	80.4	37.8
6.5	81.7	80.2	77.6	61.6	82.7	63.3
7.0	80.4	84.7	79.2	68.8	81.1	79.9
7.5	78.9	83.4	80.2	71.6	78.9	82.2
8.0	79.3	83.7	80.9	70.0	79.7	84.1

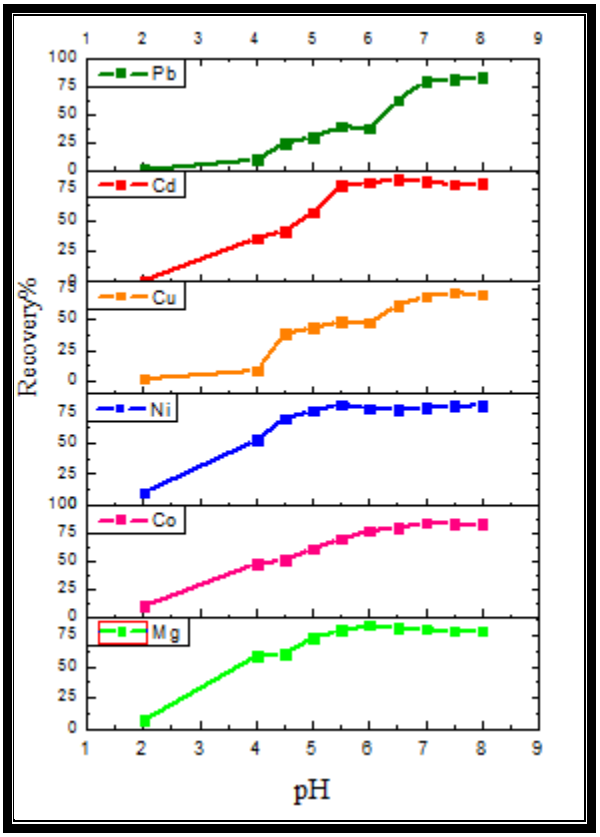

Fig. (3-12) Effect of pH on the recovery% of analyte ions

3.3.1.2 Effect of NGO mass

The recovery of analyte ions (1µg/mL) at the optimum pH for each analyte ion, increased 0.25-1.0 mg as shown in the Table (3-3) and Fig. (3-13). The obtained recovery percentage 0.5 mg explained the availability of more sorption sites on NGO surface[125].

Table (3-3) Effect of the NGO mass on the recovery% of metal ions

Mass of NGO (mg)	Recovery %					
	Mg	Co	Ni	Cu	Cd	Pb
0.25	33.7	49.4	39.6	32.9	48.8	40.3
0.50	78.7	82.9	80.5	65.9	79.4	81.6
0.75	79.1	83.3	80.9	67.1	79.9	82.1
1.00	79.0	83.1	80.7	66.5	79.7	82.3

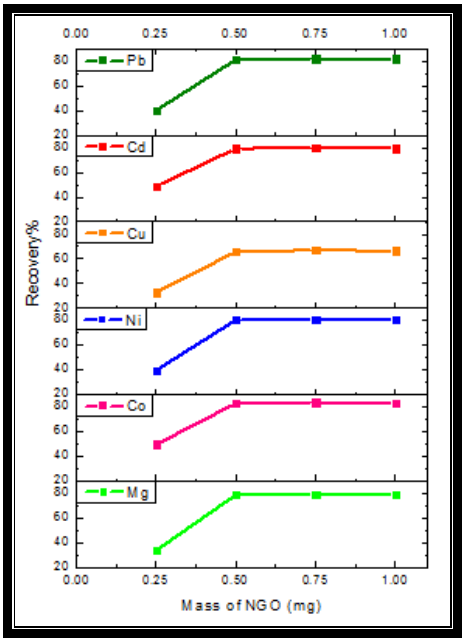

Fig. (3-13) Effect of the mass of NGO on the recovery% of metal ions

3.3.1.3 Effect of sample volume

The effect of the sample volume of each analyte (1µg/mL) on the recovery percentage was investigated by the analysis samples of volumes in the range (5, 10, 20, 25 and 50 mL), 0.5 mg of GO, at the optimum pH for each analyte ion. The results show the recovery percentage of the analyte ions remained constant within 20 – 50 mL of the sample volumes, but at less than 20 mL the recovery percentage of metal ions decreased under optimum conditions because the adsorption capacity is depended on the sample volume[133] as shown in Table (3-4) and Fig.(3-14). The chosen sample volume was 20 mL .

Table (3-4) Effect of the sample volume on the recovery% of metal ions

Sample volume (mL)	Recovery %					
	Mg	Co	Ni	Cu	Cd	Pb
5	27.9	18.8	23.2	21.9	26.5	39.4
10	36.9	30.8	38.7	38.3	37.3	52.8
20	79.7	81.1	80.9	67.7	79.6	82.7
25	80.3	80.4	81.2	67.5	79.0	83.2
50	78.7	82.9	80.5	65.9	79.4	81.6

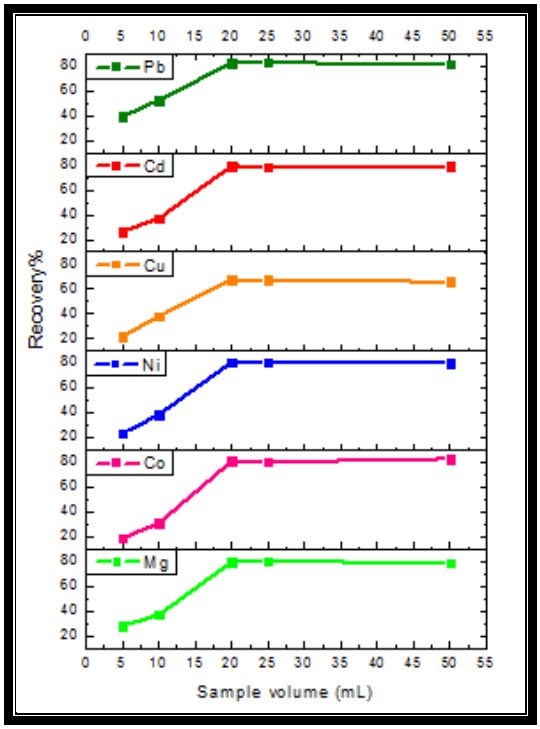

Fig. (3-14) Effect of the sample volume on the recovery% of metal ions

3.3.1.4 Effect of sonication time

The sonication time (0-10 min.) for the recovery percentage of analyte ions according to the optimum factors above remained constant in the range of (2-10 min), while the recovery percentage of the metal ions without sonicated was lower than 2 min. because the solution is not dispersed (accumulated) and therefore there is incomplete adsorption process on the surface of NGO as shown in Table (3-5) and Fig. (3-15). The chosen sonicated time was 2 min.

Table (3-5) Effect of the sonicated time on the recovery% of metal ions

Sonicated time (min)	Recovery %					
	Mg	Co	Ni	Cu	Cd	Pb
0	57.8	37.9	53.1	38.6	46.8	50.8
2	80.9	81.8	81.5	71.2	81.0	83.8
4	81.0	81.2	81.1	70.6	80.3	83.4
6	80.5	80.7	80.9	69.8	80.7	83.0
8	80.7	81.0	80.9	70.9	80.9	83.7
10	80.9	81.1	81.2	68.9	80.5	83.2

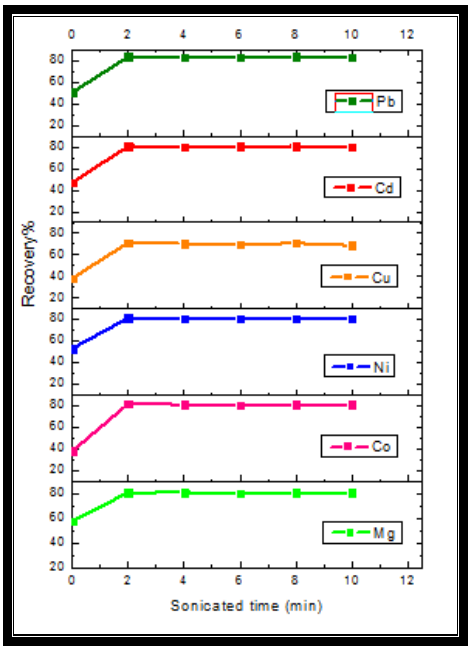

Fig.(3-15) Effect of the sonicated time on the recovery% of metal ions

3.3.1.5 Effect of stirring time

The stirring time (5-120 min) does not play a significant role in the pre-concentration of analyte ions (1µg/mL) in SPME method at the optimum pH for each analyte ion, NGO 0.5 mg and sample volume 20 mL as shown in Table (3-6) and Fig. (3-16). The results shows the adsorption process is very quick because the equilibrium reached fast, and the sorption site the available metal ions rapidly. Consequently, the sorption time 5 min was chosen .

Table (3-6) Effect of the stirring time on the recovery% of metal ions

Stirring time (min)	Recovery %					
	Mg	Co	Ni	Cu	Cd	Pb
5	80.4	81.2	80.4	68.4	79.5	83.4
15	80.9	80.7	80.9	68.0	79.1	83.0
30	79.2	80.1	80.5	67.8	80.2	83.3
60	79.6	79.8	80.6	68.2	79.6	83.1
90	80.1	81.0	80.9	67.9	80.4	83.0
120	80.8	79.5	81.3	67.5	80.2	83.6

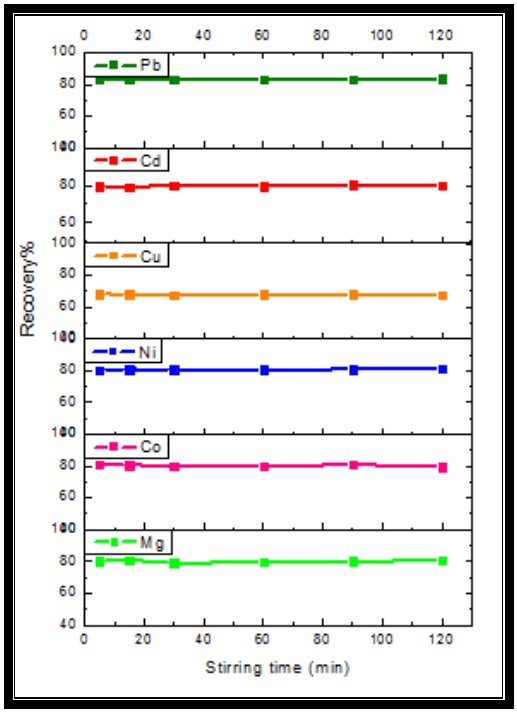

Fig. (3-16) Effect of the stirring time on the recovery of metal ions

3.3.1.6 Effect of temperature

A series of experiments was performed at the optimum factors above at (20°C - 70°C), the recovery percentage of metal ions did not change remarkably with a change of the temperature, but at 70°C the recovery percentage is decreased because of the weak electrostatic forces between the metal ions and the surface charge of the NGO at high temperatures[129] as shown in Table (3-7) and Fig. (3-17). The chosen temperature was room temperature.

Table (3-7) Effect of the temperature on the recovery% of metal ions

Temp. °C	Recovery %					
	Mg	Co	Ni	Cu	Cd	Pb
20	81.0	81.7	80.6	68.6	80.8	83.4
30	80.4	81.4	80.3	68.2	80.5	83.1
40	80.7	81.0	80.9	68.0	80.7	83.3
50	80.3	81.3	80.2	68.1	80.8	83.6
60	79.3	80.4	79.2	67.4	79.2	83.0
70	70.9	74.8	69.6	60.2	70.5	72.1

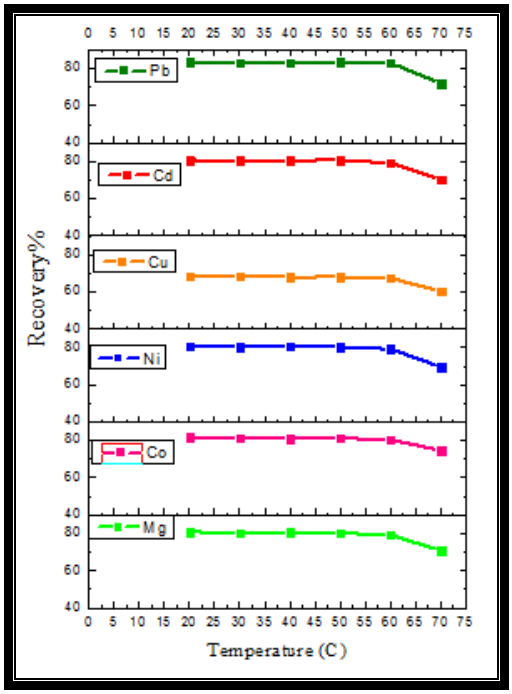

Fig. (3-17) Effect of the temperature on the recovery% of metal ions

3.3.1.7 Effect of NaCl concentration

The effect of NaCl concentration on adsorption efficiency was investigated using (1 μg/mL^{-1}) of metal ions under optimized experimental conditions. Adsorption efficiency dramatically increased with NaCl concentration increased (2 - 6.5 mg mL^{-1}) and decreased at higher concentrations of NaCl (7 - 8 mg mL^{-1}) as shown in Table (3-8) and Fig.(3-18). Lower NaCl concentration resulted inefficient NGO aggregation and low efficiency of adsorption of analyte whereas higher NaCl concentrations resulted in significant elution of analyte from NGO because of competition between positive sodium ions and analyte ions[80]. Concentration of NaCl (6.5 mg mL^{-1}) was selected for all determined elements.

Table (3-8) Effect of NaCl concentration on the recovery% of metal ions

NaCl mg/mL	Recovery %					
	Mg	Co	Ni	Cu	Cd	Pb
2	68.6	62.8	60.3	52.3	64.9	65.2
4	75.8	68.6	71.4	60.1	75.8	72.9
6	84.7	84.4	81.7	71.2	82.2	84.6
6.5	85.1	85.1	82.2	71.9	83.3	84.9
7	82.1	80.2	78.0	69.3	80.3	82.4
8	79.4	77.6	76.0	66.8	78.5	78.9

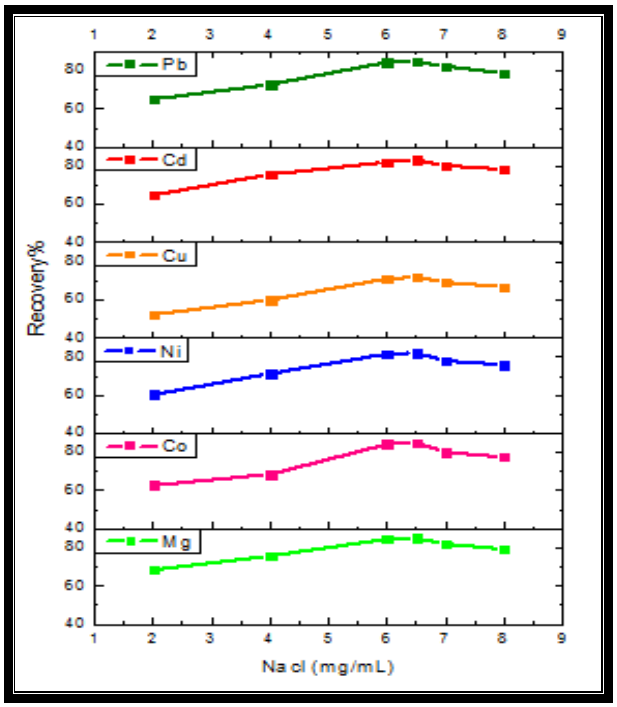

Fig. (3-18) Effect of NaCl concentration on the recovery% of metal ions

3.3.1.8 Effect of interfering ions

The interfering ions may affect the adsorption efficiencies of analytes because of the competitive adsorption between the interfering ions and analyte ions. The recovery of the determined analyte ions Mg(II), Co(II), Ni(II), Cu(II), Cd(II) and Pb(II) (1 µg/mL) was studied in the solutions containing interfering metal ions such as Cr(III), Mn(IV), As(III), Sn(II) at (0.2-1.0 µg mL^{-1}), Fe(II), Fe(III), Zn(II), Li(I) at (1-5 µg mL^{-1}), K(I), Ca(II) at (10-50 µg mL^{-1}) and Ba(II)

at (20-80 µg mL^{-1}). With tolerance limits defined as the largest concentrations of ions resulting in less than ±5% of recovery values by comparing the recovery value before and after adding the interfering ions[125] as shown in table (3-9) and figures from (3-19) to (3-30).

Table (3-9) The tolerance limit of interfering ions with the analytes

Interfering ion \ Analyte	Mg	Co	Ni	Cu	Cd	Pb
Cr(III) (µg/mL)	0.8	0.8	0.4	0.8	0.6	0.8
Mn(IV) (µg/mL)	1	0.8	0.4	0.8	0.4	1
Fe(II) (µg/mL)	5	3	4	5	5	5
Fe(III) (µg/mL)	3	2	3	4	3	4
Zn(II) (µg/mL)	5	4	2	4	1	3
As(III) (µg/mL)	0.8	0.4	0.4	1	0.4	0.6
Sn(II) (µg/mL)	0.8	0.8	0.4	0.8	0.6	0.6
Li(I) (µg/mL)	1	4	3	3	2	4
K(I) (µg/mL)	10	40	20	40	40	40
Ca(II) (µg/mL)	10	30	35	26	15	30
Ba(II) (µg/mL)	40	80	80	80	80	80

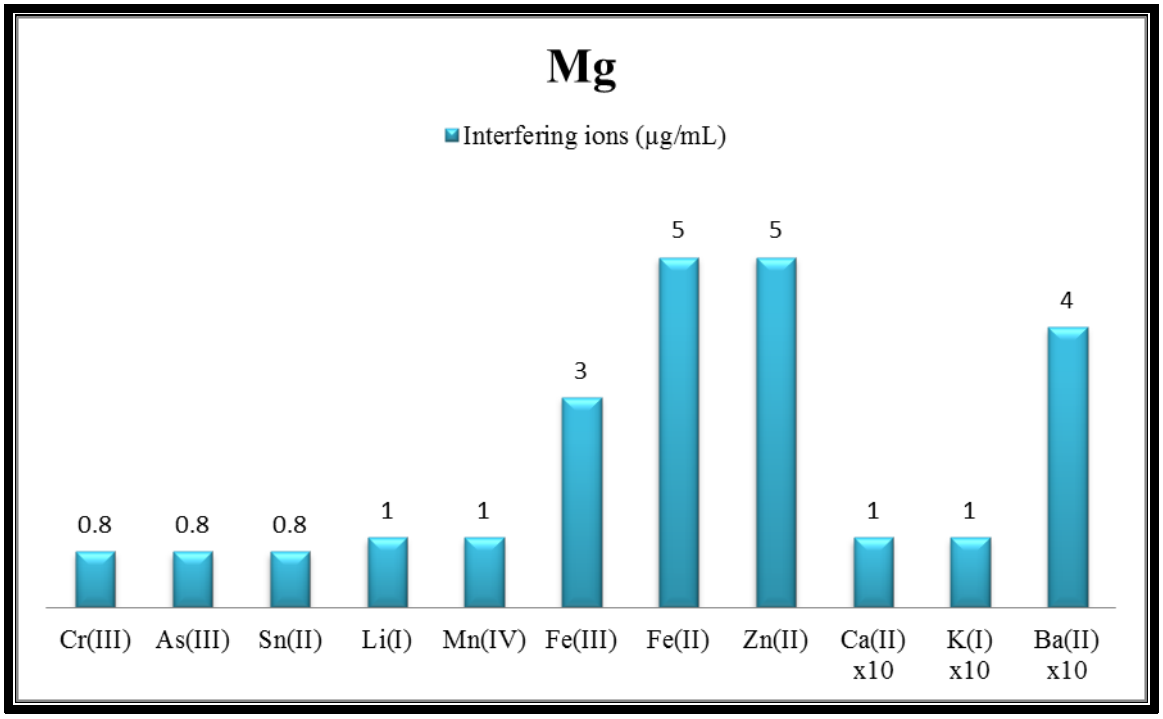

Fig. (3-19) Tolerance limit of interfering ions with Magnesium

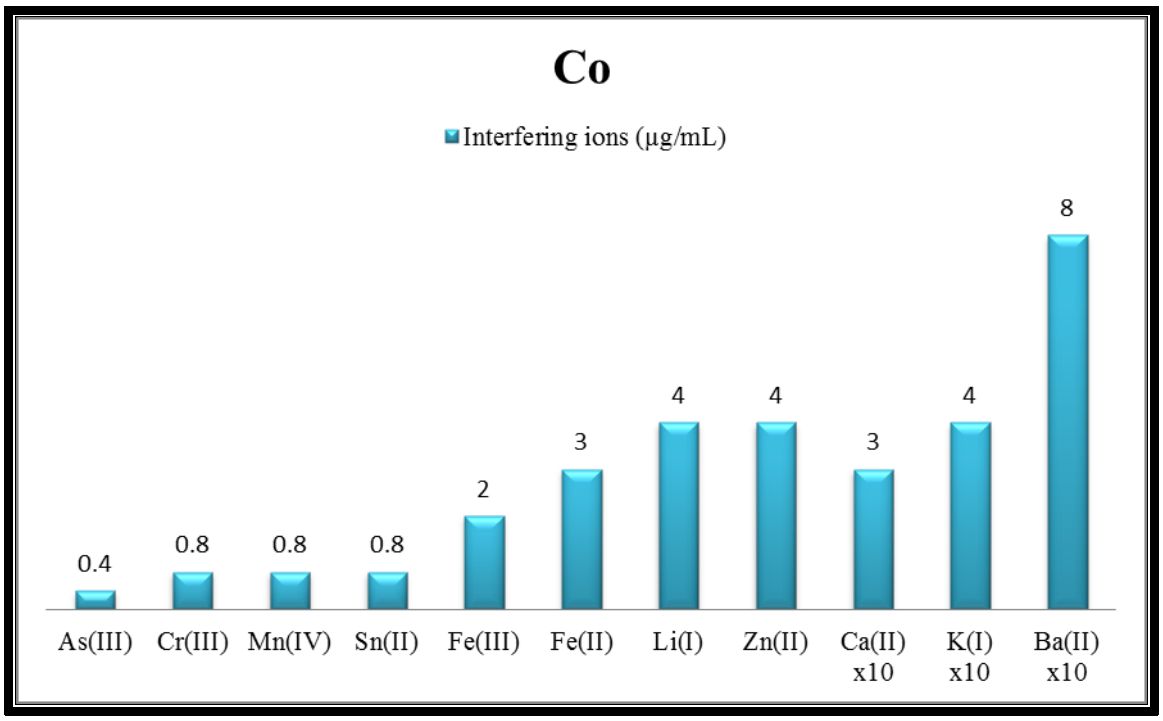

Fig. (3-20) Tolerance limit of interfering ions with Cobalt

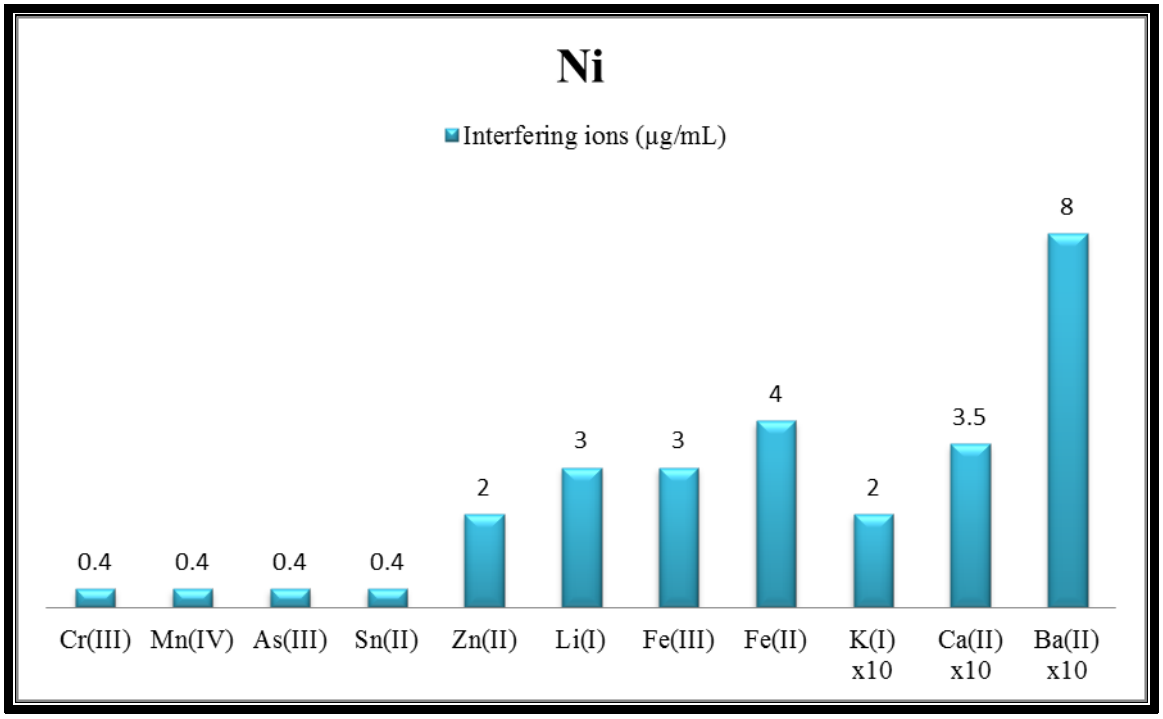

Fig. (3-21) Tolerance limit of interfering ions with Nickel

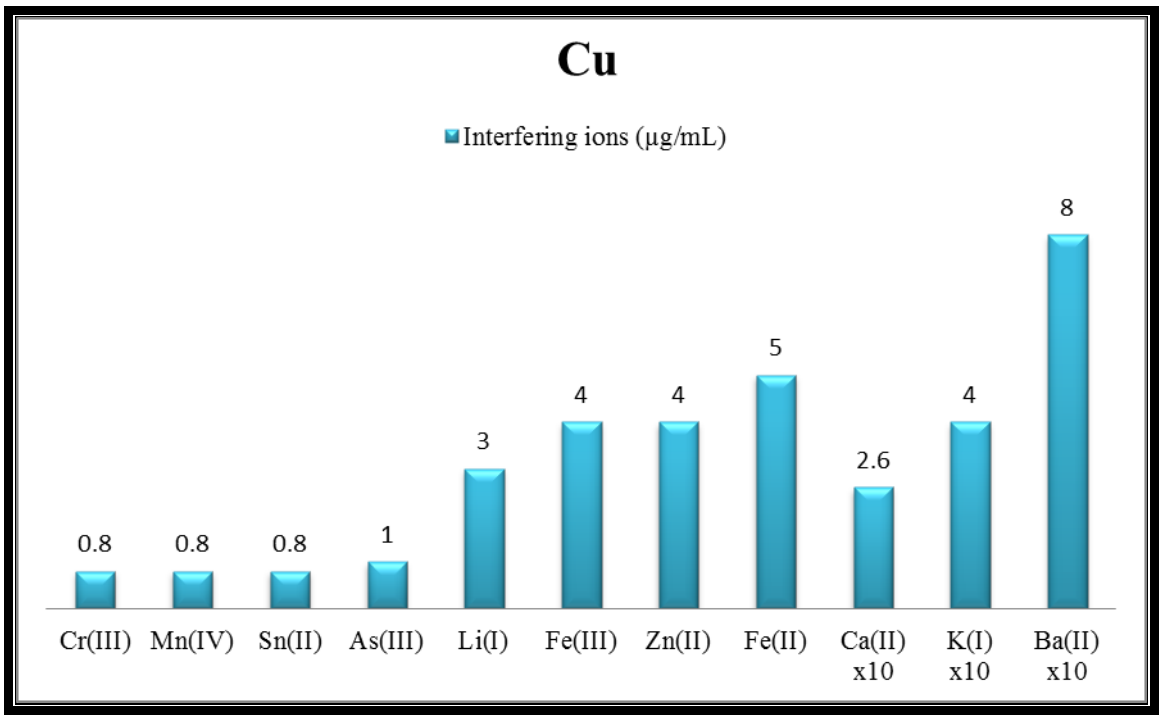

Fig. (3-22) Tolerance limit of interfering ions with Copper

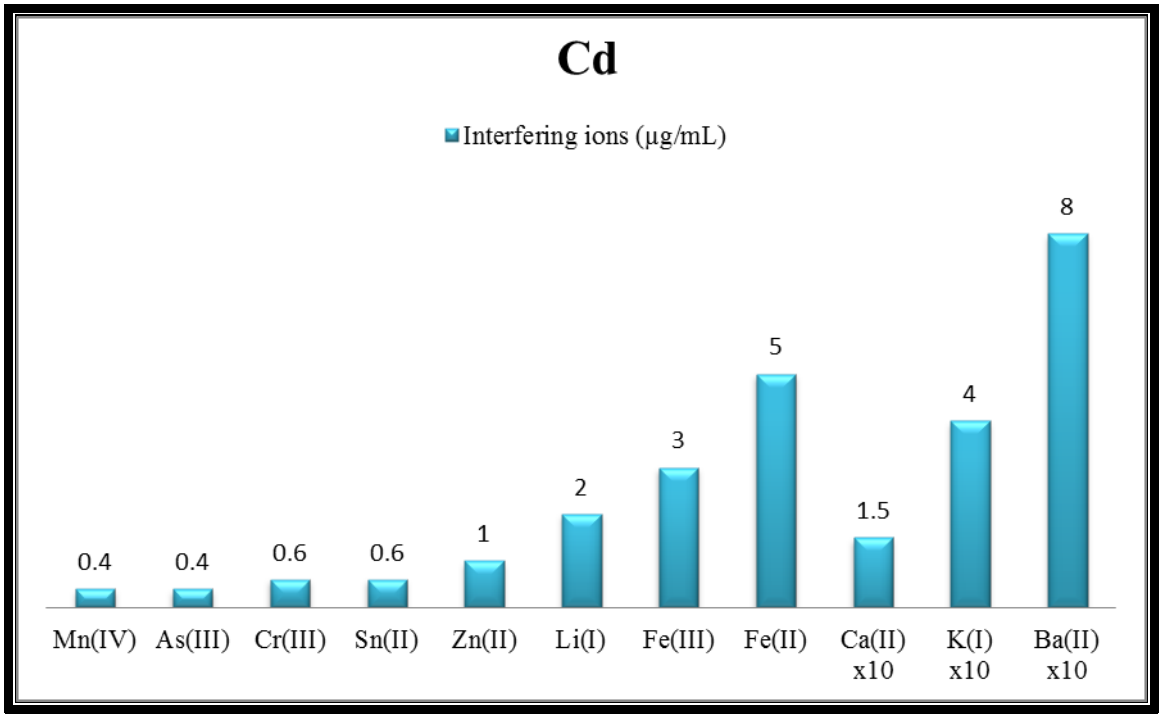

Fig. (3-23) Tolerance limit of interfering ions with Cadmium

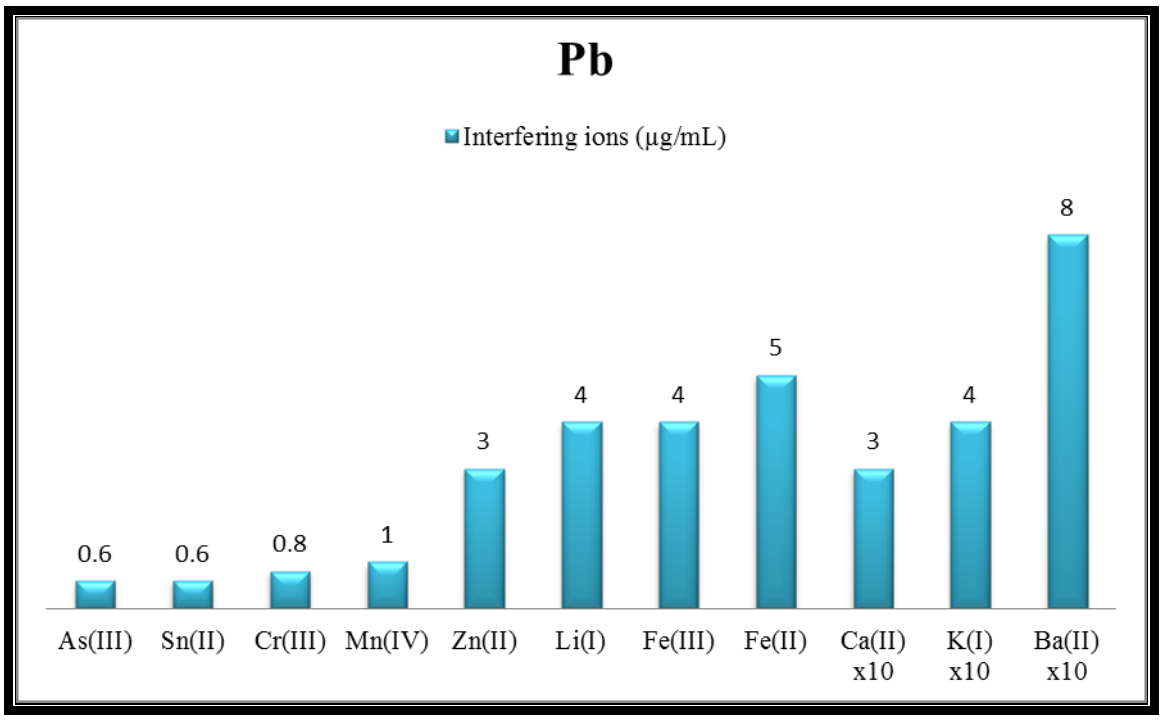

Fig. (3-24) Tolerance limit of interfering ions with Lead

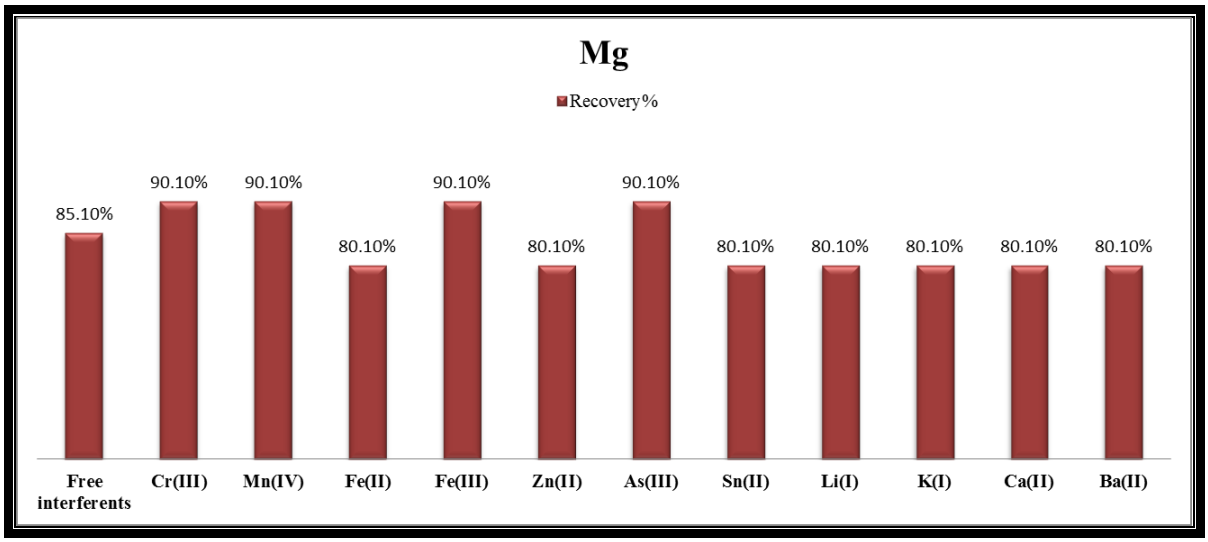

Fig. (3-25) Magnesium recovery% with tolerance limit of interfering ions

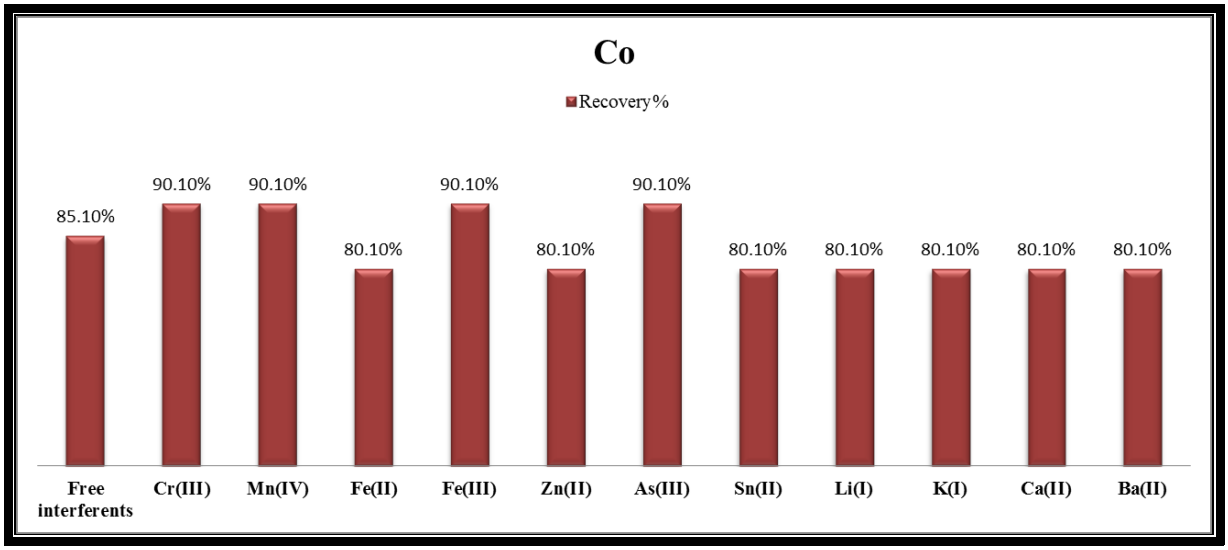

Fig. (3-26) Cobalt recovery% with tolerance limit of interfering ions

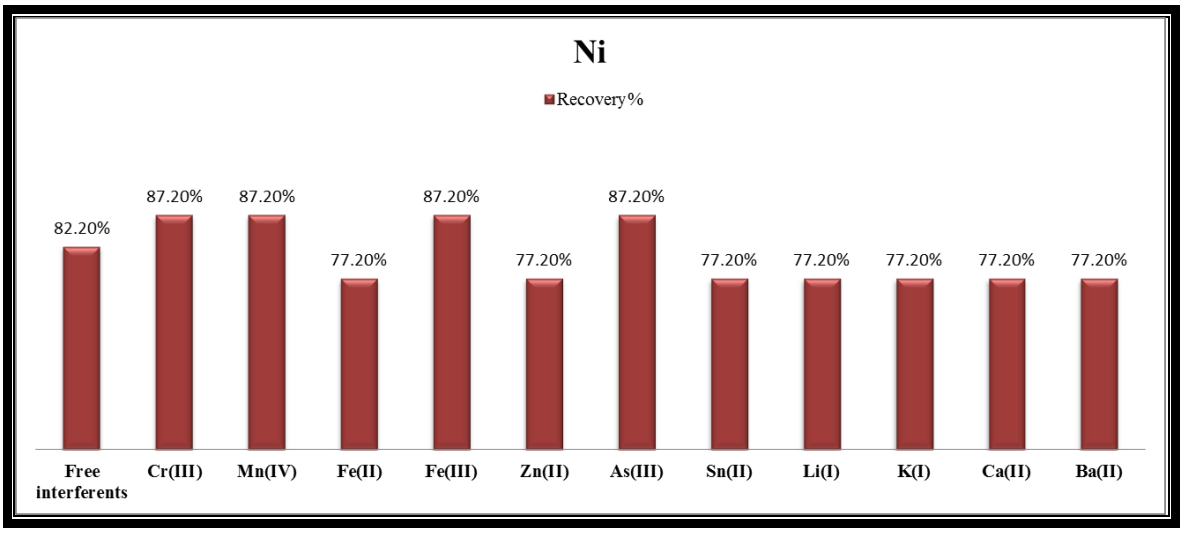

Fig. (3-27) Nickel recovery% with tolerance limit of interfering ions

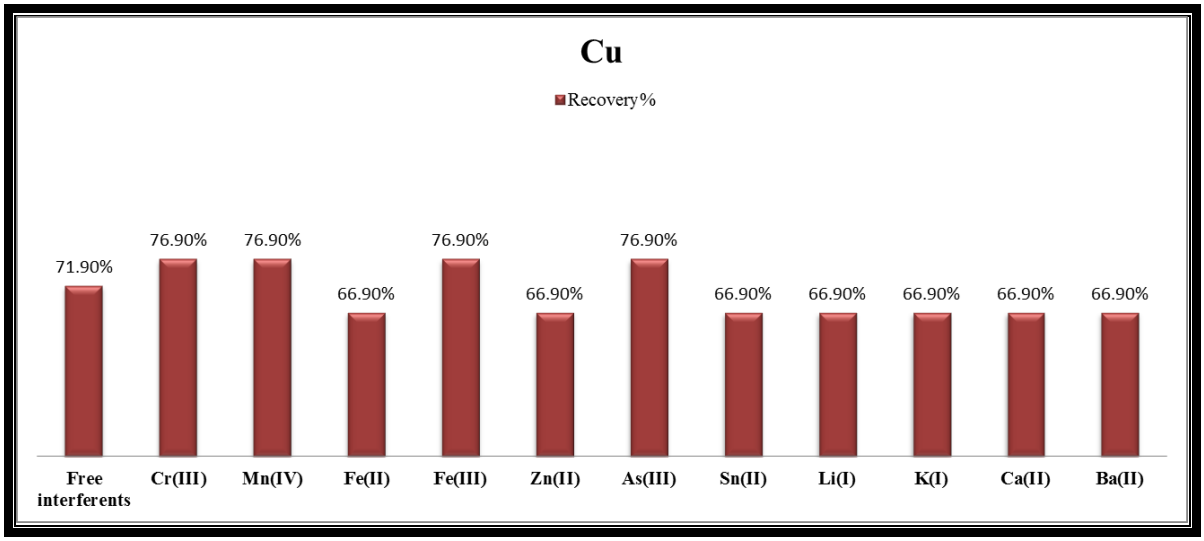

Fig. (3-28) Copper recovery% with tolerance limit of interfering ions

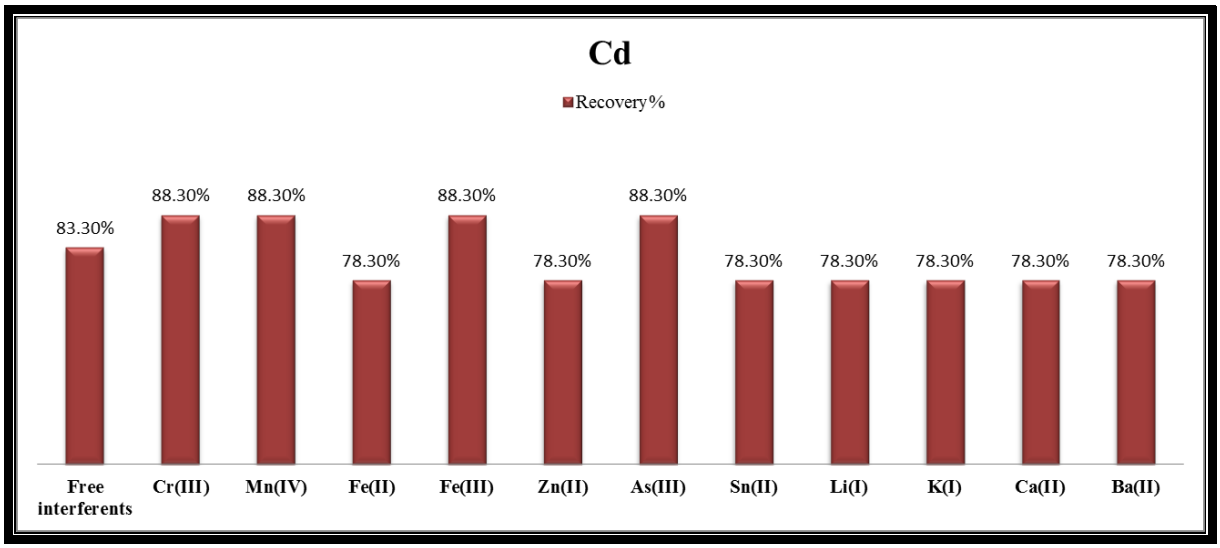

Fig. (3-29) Cadmium recovery% with tolerance limit of interfering ions

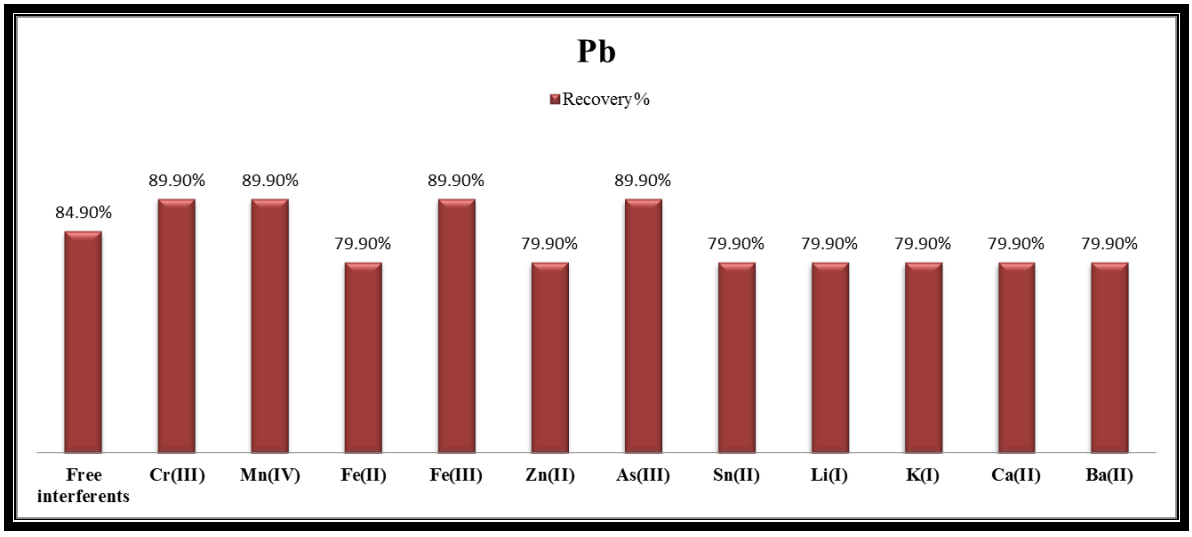

Fig. (3-30) Lead recovery% with tolerance limit of interfering ions

The tolerance limit of interfering ions (Cr^{+2}, As^{+3}, Sn^{+2}, Li^{+}, Mn^{+4}, Fe^{+3}, Fe^{+2}, Zn^{+2}, K^{+}, Ca^{+2} and Ba^{+2}) with magnesium analyte in the following concentrations are (0.8, 0.8, 0.8, 1, 1, 3, 5, 5, 10, 10 and 40 µg/mL)

respectively. The tolerance limit of interfering ions (As^{+3}, Cr^{+2}, Mn^{+4},Sn^{+2}, Fe^{+3}, Fe^{+2}, Li^{+}, Zn^{+2}, Ca^{+2}, K^{+} and Ba^{+2}) with cobalt analyte in the following concentrations are (0.4, 0.8, 0.8, 0.8, 2, 3, 4, 4, 30, 40 and 80 µg/mL) respectively. The tolerance limit of interfering ions (Cr^{+2}, Mn^{+4}, As^{+3}, Sn^{+2}, Zn^{+2},Li^{+}, Fe^{+3}, Fe^{+2}, K^{+}, Ca^{+2} and Ba^{+2}) with nickel analyte in the following concentrations are (0.4, 0.4, 0.4, 0.4, 2, 3, 3, 4, 2, 35 and 80q µg/mL) respectively. The tolerance limit of interfering ions (Cr^{+2}, Mn^{+4}, Sn^{+2}, As^{+3}, Li^{+}, Fe^{+3}, Zn^{+2}, Fe^{+2}, Ca^{+2}, K^{+} and Ba^{+2}) with copper analyte in the following concentrations are (0.8, 0.8, 0.8, 1, 3, 4, 4, 5, 26, 40 and 80 µg/mL) respectively. The tolerance limit of interfering ions (Mn^{+4}, As^{+3}, Cr^{+2}, Sn^{+2}, Zn^{+2}, Li^{+}, Fe^{+3}, Fe^{+2}, Ca^{+2}, K^{+} and Ba^{+2}) with cadmium analyte in the following concentrations are (0.4, 0.4, 0.6, 0.6, 1, 2, 3, 5, 15, 40 and 80 µg/mL) respectively. The tolerance limit of interfering ions (As^{+3}, Sn^{+2}, Cr^{+2}, Mn^{+4}, Zn^{+2},Li^{+}, Fe^{+3}, Fe^{+2}, Ca^{+2}, K^{+} and Ba^{+2}) with lead analyte in the following concentrations are (0.6,0.6, 0.8, 1, 3, 4, 4, 5, 30, 40 and 80 µg/mL) respectively.

According to the results above, in the presence of the interfering ions in higher concentration than the tolerance limit affects the recovery% and adsorption efficiency, may be the recovery decreased or in other studied cases, although NGO can be utilized by competing metal ions, the sorption capabilities of NGO towards the determined elements expressed as recovery can remain high. Magnesium, cobalt, nickel, copper, cadmium and lead recoveries% increased in the presence of the matrix ions (Cr^{+3}, Mn^{+4}, Fe^{+3} and As^{+3}) with tolerance limit due to the high positive charge of this interfering ions, the sorbent sites of NGO activated, but the recoveries% decreased in presence the matrix ions (Fe^{+2}, Zn^{+2}, Sn^{+2}, Li^{+}, K^{+}, Ca^{+2} and Ba^{+2}) with tolerance limit due to high competing with analytes because them have similar properties in attraction electrostatic with NGO.

3.3.2 Adsorption capacity

The adsorption capacity (q) of analytes calculated using the following equation, $q\ (\mu g/mg) = \frac{(C_\circ - C)V}{W}$ Where q is the amount of analyte adsorbed per unit weight of NGO, C_o and C are the analyte concentrations related to initial and residual respectively, V is the volume of sample and W is weight of NGO[133]. Adsorption capacity of Mg, Co, Ni, Cu, Cd and Pb (1µg/mL) calculated at optimum conditions of SPME method as shown in Table (3-10) and Fig. (3-31).

Table(3-10) Adsorption capacity of analytes (1µg/mL) on NGO surface

Analyte	Recovery %	Adsorption capacity (µg/mg)
Mg	85.1	34.04
Co	85.1	34.04
Ni	82.2	32.88
Cu	71.9	28.76
Cd	83.3	33.32
Pb	84.9	33.96

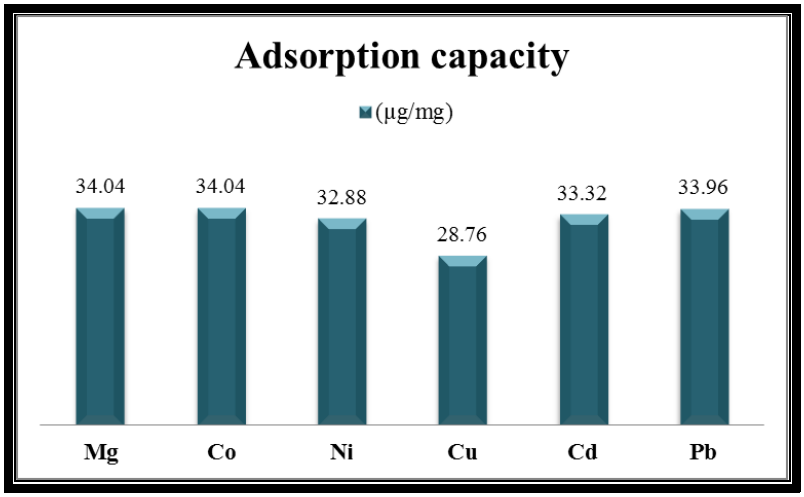

Fig. (3-31) Adsorption capacity of analytes (1µg/mL) on NGO surface

3.4 Determination of metal ions and recovery in the samples by SPME method

The analyte ions (Mg, Co, Ni, Cu, Cd and Pb) in the samples determined by flame atomic absorption spectroscopy (FAAS) according to the manual instructions of (Aurora AI 1200) for each analyte with the limit of detection (LOD) is the lowest concentration level that can be determined to be statistically different from an analyte blank, gives a signal that is above the background signal by three times the standard deviation of the background signal as in equation $LOD = 3.3 * \frac{S}{Slope}$,where the slope of calibration curve of the analyte, Standard deviation (S) in statistics, the standard deviation is a measure of the variation or dispersion amount of a set of values as in equation $S = \sqrt{\frac{\sum(xi-\bar{x})^2}{n-1}}$ where, xi, absorbance values of standard solution at same concentration, $\bar{x}$, average of absorbance values, n: number of absorbance values[140], as shown in Table (3-11). The standard calibration curves of the analyte ions as shown in Figures from (3-32) to (3-37).

Table (3-11) The analytical conditions for determination of metal ions

Ser.	Metal	Wave length (nm)	Slit width (nm)	Current of HCLamp (mA)	Flame type	LOD (µg/mL)
1	Mg	285.2	0.2	5	Air / Acetylene (99.99%)	0.001
2	Co	240.7	0.2	7	Air / Acetylene (99.99%)	0.022
3	Ni	232	0.2	7	Air / Acetylene (99.99%)	0.02
4	Cu	324.7	0.2	6	Air / Acetylene (99.99%)	0.015
5	Cd	288.8	0.2	5	Air / Acetylene (99.99%)	0.005
6	Pb	217	0.2	5	Air / Acetylene (99.99%)	0.053

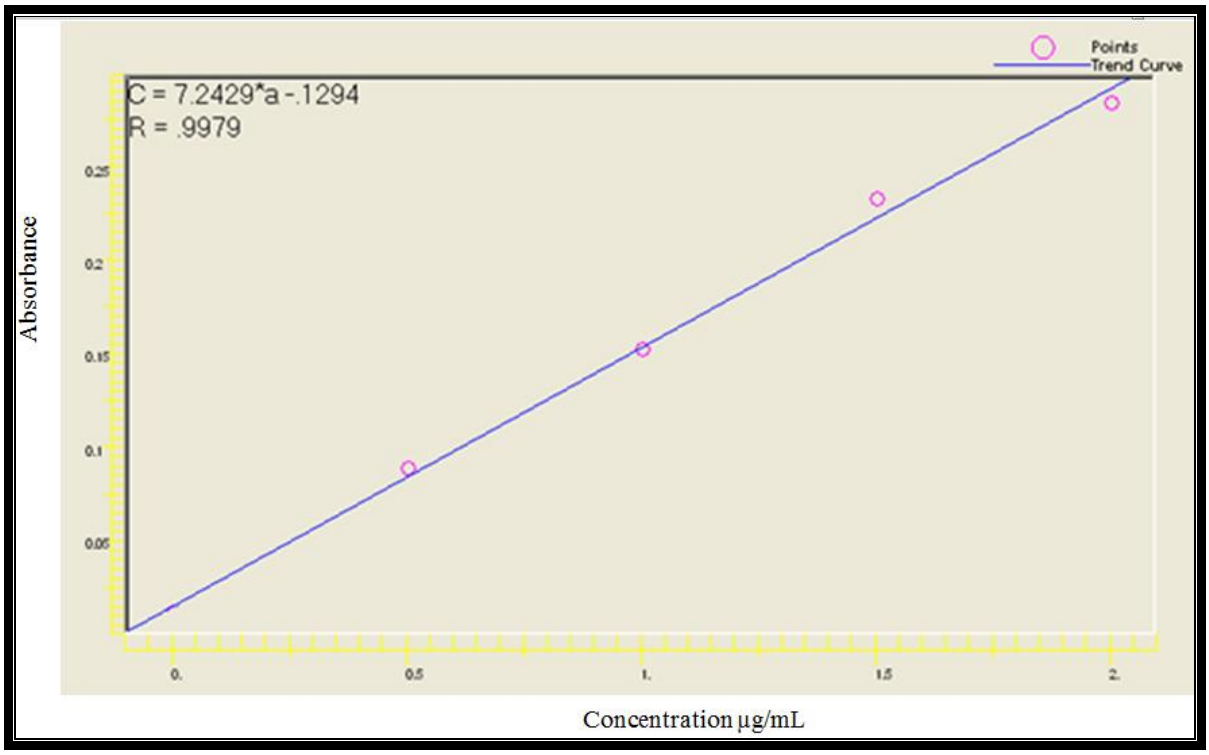

Fig. (3-32) Calibration curve of Magnesium

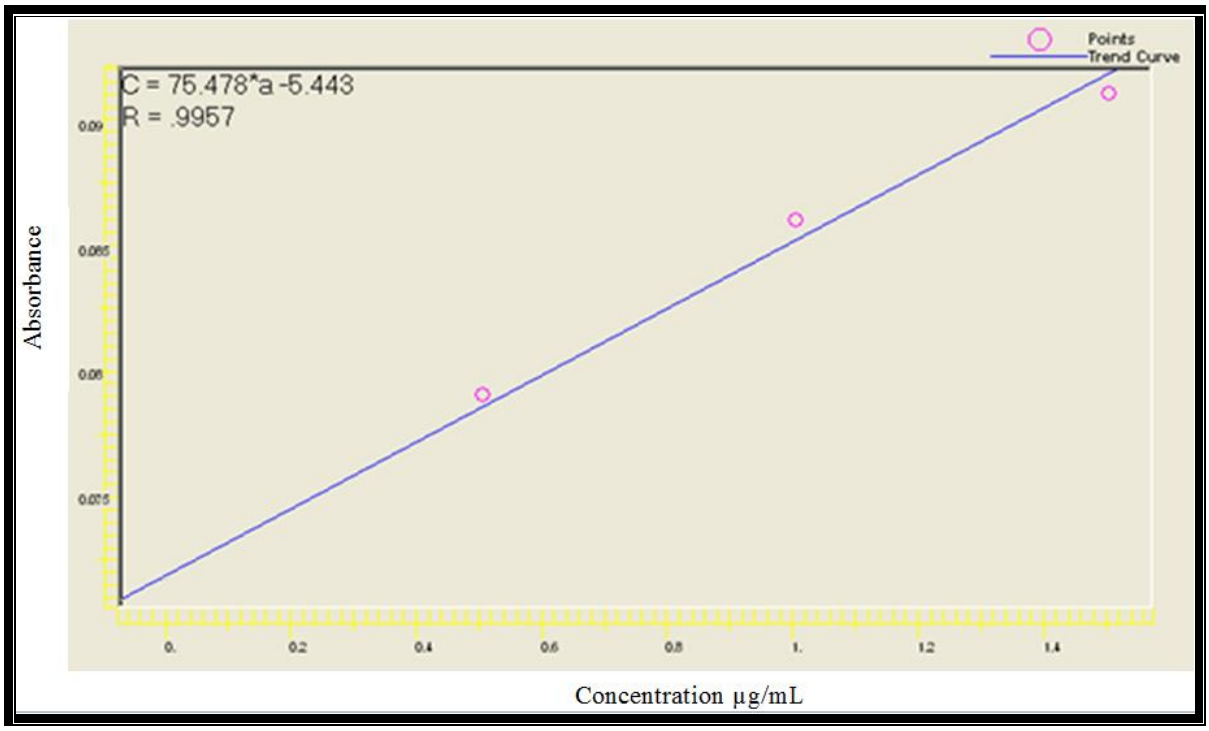

Fig. (3-33) Calibration curve of Cobalt

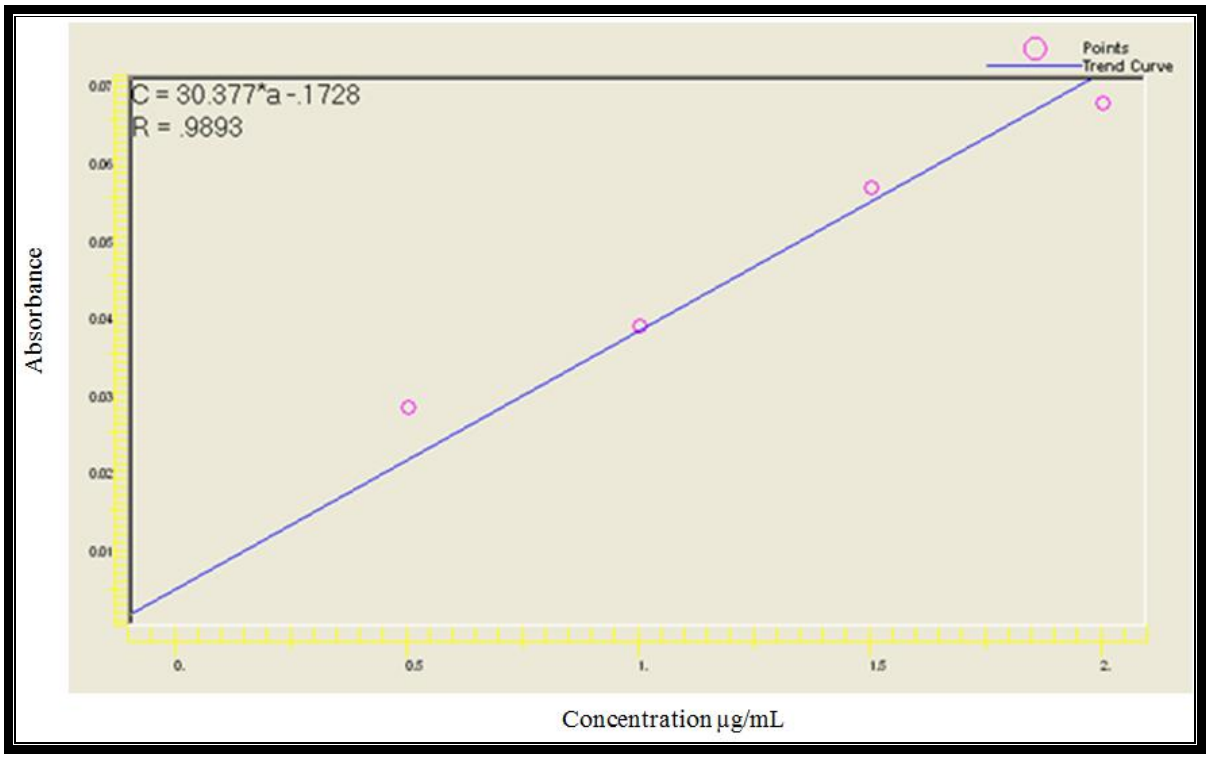

Fig. (3-34) Calibration curve of Nickel

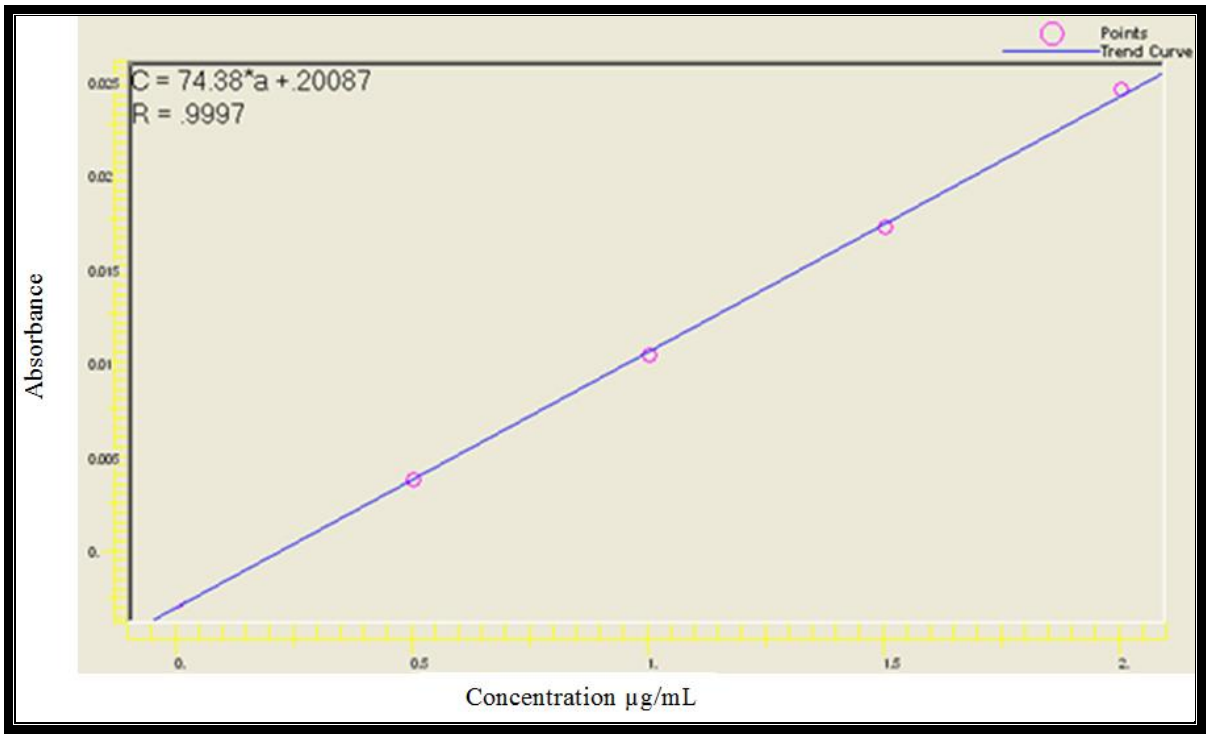

Fig. (3-35) Calibration curve of Copper

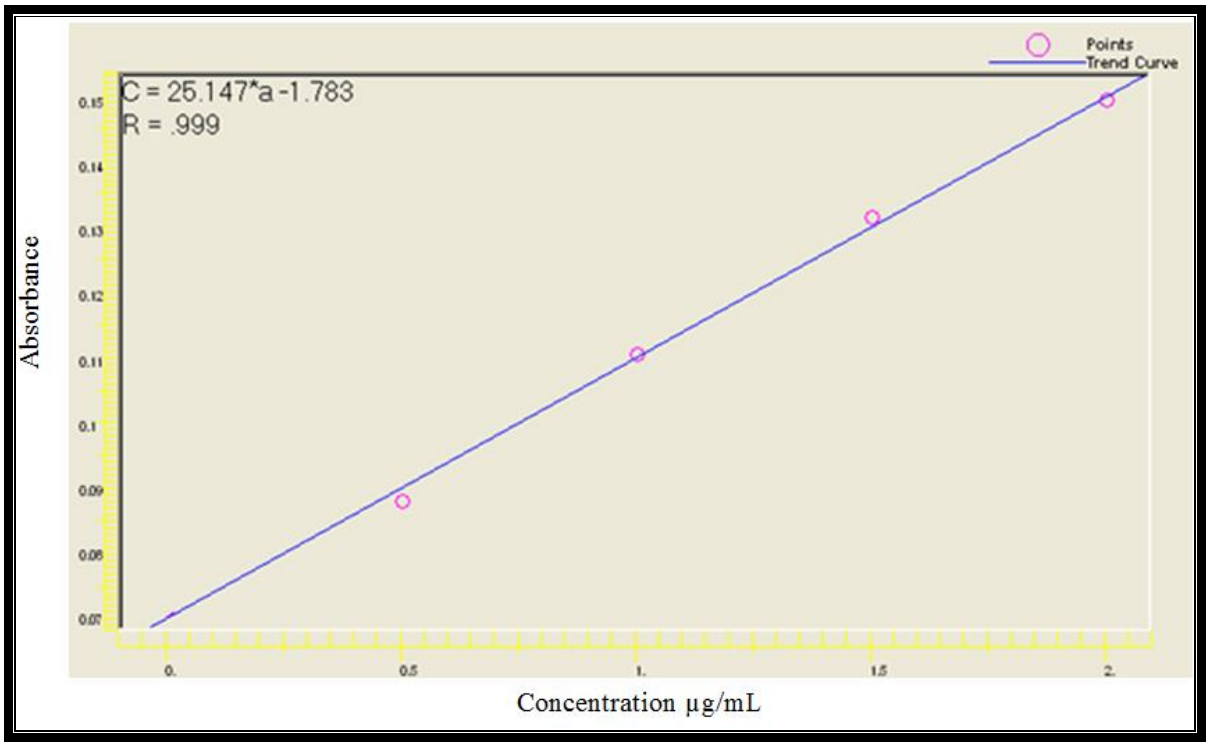

Fig. (3-36) Calibration curve of Cadmium

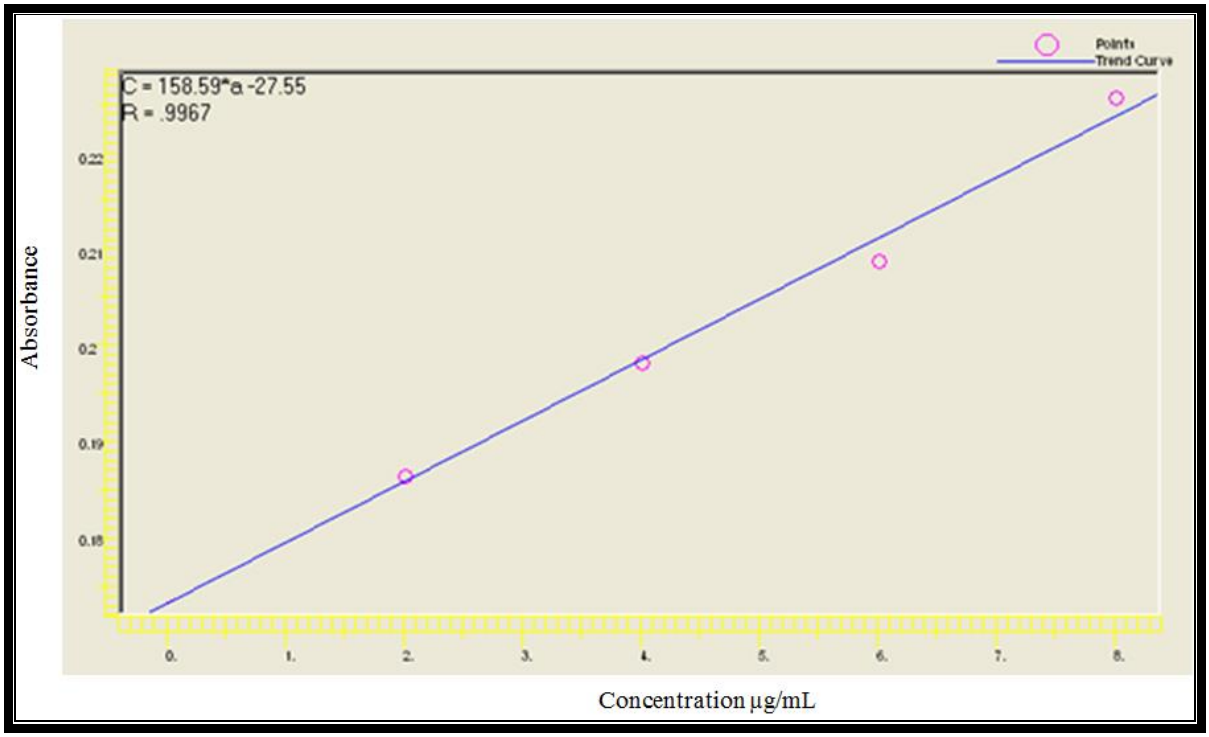

Fig. (3-37) Calibration curve of Lead

3.4.1 Determination of metal ions and recovery in cutting rock samples by SPME method

The analytes determined directly (without NGO), with SPME method (with NGO) according to the optimum conditions, five samples were collected from each oil field as shown in Table (3-12) , Figures from (3-38) to (3-49).

Table (3-12) The concentration of analytes by direct, SPME methods and recovery in cutting rock samples

Oil field	Analyte																	
	Mg			Co			Ni			Cu			Cd			Pb		
	µg/mL		Recovery %	µg/mL		Recovery %	µg/mL		Recovery %	µg/mL		Recovery %	µg/mL		Recovery %	µg/mL		Recovery %
	Direct method	SPME method		Direct method	SPME method		Direct method	SPME method		Direct method	SPME method		Direct method	SPME method		Direct method	SPME method	
Halfayah (n=5)	9.342	1.944	79.2	1.307	0.222	83	4.292	0.73	83	0.621	0.16	74.2	0.419	0.011	97.4	3.095	0.557	82
Noor (n=5)	9.649	2.093	78.3	1.371	0.239	82.6	4.464	0.785	82.4	1.31	0.369	71.8	0.522	0.035	93.3	31.33	8.205	73.8
Amarah (n=5)	10.545	2.364	77.6	1.38	0.254	81.6	7.113	1.48	79.2	0.51	0.134	73.7	0.548	0.058	89.4	2.508	0.434	82.7
North Buzurgan (n=5)	9.859	2.169	78	1.271	0.238	81.3	6.727	1.298	80.7	0.46	0.101	78.3	0.636	0.081	87.3	4.38	0.71	83.8
South Buzurgan (n=5)	9.205	1.842	80	1.262	0.245	80.6	5.636	1.037	81.6	0.181	0.047	73.7	0.71	0.091	87.2	5.166	0.858	83.4

* Note: n= 5 (number of samples)

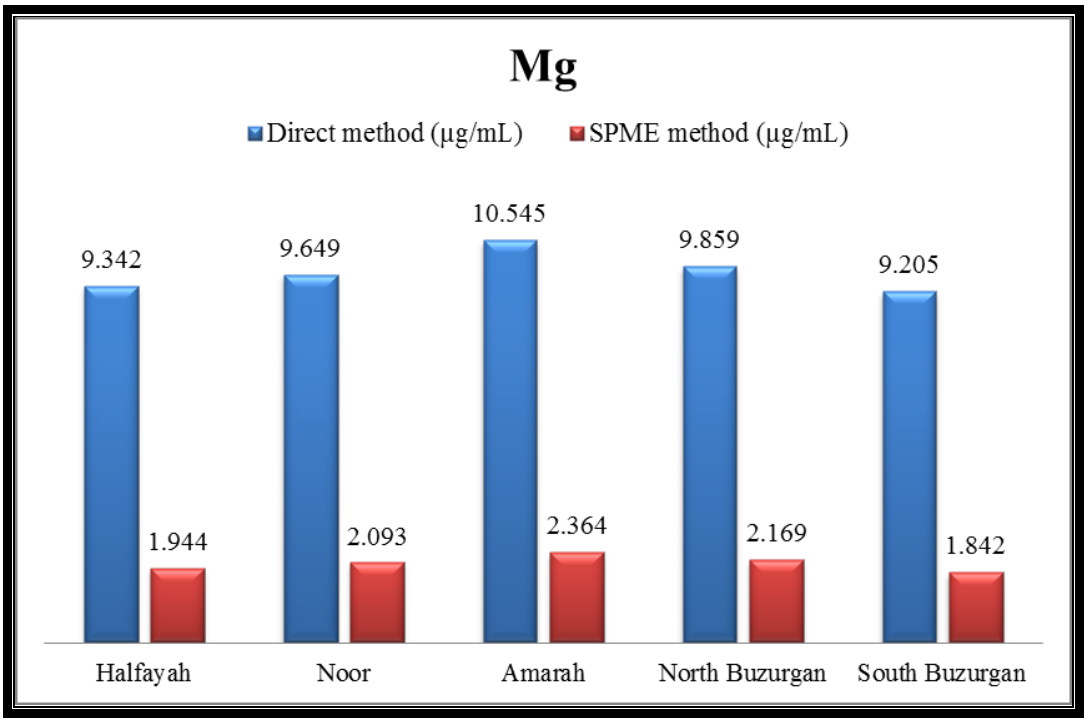

Fig. (3-38) Magnesium concentration (µg/mL) by direct, SPME methods for cutting rock samples in oil fields

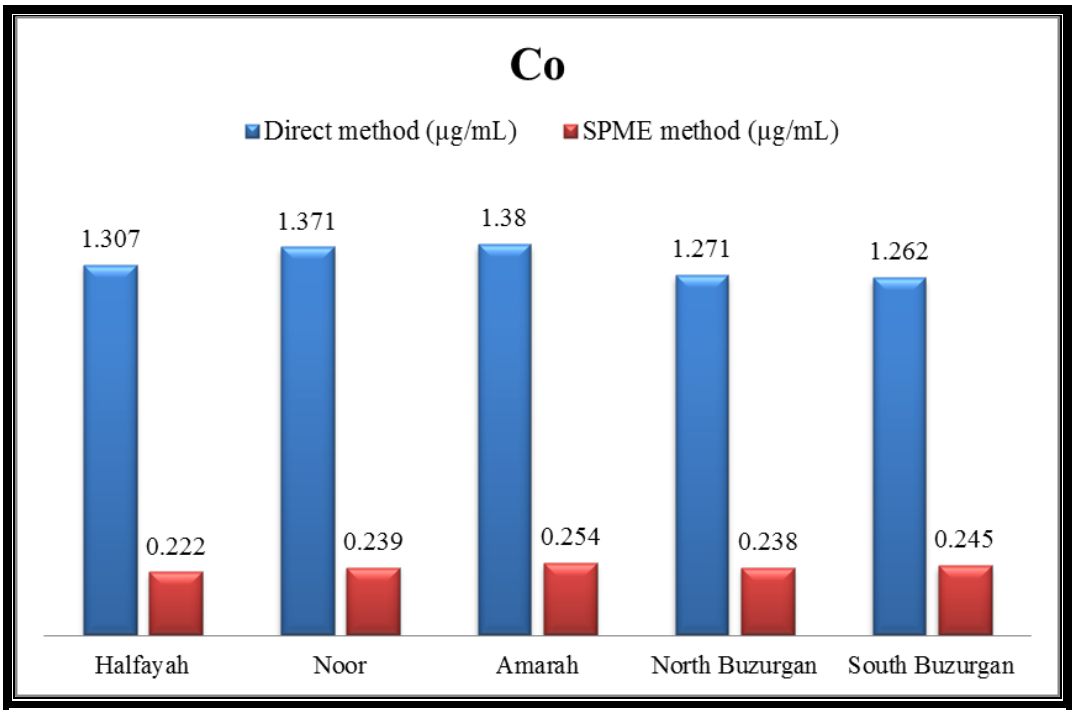

Fig. (3-39) Cobalt concentration (µg/mL) by direct, SPME methods for cutting rock samples in oil fields

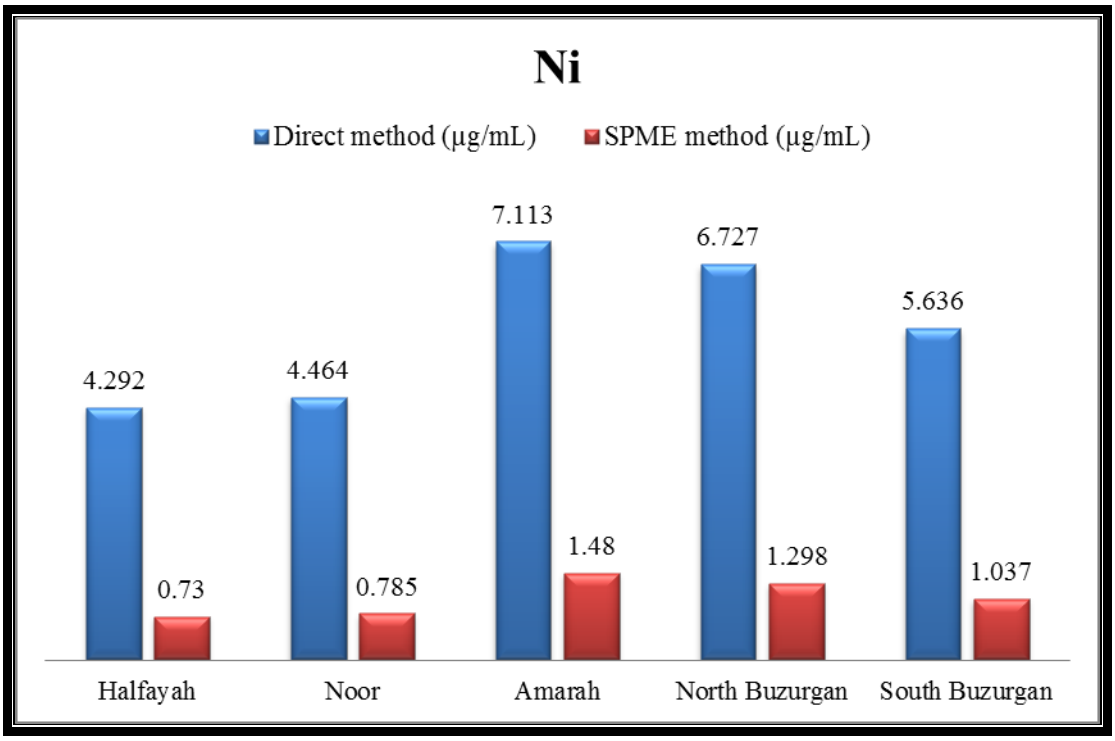

Fig. (3-40) Nickel concentration (µg/mL) by direct, SPME methods for cutting rock samples in oil fields

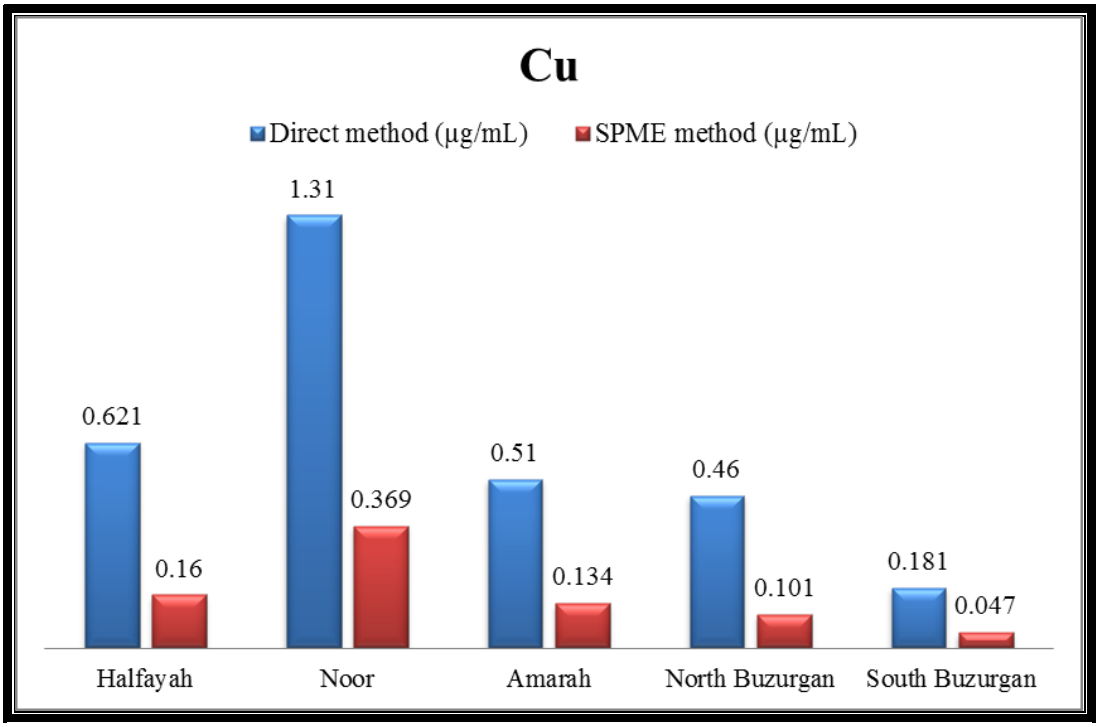

Fig. (3-41) Cupper concentration (µg/mL) by direct, SPME methods for cutting rock samples in oil fields

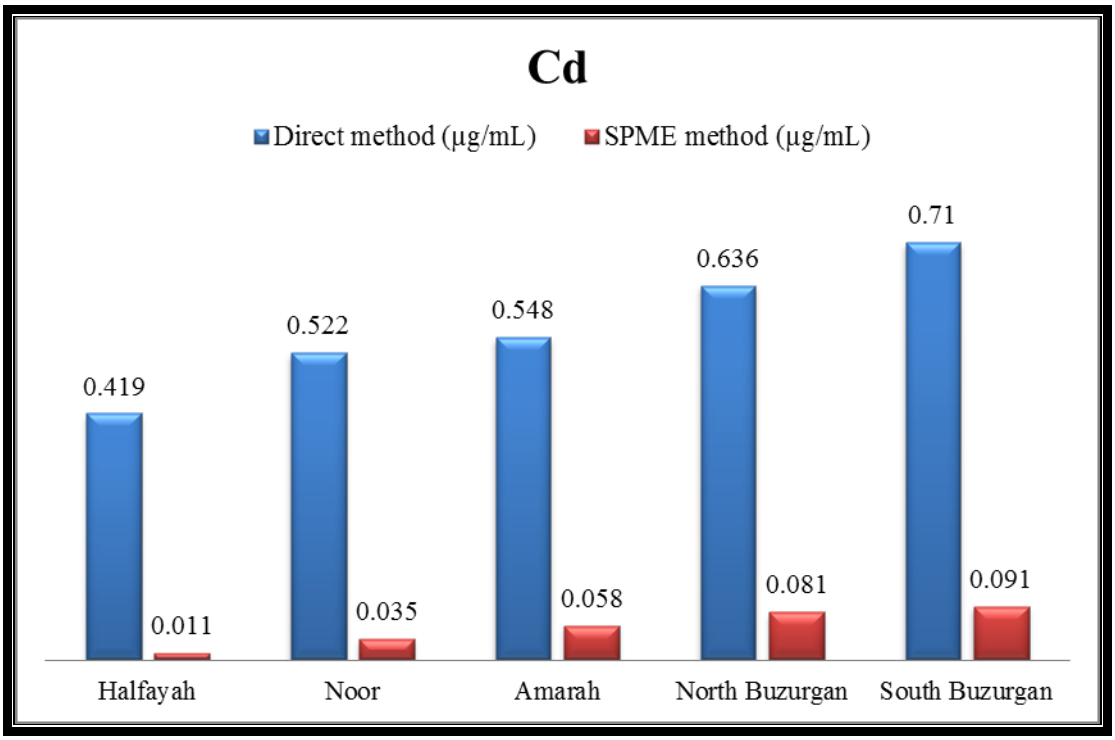

Fig. (3-42) Cadmium concentration (µg/mL) by direct, SPME methods for cutting rock samples in oil fields

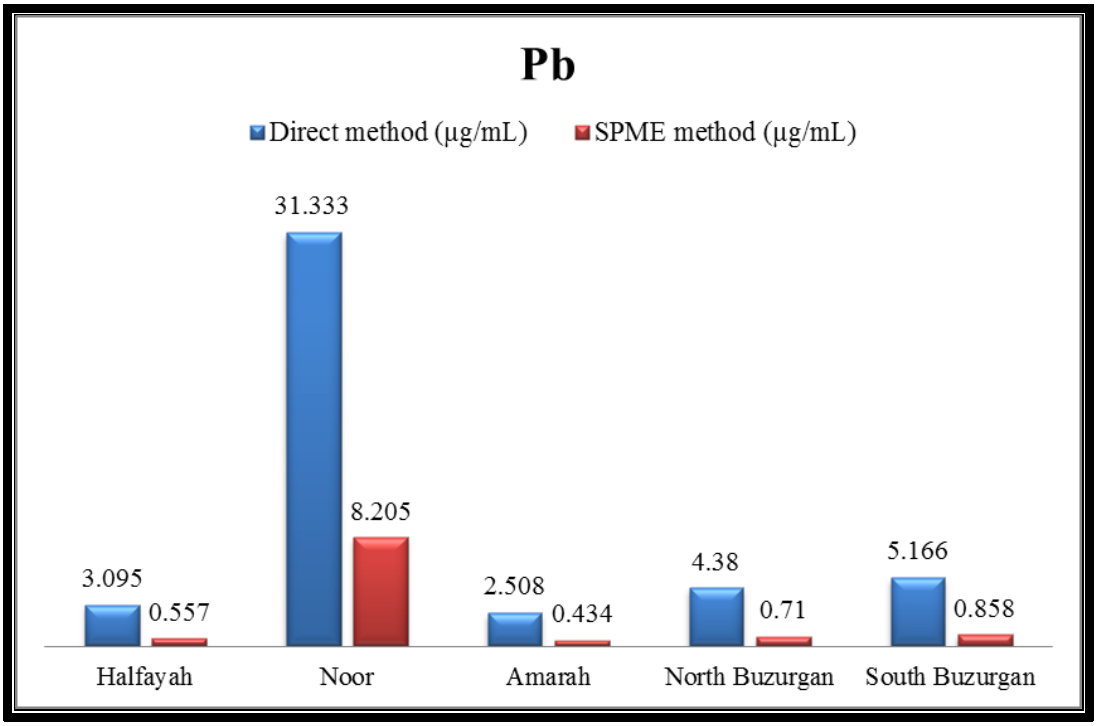

Fig. (3-43) Lead concentration (µg/mL) by direct, SPME methods for cutting rock samples in oil fields

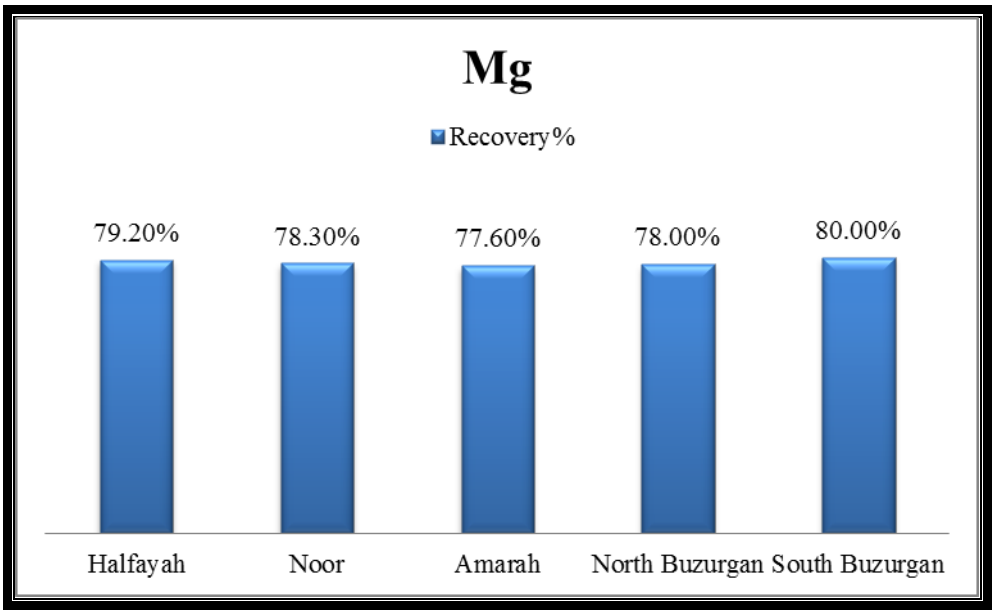

Fig. (3-44) Magnesium recovery% for cutting rock samples in oil fields

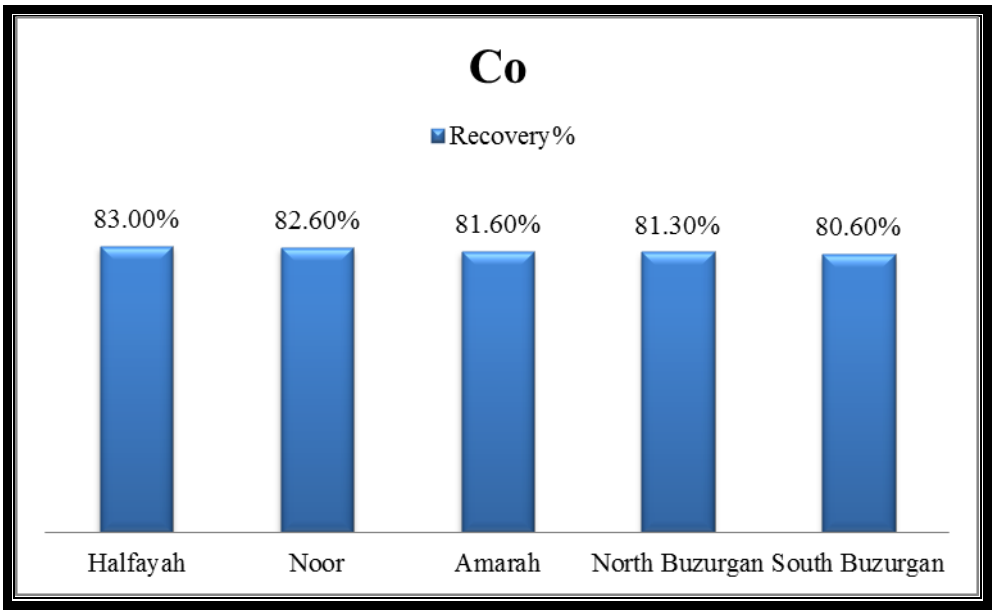

Fig. (3-45) Cobalt recovery% for cutting rock samples in oil fields

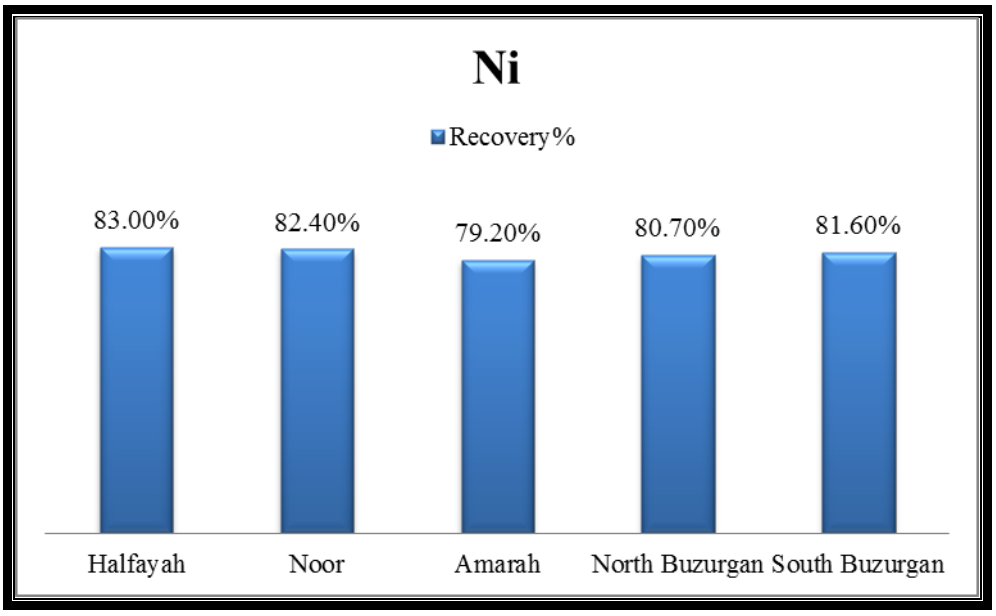

Fig. (3-46) Nickel recovery% for cutting rock samples in oil fields

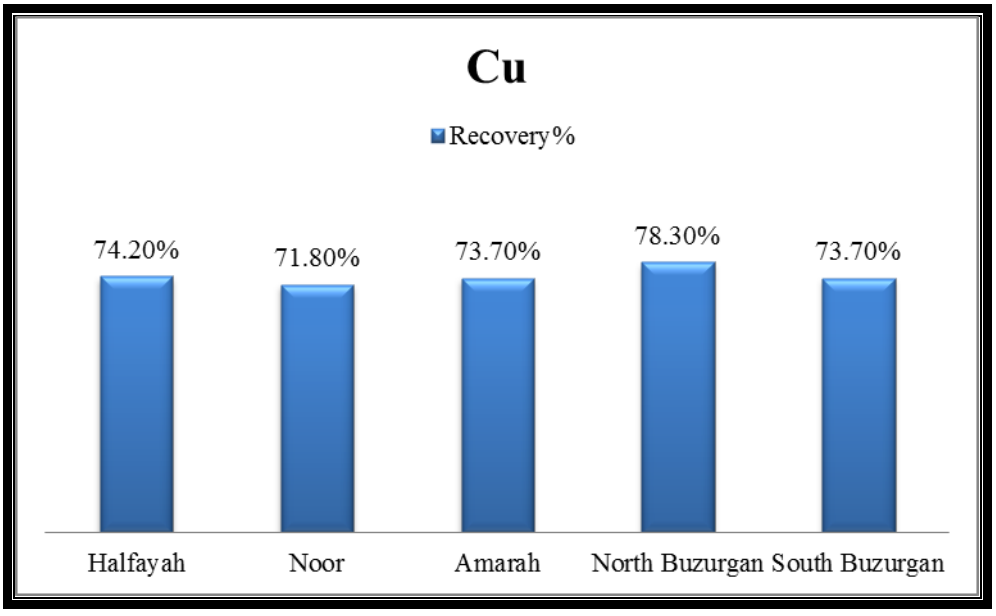

Fig. (3-47) Copper recovery% for cutting rock samples in oil fields

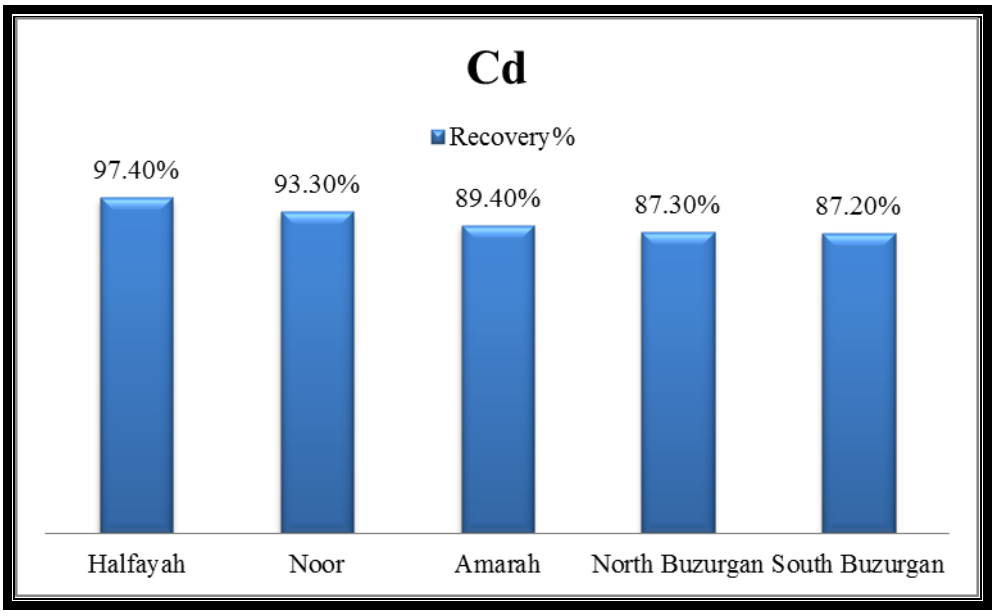

Fig. (3-48) Cadmium recovery% for cutting rock samples in oil fields

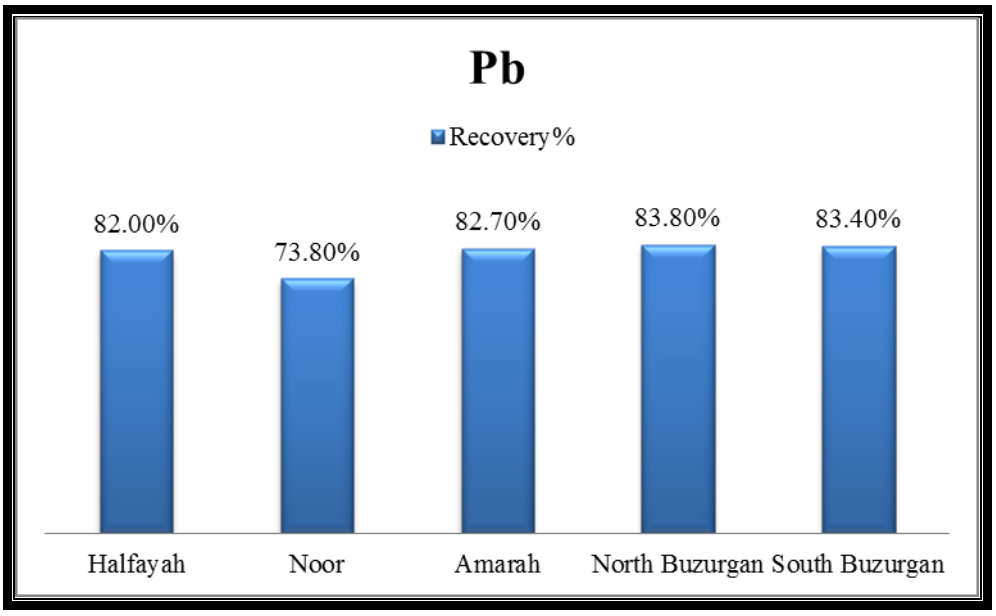

Fig. (3-49) Lead recovery % for cutting rock samples in oil fields

Magnesium concentrations by the direct method (9.205, 9.342, 9.649, 9.859 and 10.545 µg/mL) in the cutting rock samples in the following oil fields: south Buzurgan, Halfayah, Noor, north Buzurgan and Amarah respectively. Cobalt concentrations by the direct method (1.262, 1.271, 1.307, 1.371 and 1.38 µg/mL) in the cutting rock samples in the following oil fields: south Buzurgan, north Buzurgan, Halfayah, Noor and Amarah respectively. Nickel concentrations by the direct method (4.292, 4.464, 5.636, 6.727 and 7.113 µg/mL) in the cutting rock samples in the following oil fields: Halfayah, Noor, south Buzurgan, north Buzurgan and Amarah respectively. Copper concentrations by the direct method (0.181, 0.46, 0.51, 0.621 and 1.31 µg/mL) in the cutting rock samples in the following oil fields: south Buzurgan, north Buzurgan, Amarah, Halfayah and Noor respectively. Cadmium concentrations by the direct method (0.419, 0.522, 0.548, 0.636 and 0.71 µg/mL) in the cutting rock samples in the following oil fields: Halfayah, Noor, Amarah, north Buzurgan and south Buzurgan respectively. Lead concentrations by the direct method (2.508, 3.095, 4.38, 5.166 and 31.333 µg/mL) in the cutting rock samples in the following oil fields: Amarah, Halfayah, north Buzurgan, south Buzurgan and Noor respectively.

Magnesium concentrations by the SPME method (1.842, 1.944, 2.093, 2.169 and 2.364 µg/mL) in the cutting rock samples in the following oil fields: Buzurgan south region, Halfayah, Noor, Buzurgan north region and Amarah respectively. Cobalt concentrations by the SPME method (0.222, 0.238, 0.239, 0.245 and 0.254 µg/mL) in the cutting rock samples in the following oil fields: Halfayah, north Buzurgan, Noor, south Buzurgan and Amarah respectively. Nickel concentrations by the SPME method (0.73, 0.785, 1.037, 1.298 and 1.48 µg/mL) in the cutting rock samples in the following oil fields: Halfayah, Noor, south Buzurgan, north Buzurgan and Amarah respectively. Copper concentrations by the SPME method (0.047, 0.101, 0.134, 0.16 and 0.369

µg/mL) in the cutting rock samples in the following oil fields: south Buzurgan, north Buzurgan, Amarah, Halfayah and Noor respectively. Cadmium concentrations by the SPME method (0.011, 0.035, 0.058, 0.081 and 0.091 µg/mL) in the cutting rock samples in the following oil fields: Halfayah, Noor, Amarah, north Buzurgan and south Buzurgan respectively. Lead concentrations by the SPME method (0.434, 0.557, 0.71, 0.858 and 8.205 µg/mL) in the cutting rock samples in the following oil fields: Amarah, Halfayah, north Buzurgan, south Buzurgan and Noor respectively.

The concentrations of the analytes in cutting rock samples decreased by using SPME method because of the electrostatic attraction with NGO surface.

Magnesium recovery% (77.6%, 78%, 78.3%, 79.2% and 80%) in the cutting rock samples in the following oil fields: Amarah, north Buzurgan, Noor, Halfayah and south Buzurgan respectively. Cobalt recovery% (80.6%, 81.3%, 81.6%, 82.6% and 83%) in the cutting rock samples in the following oil fields: south Buzurgan, north Buzurgan, Amarah, Noor and Halfayah respectively. Nickel recovery% (79.2%, 80.7%, 81.6%, 82.4% and 83%) in the cutting rock samples in the following oil fields: Amarah, north Buzurgan, south Buzurgan, Noor and Halfayah respectively. Copper recovery% (71.8%, 73.7%, 73.7%, 74.2% and 78.3%) in the cutting rock samples in the following oil fields: Noor, south Buzurgan, Amarah, Halfayah and north Buzurgan respectively. Cadmium recovery% (87.2%, 87.3%, 89.4%, 93.3% and 97.4%) in the cutting rock samples in the following oil fields: south Buzurgan, north Buzurgan Amarah, Noor and Halfayah respectively. Lead recovery% (73.8%, 82%, 82.7%, 83.4% and 83.8%) in the cutting rock samples in the following oil fields: Noor, Halfayah, Amarah, south Buzurgan and north Buzurgan respectively.

The average recovery% (78.62%, 81.14%, 81.2% and 81.3%) of the analytes in cutting rock samples deceased than the recovery% (85.1%, 84.9%, 85.1% and 82.2%) of the analytes (1 µg/mL), at optimum conditions for (Mg, Pb, Co and

Ni) respectively, because the mass of NGO (0.5 mg) was insufficient for adsorption of the analytes on the NGO surface.

The average recovery% (74.34% and 90.92%) of the analytes in cutting rock samples increased than the recovery% (71.9% and 83.3%) of the analytes (1µg/mL), at optimum conditions for (Cu and Cd) respectively, because the mass of NGO (0.5 mg) was sufficient for adsorption of the analytes on the NGO surface.

The interfering ions present in cutting rock sample at concentration higher than tolerance limit effect on the recovery% of analyte, therefore investigated them.

3.4.2 Determination of trace elements in cutting rock samples

The trace elements (Cr, Mn, Fe, Co, Ni, Cu, Zn, As, Cd, Sn and Pb) determined by flame atomic absorption spectroscopy (FAAS), but (Li, Mg, K, Ca and Ba) determined by flame photometer (atomic emission spectroscopy) in cutting rock sample with standard deviation (SD±) as in equation $S = \sqrt{\frac{\sum(xi-\bar{x})^2}{n-1}}$ where, xi : concentration of analyte for each oil field, $\bar{x}$: average of concentrations, n: number of concentration value, and relative standard deviation (RSD%) as in equation $RSD\% = \frac{S}{\bar{x}} * 100\%$ where, S: standard deviation, $\bar{x}$: average of concentrations[141] as shown in Table (3-13) and Figures from (3-50) to (3-54).

Table (3-13): Concentration of trace elements in cutting rock samples in oil fields

Oil field	Analyte															
	Cr (µg/mL)	Mn (µg/mL)	Fe (µg/mL)	Co (µg/mL)	Ni (µg/mL)	Cu (µg/mL)	Zn (µg/mL)	As (µg/mL)	Cd (µg/mL)	Sn (µg/mL)	Pb (µg/mL)	Li (µg/mL)	Mg (µg/mL)	K (µg/mL)	Ca (µg/mL)	Ba (µg/mL)
Halfayah (n = 5)	0.261	0.312	2.541	1.307	4.292	0.621	2.056	0.105	0.419	0.321	3.095	1.032	9.342	7.673	14.19	4.231
Noor (n = 5)	0.343	0.387	4.256	1.371	4.464	1.31	1.238	0.212	0.522	0.537	31.333	1.134	9.649	13.52	17.45	6.427
Amarah (n = 5)	0.372	0.353	3.248	1.38	7.113	0.51	1.623	0.126	0.548	0.482	2.508	1.062	10.55	11.82	19.31	6.928
North Buzurgan (n = 5)	0.281	0.278	2.873	1.271	6.727	0.46	0.953	0.167	0.636	0.157	4.38	0.953	9.859	8.867	14.87	4.173
South Buzurgan (n = 5)	0.217	0.333	3.027	1.262	5.636	0.181	0.979	0.139	0.71	0.149	5.166	0.842	9.205	7.395	15.43	3.989
SD ± (µg/mL)	0.063	0.041	0.65	0.055	1.28	0.42	0.469	0.041	0.111	0.179	12.363	0.112	0.528	2.696	2.099	1.409
RSD%	21.23	12.38	20.37	4.176	22.67	68.18	34.22	27.63	19.62	54.49	132.99	11.12	5.427	27.36	12.92	27.36

* Note: n = 5 (number of samples)

SD ± : standard deviation, RSD% : relative standard deviation

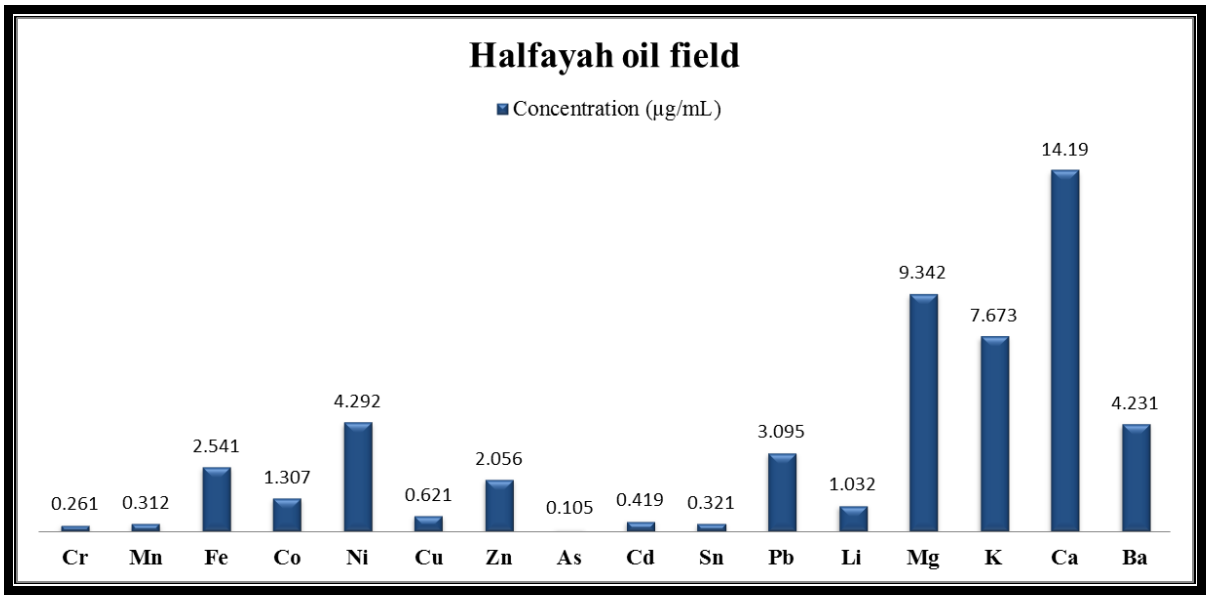

Fig. (3-50) Concentration of trace elements in cutting rock samples in Halfayah oil field

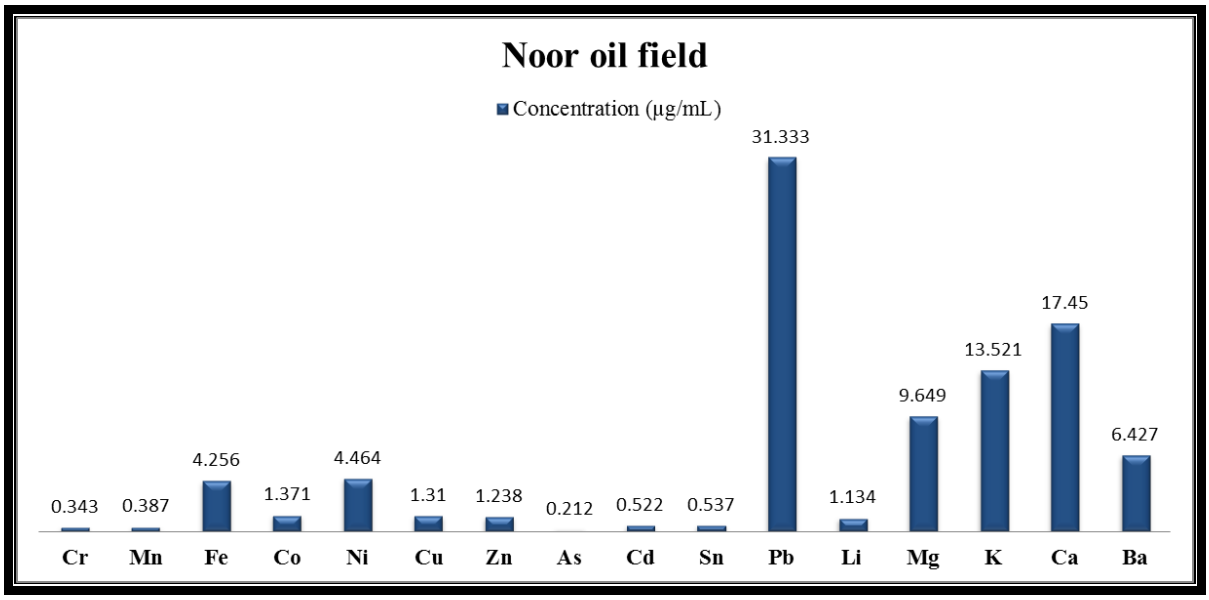

Fig. (3-51) Concentration of trace elements in cutting rock samples in Noor oil field

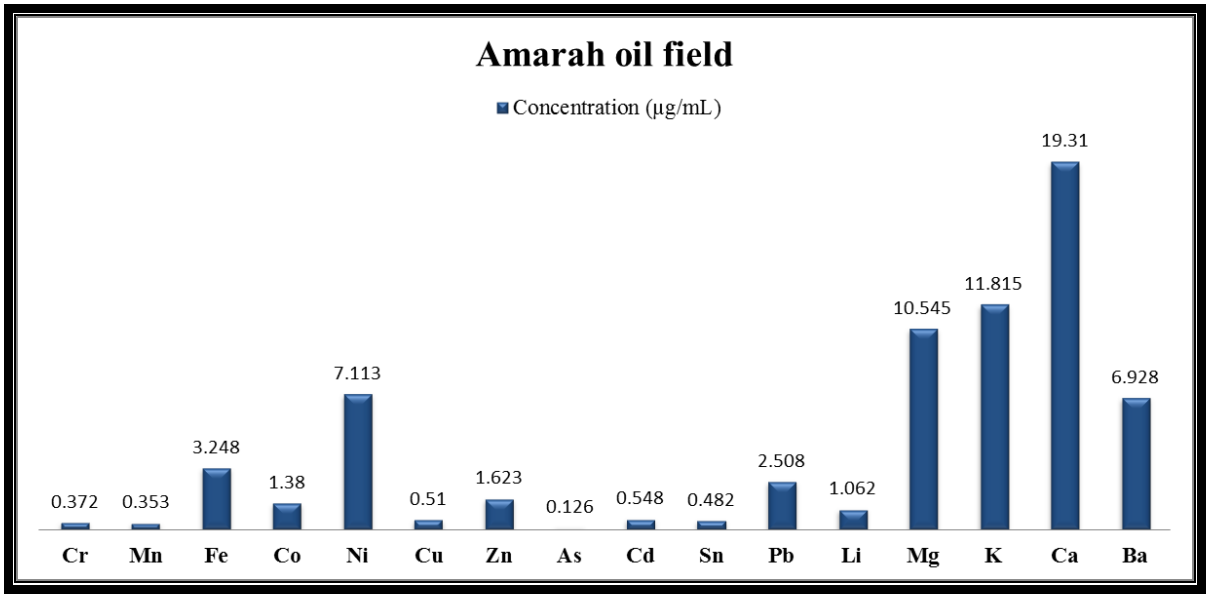

Fig. (3-52) Concentration of trace elements in cutting rock samples in Amarah oil field

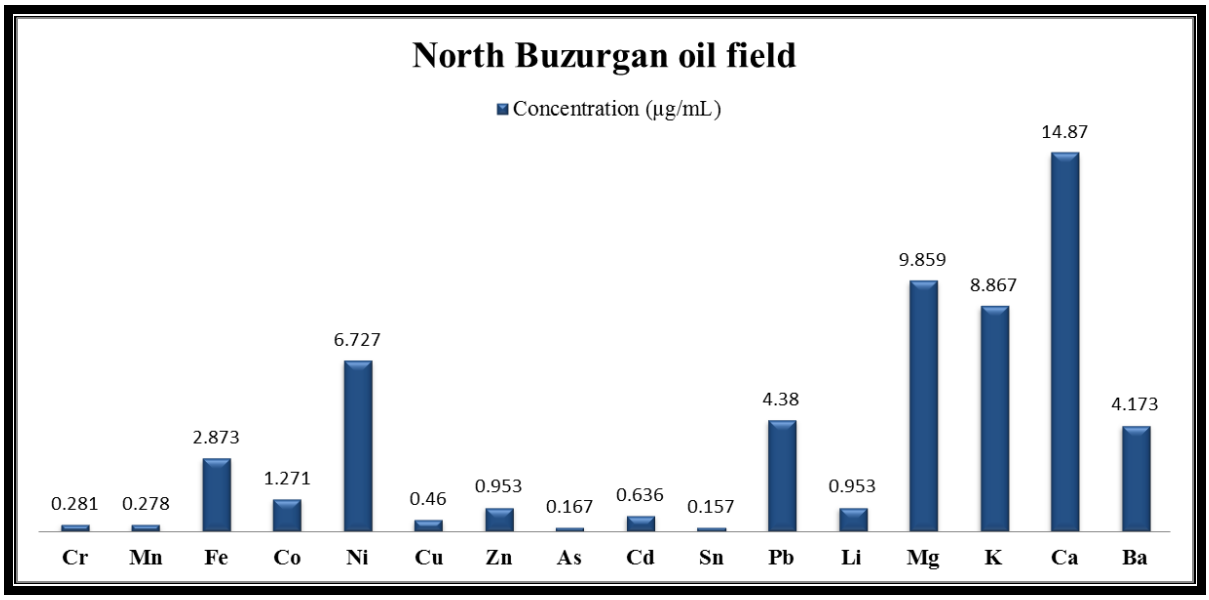

Fig. (3-53) Concentration of trace elements in cutting rock samples in North Buzurgan oil field

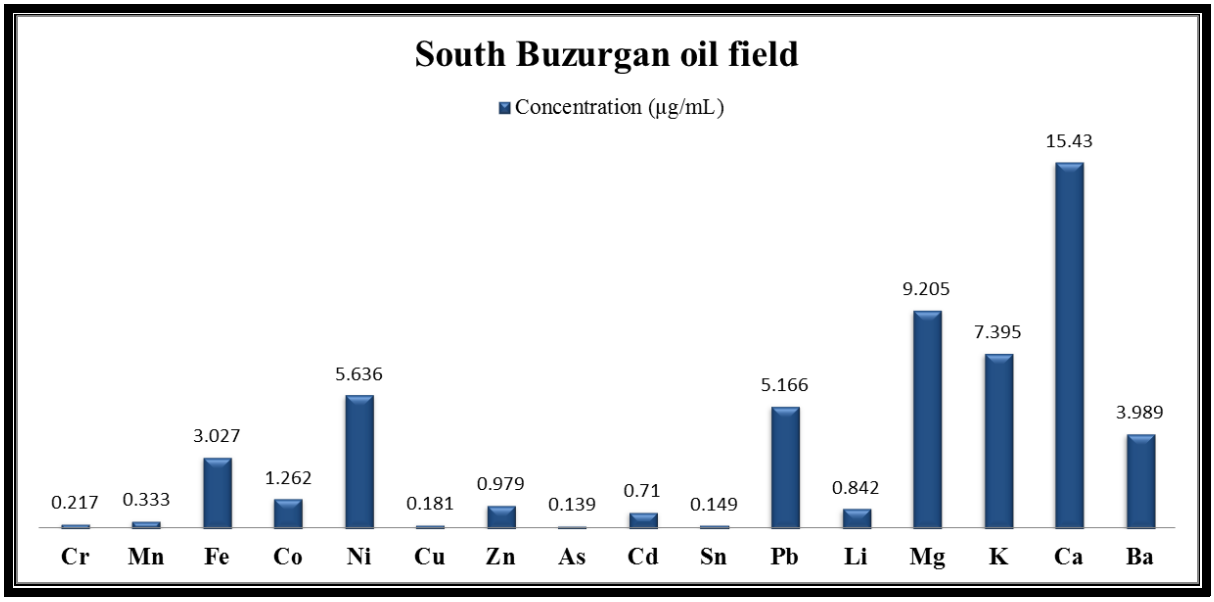

Fig. (3-54) Concentration of trace elements in cutting rock samples in south Buzurgan oil field

The concentration of trace elements (As, Cr, Mn, Sn, Cd, Cu, Li, Co, Zn, Fe, Pb, Ba, Ni, K, Mg and Ca) in cutting rock samples in Halfayah oil field were (0.105, 0.261, 0.312, 0.321, 0.419, 0.621, 1.032, 1.307, 2.056, 2.541, 3.095, 4.231, 4.292, 7.673, 9.342 and 14.19 µg/mL) respectively. The concentration of trace elements (As, Cr, Mn, Cd, Sn, Li, Zn, Cu, Co, Fe, Ni, Ba, Mg, K, Ca and Pb) in cutting rock samples in Noor oil field were (0.212, 0.343, 0.387, 0.522, 0.537, 1.134, 1.238, 1.31, 1.371, 4.256, 4.464, 6.427, 9.649, 13.521, 17.45 and 31.333 µg/mL) respectively. The concentration of trace elements (As, Mn, Cr, Sn, Cu, Cd, Li, Co, Zn, Pb, Fe, Ba, Ni, Mg, K and Ca) in cutting rock samples in Amarah oil field were (0.126, 0.353, 0.372, 0.482, 0.51, 0.548, 1.062, 1.38, 1.623, 1.623, 3.248, 6.928, 7.113, 10.545, 11.815 and 19.31 µg/mL) respectively. The concentration of trace elements (Sn, As, Mn, Cr, Cu, Cd, Li, Zn, Co, Fe, Ba, Pb, Ni, K, Mg and Ca) in cutting rock samples in north Buzurgan oil field were (0.157, 0.167, 0.278, 0.281, 0.46, 0.636, 0.953, 0.953, 1.271, 2.873, 4.173, 4.38, 6.727, 8.867, 9.859 and 14.87 µg/mL) respectively. The concentration of trace elements (As, Sn, Cu, Cr, Mn, Cd, Li, Zn, Co, Fe, Ba, Pb, Ni, K, Mg and Ca) in cutting rock samples in south Buzurgan oil field were (0.139, 0.149, 0.181, 0.217, 0.333, 0.71, 0.842, 0.979, 1.262, 3.027, 3.989, 5.166, 5.636, 7.395, 9.205 and 15.43 µg/mL) respectively.

Calcium concentration observed higher in Halfayah, Amarah, north and south Buzurgan oil fields, but lead concentration observed higher in Noor oil field. Arsine concentration observed lower in Halfayah, Amarah, Noor and south Buzurgan oil fields, but tin concentration observed lower in north Buzurgan oil field. Concentration of chromium (0.217, 0.261, 0.281, 0.343 and 0.372 µg/mL) in cutting rock sample in the following oil fields (south Buzurgan, Halfayah, north Buzurgan, Noor and Amarah) respectively. The concentration of manganese (0.278, 0.312, 0.333, 0.353 and 0.387 µg/mL) in cutting rock sample in the following oil fields (north Buzurgan, Halfayah, south Buzurgan,

Amarah and Noor) respectively. The concentration of iron (2.541, 2.873, 3.027, 3.248 and 4.256 µg/mL) in cutting rock sample in the following oil fields (Halfayah, north Buzurgan, south Buzurgan, Amarah and Noor) respectively. The concentration of cobalt (1.262, 1.271, 1.307, 1.371 and 1.38 µg/mL) in cutting rock sample in the following oil fields (south Buzurgan, north Buzurgan, Halfayah, Noor and Amarah) respectively. The concentration of nickel (4.292, 4.464, 5.636, 6.727 and 7.113 µg/mL) in cutting rock sample in the following oil fields (Halfayah, Noor, south Buzurgan, north Buzurgan and Amarah) respectively. The concentration of copper (0.181, 0.46, 0.51, 0.621 and 1.31 µg/mL) in cutting rock sample in the following oil fields (south Buzurgan, north Buzurgan, Amarah, Halfayah and Noor) respectively. The concentration of zinc (0.953, 0.979, 1.238, 1.623 and 2.056 µg/mL) in cutting rock sample in the following oil fields (north Buzurgan, south Buzurgan, Noor, Amarah and Halfayah) respectively. The concentration of arsine (0.105, 0.126, 0.139, 0.167 and 0.212 µg/mL) in cutting rock sample in the following oil fields (Halfayah, Amarah, south Buzurgan, north Buzurgan and Noor) respectively. The concentration of cadmium (0.419, 0.522, 0.548, 0.636 and 0.71 µg/mL) in cutting rock sample in the following oil fields (Halfayah, Noor, Amarah, north Buzurgan and south Buzurgan) respectively. The concentration of tin (0.149, 0.157, 0.321, 0.482 and 0.537 µg/mL) in cutting rock sample in the following oil fields (south Buzurgan, north Buzurgan, Halfayah, Amarah and Noor) respectively. The concentration of lead (2.508, 3.095, 4.38, 5.166 and 31.333 µg/mL) in cutting rock sample in the following oil fields (Amarah, Halfayah, north Buzurgan, south Buzurgan and Noor) respectively. The concentration of lithium (0.842, 0.953, 1.032, 1.062 and 1.134 µg/mL) in cutting rock sample in the following oil fields (south Buzurgan, north Buzurgan, Halfayah, Amarah and Noor) respectively. The concentration of magnesium (9.205, 9.342, 9.649, 9.859 and 10.545 µg/mL) in cutting rock sample in the following oil fields (south Buzurgan, Halfayah, Noor, north

Buzurgan and Amarah) respectively. The concentration of potassium (7.395, 7.673, 8.867, 11.815 and 13.521 µg/mL) in cutting rock sample in the following oil fields (south Buzurgan, Halfayah, north Buzurgan, Amarah and Noor) respectively. The concentration of calcium (14.19, 14.87, 15.43, 17.45 and 19.31 µg/mL) in cutting rock sample in the following oil fields (Halfayah, north Buzurgan, south Buzurgan, Noor and Amarah) respectively. The concentration of barium (3.989, 4.173, 4.231, 6.427 and 6.928 µg/mL) in cutting rock sample in the following oil fields (south Buzurgan, north Buzurgan, Halfayah, Noor and Amarah) respectively.

3.4.3 Determination of metal ions and recovery in crude oil samples by SPME method

The analytes determined directly (without NGO), with SPME method (with NGO) according to the optimum conditions, one sample collected from each oil field as shown in Table (3-14) , Figures from (3-55) to (3-66).

Table (3-14): Concentration of analytes by direct, SPME methods and recovery in crude oil samples

Oil field	Analyte																	
	Mg			Co			Ni			Cu			Cd			Pb		
	µg/mL		Recovery %	µg/mL		Recovery %	µg/mL		Recovery %	µg/mL		Recovery %	µg/mL		Recovery %	µg/mL		Recovery %
	Direct method	SPME method		Direct method	SPME method		Direct method	SPME method		Direct method	SPME method		Direct method	SPME method		Direct method	SPME method	
Halfayah	4.351	0.705	83.8	0.561	0.075	86.6	20.143	4.149	79.4	0.283	0.044	84.3	0.613	0.089	85.5	2.836	0.448	84.2
Noor	7.182	1.285	82.1	0.732	0.084	88.5	27.621	6.684	75.8	0.871	0.173	80.1	0.362	0.045	87.7	9.892	1.949	80.3
Amarah	9.724	1.769	81.8	0.924	0.09	90.3	28.103	6.66	76.3	0.592	0.104	82.4	0.212	0.022	89.7	7.492	1.446	80.7
North Buzurgan	3.869	0.634	83.6	0.572	0.073	87.3	21.763	4.592	78.9	0.412	0.067	83.7	0.187	0.016	91.6	4.474	0.774	82.7
South Buzurgan	4.937	0.829	83.2	0.483	0.066	86.3	20.795	4.242	79.6	0.389	0.066	83.1	0.213	0.021	90.3	3.631	0.595	83.6

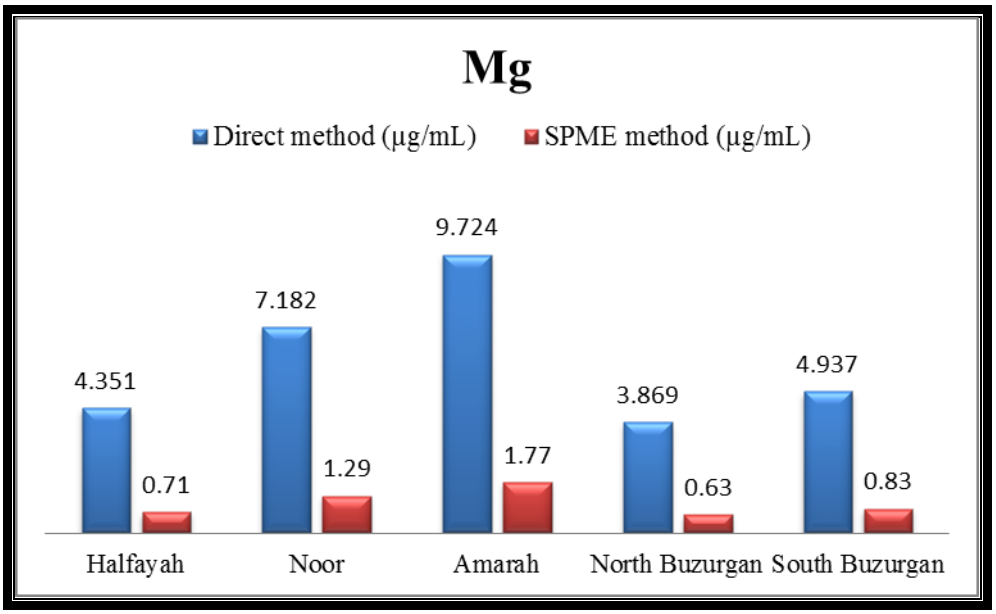

Fig. (3-55) Magnesium concentration (µg/mL) by direct, SPME methods for crude oil samples in oil fields

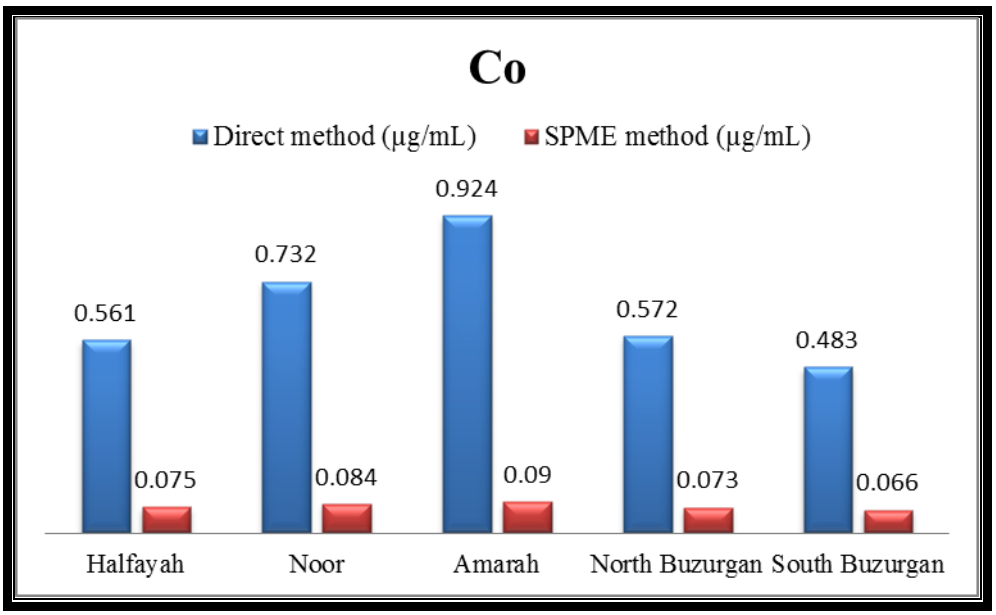

Fig. (3-56) Cobalt concentration (µg/mL) by direct, SPME methods for crude oil samples in oil fields

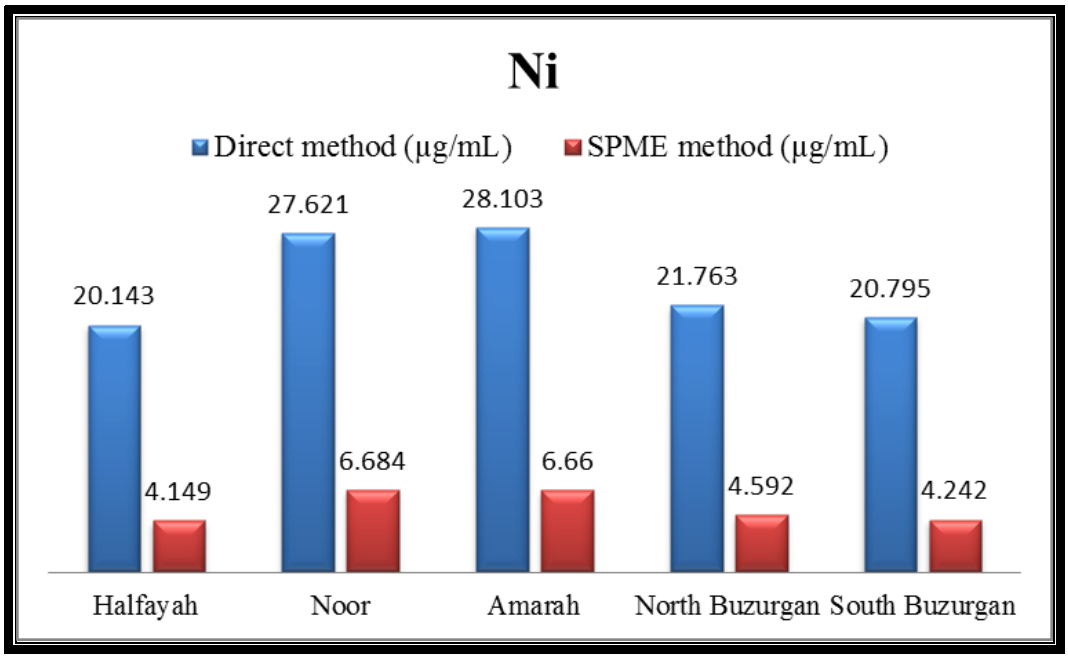

Fig. (3-57) Nickel concentration (µg/mL) by direct, SPME methods for crude oil samples in oil fields

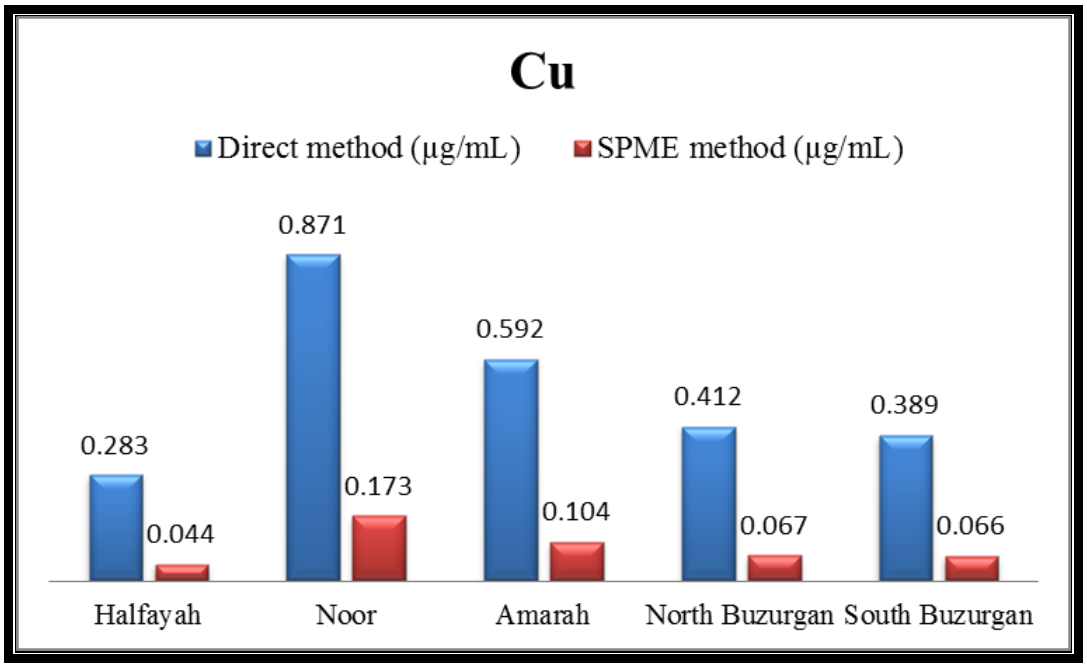

Fig. (3-58) Copper concentration (µg/mL) by direct, SPME methods for crude oil samples in oil fields

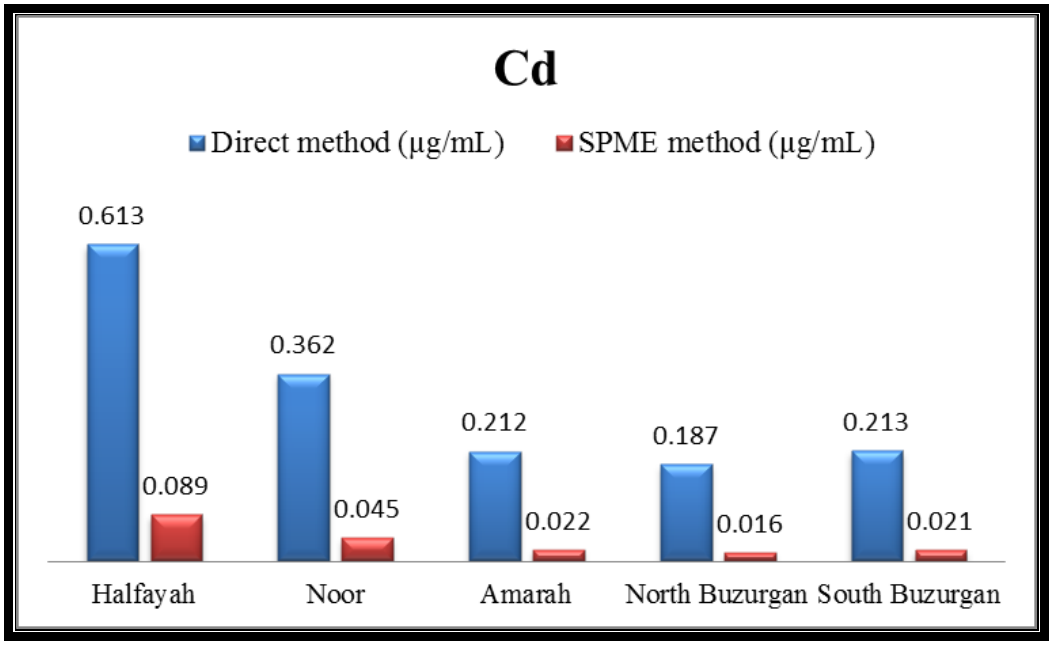

Fig. (3-59) Cadmium concentration (µg/mL) by direct, SPME methods for crude oil samples in oil fields

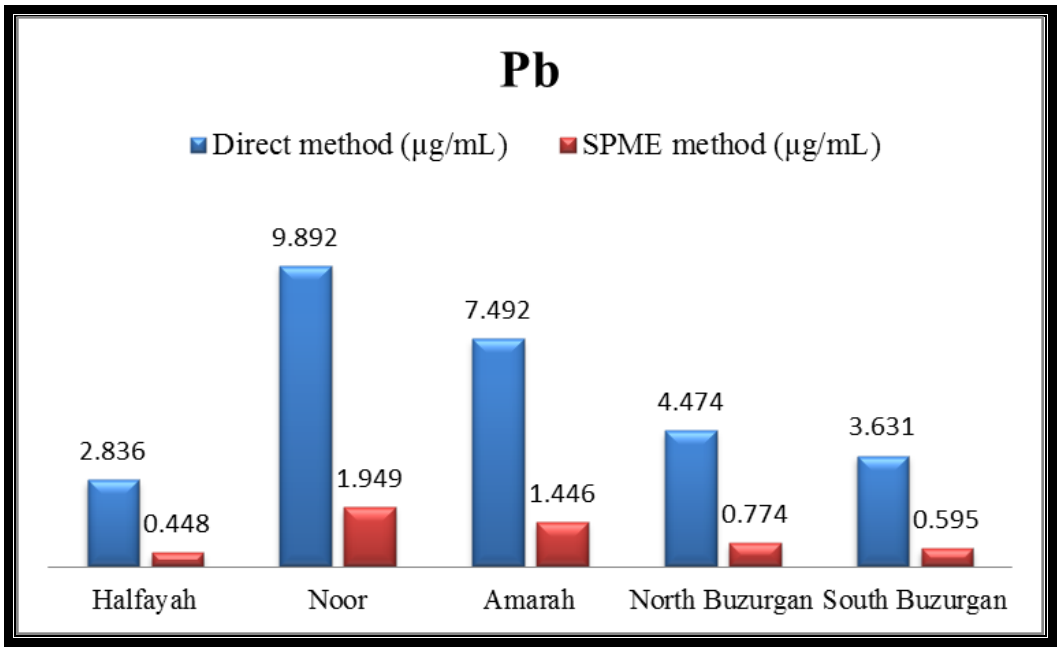

Fig. (3-60) Lead concentration (µg/mL) by direct, SPME methods for crude oil samples in oil fields

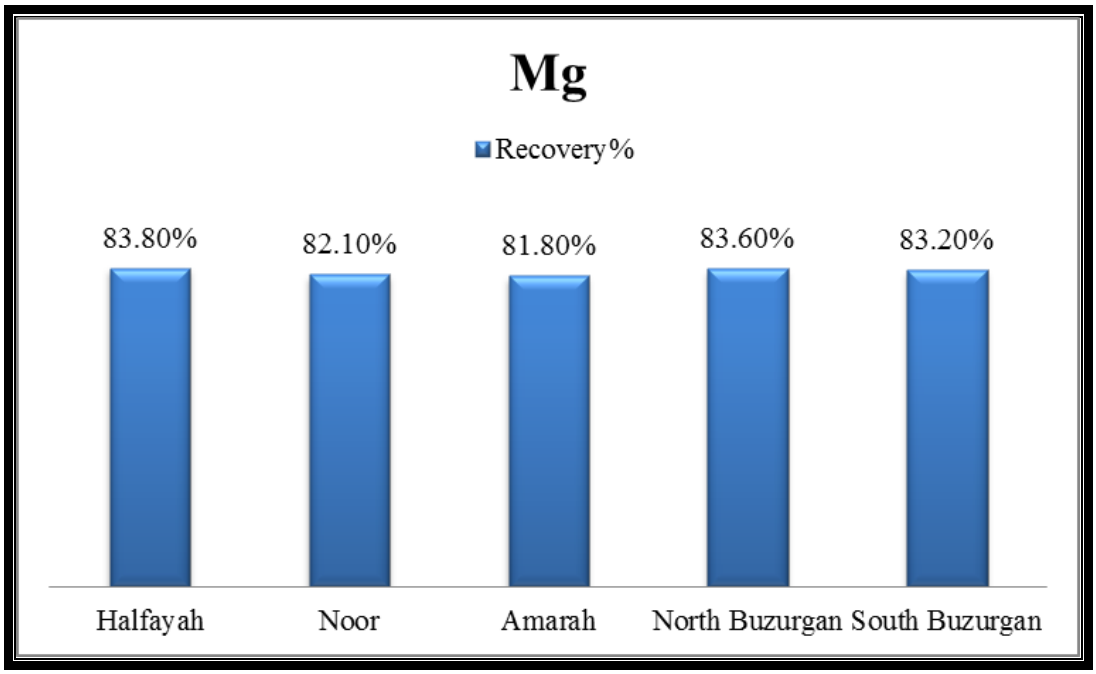

Fig. (3-61) Magnesium recovery % for crude oil samples in oil fields

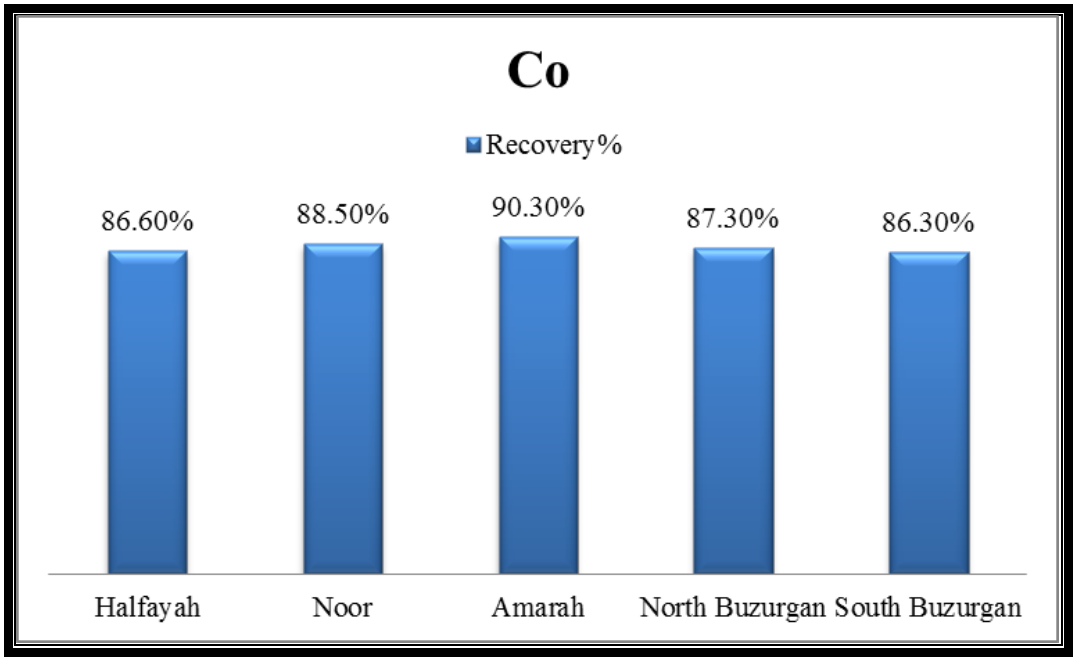

Fig. (3-62) Cobalt recovery % for crude oil samples in oil fields

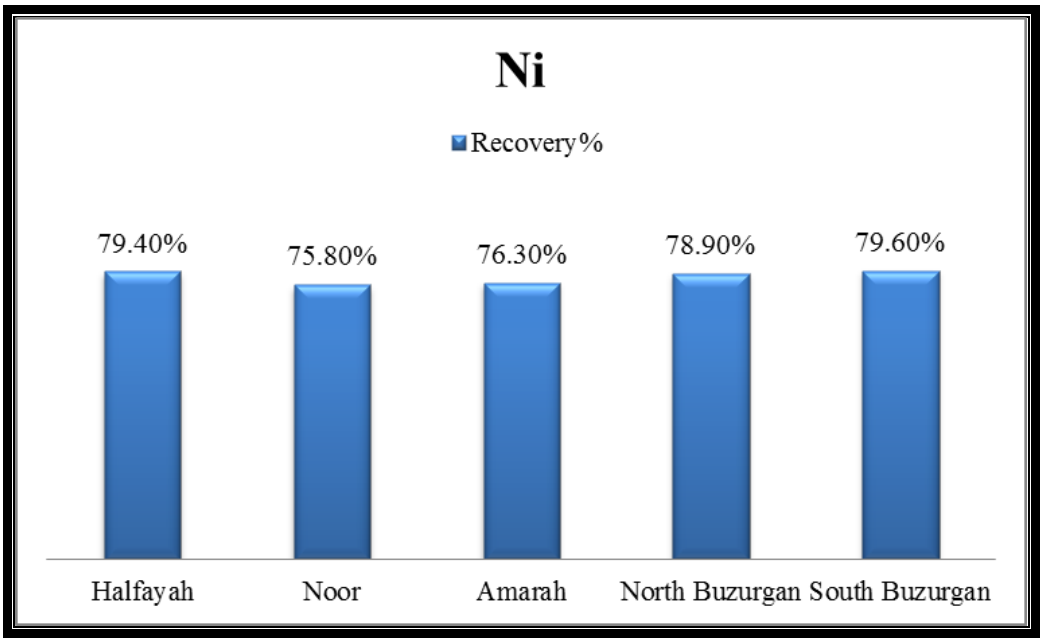

Fig. (3-63) Nickel recovery% for crude oil samples in oil fields

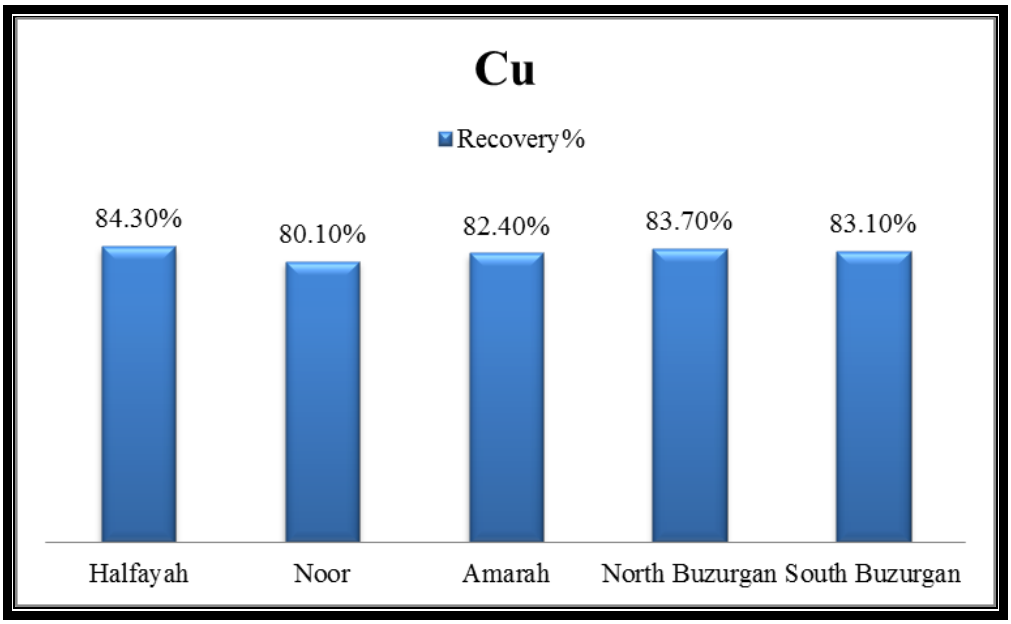

Fig. (3-64) Copper recovery % for crude oil samples in oil fields

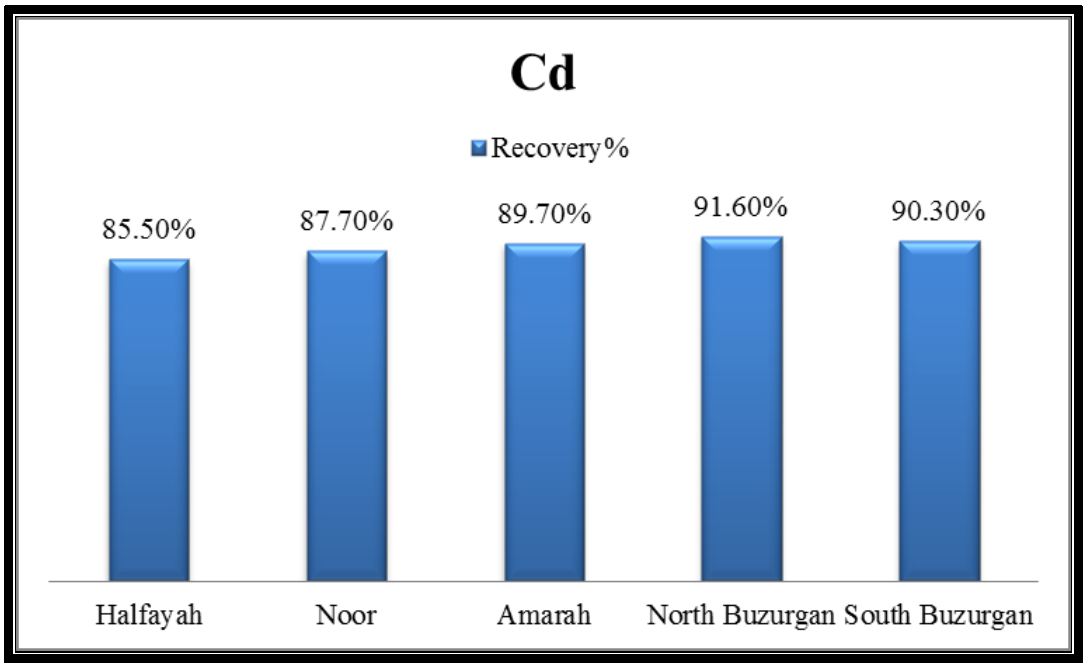

Fig. (3-65) Cadmium recovery % for crude oil samples in oil fields

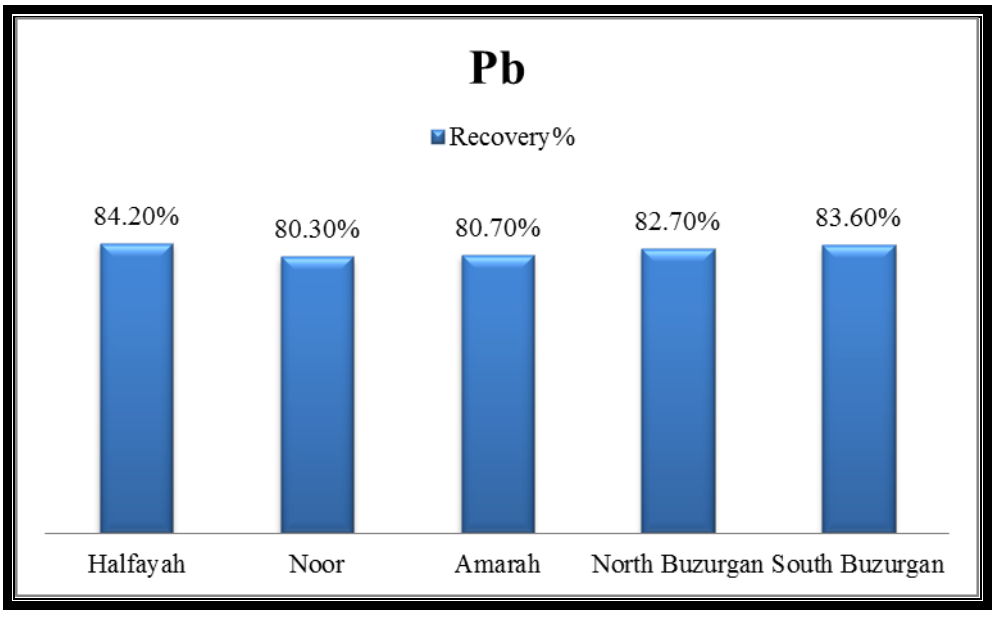

Fig. (3-66) Lead recovery % for crude oil samples in oil fields

Magnesium concentrations by the direct method (3.869, 4.351, 4.937, 7.182 and 9.724 µg/mL) in the crude oil samples in the following oil fields: north Buzurgan, Halfayah, south Buzurgan, Noor and Amarah respectively. Cobalt concentrations by the direct method (0.483, 0.561, 0.572, 0.732 and 0.924 µg/mL) in the crude oil samples in the following oil fields: south Buzurgan, Halfayah, north Buzurgan, Noor and Amarah respectively. Nickel concentrations by the direct method (20.143, 20.795, 21.763, 27.621 and 28.103 µg/mL) in the crude oil samples in the following oil fields: Halfayah, south Buzurgan, north Buzurgan, Noor and Amarah respectively. Copper concentrations by the direct method (0.283, 0.389, 0.412, 0.592 and 0.871 µg/mL) in the crude oil samples in the following oil fields: Halfayah, south Buzurgan, north Buzurgan, Amarah, and Noor respectively. Cadmium concentrations by the direct method (0.187, 0.212, 0.213, 0.362 and 0.613 µg/mL) in the crude oil samples in the following oil fields: north Buzurgan, Amarah, south Buzurgan, Noor and Halfayah respectively. Lead concentrations by the direct method (2.836, 3.631, 4.474, 7.492 and 9.892 µg/mL) in the crude oil samples in the following oil fields: Halfayah, south Buzurgan, north Buzurgan, Amarah and Noor respectively.

Magnesium concentrations by the SPME method (0.63, 0.71, 0.83, 1.29 and 1.77 µg/mL) in the crude oil samples in the following oil fields: north Buzurgan, Halfayah, south Buzurgan, Noor and Amarah respectively. Cobalt concentrations by the SPME method (0.066, 0.073, 0.075, 0.084 and 0.09 µg/mL) in the crude oil samples in the following oil fields: south Buzurgan, north Buzurgan, Halfayah, Noor and Amarah respectively. Nickel concentrations by the SPME method (4.149, 4.242, 4.592, 6.66 and 6.684 µg/mL) in the crude oil samples in the following oil fields: Halfayah, south Buzurgan, north Buzurgan, Amarah and Noor respectively. Copper concentrations by the SPME method (0.044, 0.066, 0.067, 0.104 and 0.173

µg/mL) in the crude oil samples in the following oil fields: Halfayah, south Buzurgan, north Buzurgan, Amarah, and Noor respectively. Cadmium concentrations by the SPME method (0.016, 0.021, 0.022, 0.045 and 0.089 µg/mL) in the crude oil samples in the following oil fields: north Buzurgan, south Buzurgan, Amarah, Noor, and Halfayah respectively. Lead concentrations by the SPME method (0.448, 0.595, 0.774, 1.446 and 1.949 µg/mL) in the crude oil samples in the following oil fields: Halfayah, south Buzurgan, north Buzurgan, Amarah and Noor respectively.

The concentrations of the analytes in crude oil samples decreased by using SPME method because of the electrostatic attraction with NGO surface.

Magnesium recovery% (81.8%, 82.1%, 83.2%, 83.6% and 83.8%) in the crude oil samples in the following oil fields: Amarah, Noor, south Buzurgan, north Buzurgan and Halfayah respectively. Cobalt recovery% (86.3%, 86.6%, 87.3%, 88.5% and 90.3%) in the crude oil samples in the following oil fields: south Buzurgan, Halfayah, north Buzurgan, Noor and Amarah respectively. Nickel recovery% (75.8%, 76.3%, 78.9%, 79.4% and 79.6%) in the crude oil samples in the following oil fields: Noor, Amarah, north Buzurgan, , Halfayah and south Buzurgan respectively. Copper recovery% (80.1%, 82.4%, 83.1%, 83.7% and 84.3%) in the crude oil samples in the following oil fields: Noor, Amarah, south Buzurgan, north Buzurgan and Halfayah respectively. Cadmium recovery% (85.5%, 87.7%, 89.7%, 90.3% and 91.6%) in the crude oil samples in the following oil fields: Halfayah, Noor, Amarah, south Buzurgan and north Buzurgan respectively. Lead recovery% (80.3%, 80.7%, 82.7%, 83.6% and 84.2%) in the crude oil samples in the following oil fields: Noor, Amarah, north Buzurgan, south Buzurgan and Halfayah respectively.

The average recovery% (78%, 82.3% and 82.9%) of the analytes in crude oil samples deceased than the recovery% (82.2%, 84.9% and 85.1%, and) of the analytes (1 µg/mL), at optimum conditions for (Ni, Pb and Mg) respectively,

because the mass of NGO (0.5 mg) was insufficient for adsorption of the analytes on the NGO surface.

The average recovery% (82.72%, 87.8% and 89%) of the analytes in crude oil samples increased than the recovery% (71.9%, 85.1% and 83.3%) of the analytes (1 µg/mL), at optimum conditions for (Cu, Co and Cd) respectively, because the mass of NGO (0.5 mg) was sufficient for adsorption of the analytes on the NGO surface.

The interfering ions present in crude oil sample at concentration higher than tolerance limit effect on the recovery% of analyte, therefore investigated them.

3.4.4 Determination of trace elements in crude oil samples

The trace elements (Cr, Mn, Fe, Co, Ni, Cu, Zn, As, Cd, Sn and Pb) determined by flame atomic absorption spectroscopy (FAAS), but (Li, Mg, K, Ca and Ba) determined by flame photometer (atomic emission spectroscopy) in crude oil samples with standard deviation (SD ±) and relative standard deviation (RSD%) as shown in Table (3-15) and Figures from (3-67) to (3-71).

Table (3-15) Concentration of trace elements in crude oil samples in oil fields

Oil field	Analyte															
	Cr (µg/mL)	Mn (µg/mL)	Fe (µg/mL)	Co (µg/mL)	Ni (µg/mL)	Cu (µg/mL)	Zn (µg/mL)	As (µg/mL)	Cd (µg/mL)	Sn (µg/mL)	Pb (µg/mL)	Li (µg/mL)	Mg (µg/mL)	K (µg/mL)	Ca (µg/mL)	Ba (µg/mL)
Halfayah	0.374	0.662	3.212	0.561	20.143	0.283	5.142	0.132	0.613	0.287	2.836	2.175	4.351	6.631	4.441	2.211
Noor	0.412	1.042	5.872	0.732	27.621	0.871	6.895	0.252	0.362	0.211	9.892	3.376	7.182	5.242	6.629	3.377
Amarah	0.283	0.844	5.212	0.924	28.103	0.592	8.723	0.106	0.212	0.312	7.492	4.573	9.724	4.122	5.783	2.976
North Buzurgan	0.613	0.878	2.143	0.572	21.763	0.412	5.535	0.163	0.187	0.189	4.474	4.553	3.869	6.118	9.424	2.513
South Buzurgan	0.731	0.756	2.016	0.483	20.795	0.389	6.628	0.181	0.213	0.206	3.631	4.897	4.937	5.811	8.829	3.792
SD ± (µg/mL)	0.184	0.142	1.768	0.176	3.86	0.231	1.401	0.056	0.179	0.055	2.948	1.132	2.4318	0.96	2.085	0.638
RSD%	38.11	17.01	47.9	26.86	16.3	45.28	21.28	33.36	56.44	22.71	52.04	28.91	40.445	17.19	29.69	21.44

* SD ± : standard deviation, RSD% : relative standard deviation

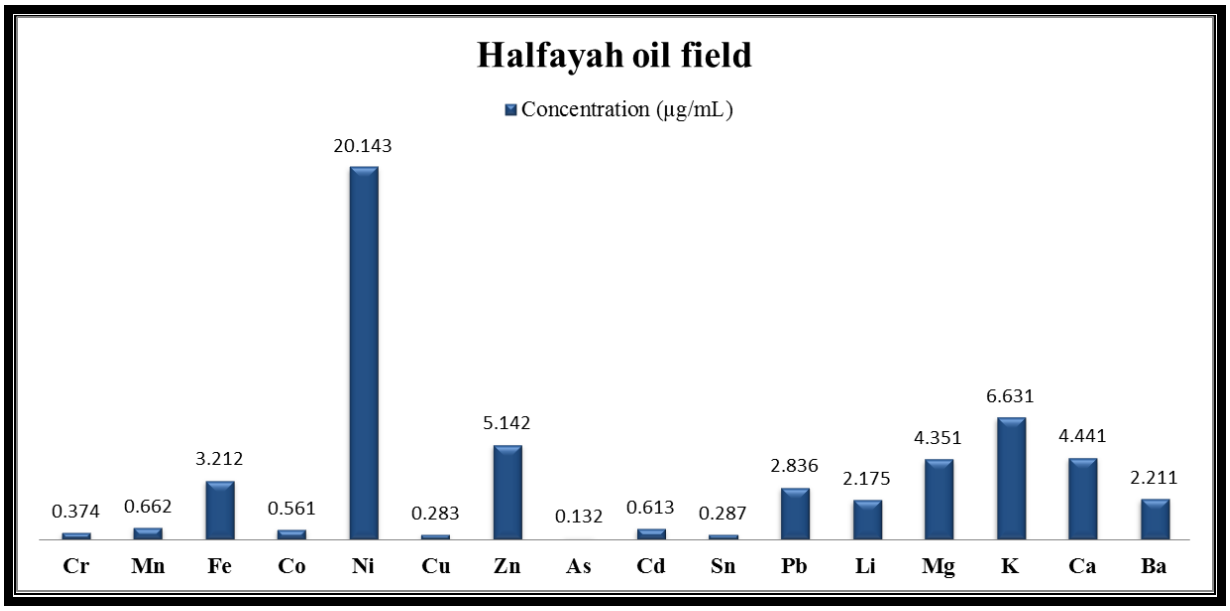

Fig. (3-67) Concentration of trace elements in crude oil samples in Halfayah oil field

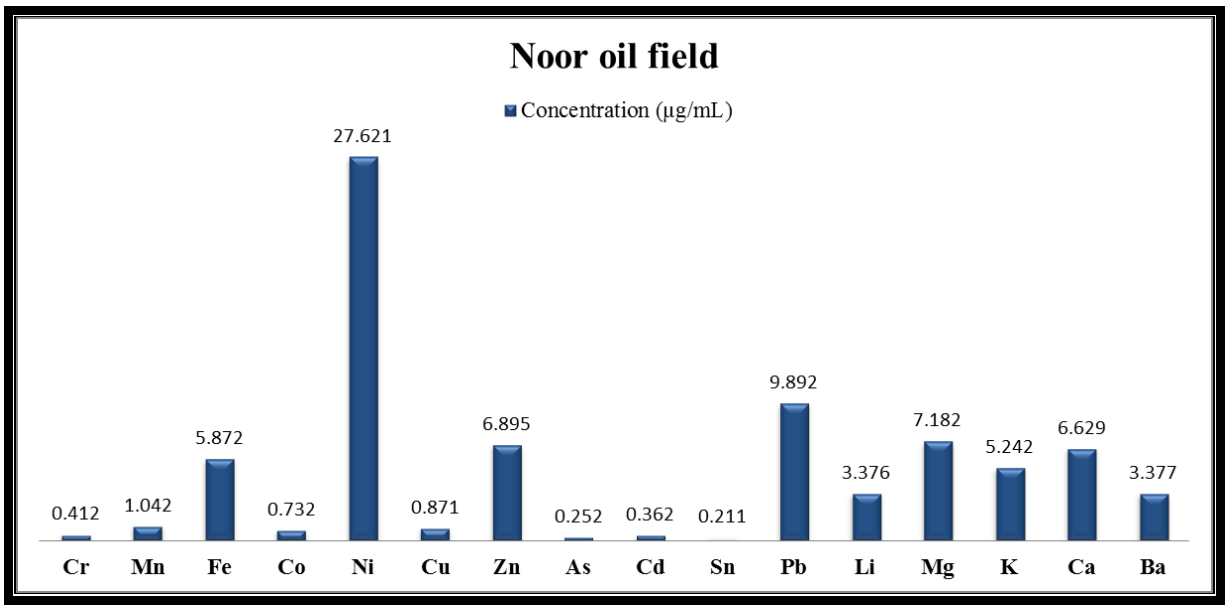

Fig. (3-68) Concentration of trace elements in crude oil samples in Noor oil field

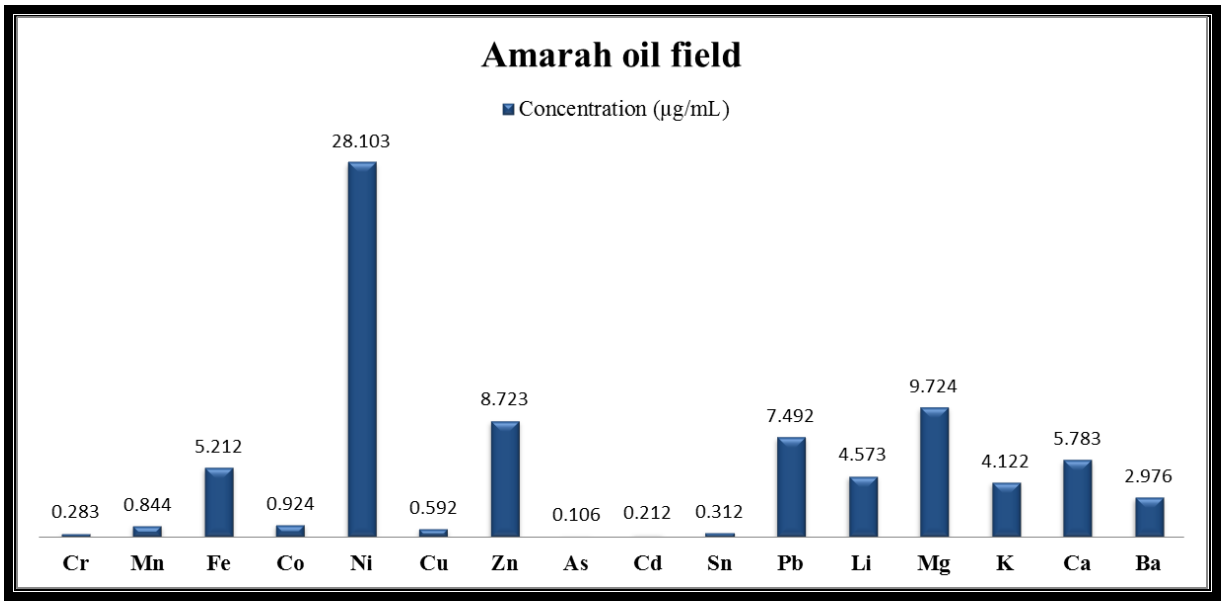

Fig. (3-69) Concentration of trace elements in crude oil samples in Amarah oil field

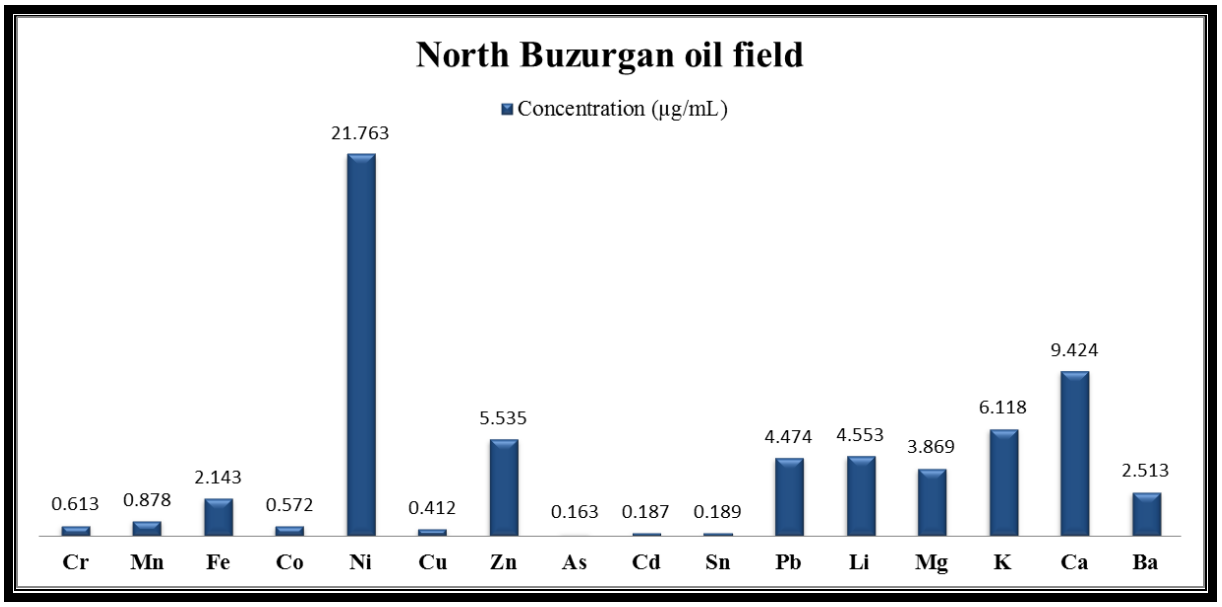

Fig. (3-70) Concentration of trace elements in crude oil samples in North Buzurgan oil field

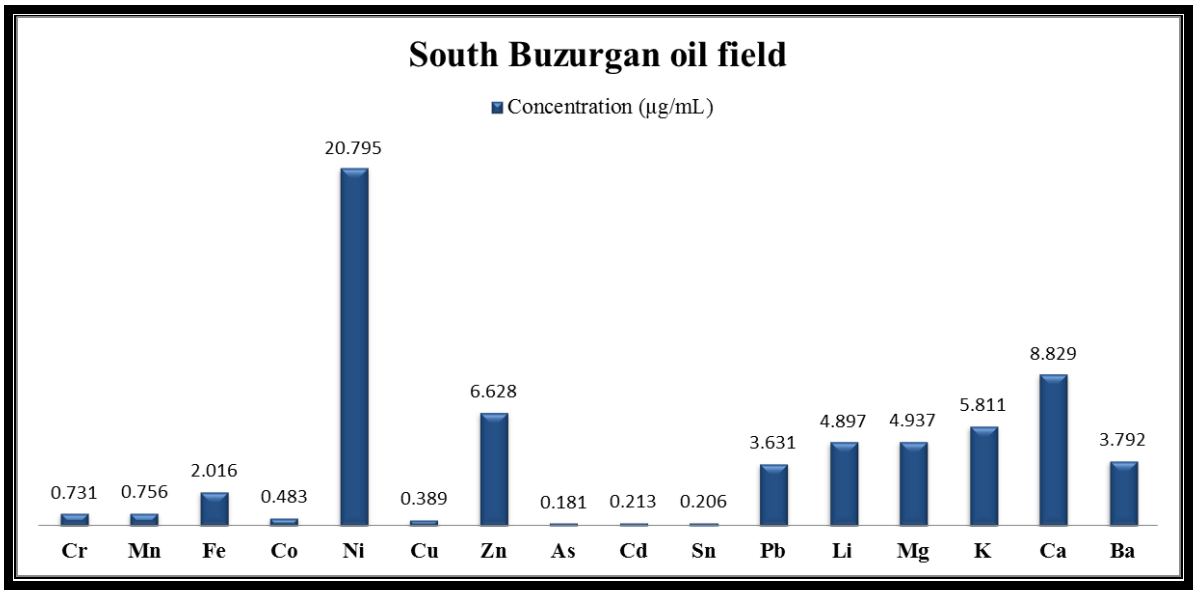

Fig. (3-71) Concentration of trace elements in crude oil samples in south Buzurgan oil field

The concentration of trace elements (As, Cu, Sn, Cr, Co, Cd, Mn, Li, Ba, Pb, Fe, Mg, Ca, Zn, K and Ni) in crude oil samples in Halfayah oil field were (0.132, 0.283, 0.287, 0.374, 0.561, 0.613, 0.662, 2.175, 2.211, 2.836, 3.212, 4.351, 4.441, 5.142, 6.631 and 20.143 µg/mL) respectively. The concentration of trace elements (Sn, As, Cd, Cr, Co, Cu, Mn, Li, Ba, K, Fe, Ca, Zn, Mg, Pb and Ni) in cutting crude oil in Noor oil field were (0.211, 0.252, 0.362, 0.412, 0.732, 0.871, 1.042, 3.376, 3.377, 5.242, 5.872, 6.629, 6.895, 7.182, 9.892 and 27.621 µg/mL) respectively. The concentration of trace elements (As, Cd, Cr, Sn, Cu, Mn, Co, Ba, K, Li, Fe, Ca, Pb, Zn, Mg and Ni) in crude oil samples in Amarah oil field were (0.106, 0.212, 0.283, 0.312, 0.592, 0.844, 9.242, 2.976, 4.122, 4.573, 5.212, 5.783, 7.492, 8.723, 9.724 and 28.103 µg/mL) respectively. The concentration of trace elements (As, Cd, Sn, Cu, Co, Cr, Mn, Fe, Ba, Mg, Pb, Li, Zn, K, Ca and Ni) in crude oil samples in north Buzurgan oil field were (0.163, 0.187, 0.189, 0.412, 0.572, 0.613, 0.878, 2.143, 2.513,

3.869, 4.474, 4.553, 5.535, 6.118, 9.424 and 21.763 µg/mL) respectively. The concentration of trace elements (As, Sn, Cd, Cu, Co, Cr, Mn, Fe, Pb, Ba, Li, Mg, K, Zn, Ca and Ni) in crude oil samples in south Buzurgan oil field were (0.181, 0.206, 0.213, 0.389, 0.483, 0.731, 0.756, 2.016, 3.631, 3.792, 4.897, 4.937, 5.811, 6.628, 8.829 and 20.795 µg/mL) respectively.

Nickel concentration observed higher in Halfayah, Amarah, Noor, north and south Buzurgan oil fields. Arsine concentration observed lower in Halfayah, Amarah, north Buzurgan and south Buzurgan oil fields, but tin concentration observed lower in Noor oil field.

The concentration of chromium (0.283, 0.374, 0.412, 0.613 and 0.731 µg/mL) in crude oil sample in the following oil fields (Amarah, Halfayah, Noor, north Buzurgan and south Buzurgan) respectively. The concentration of manganese (0.662, 0.756, 0.844, 0.878 and 1.042 µg/mL) in crude oil sample in the following oil fields (Halfayah, south Buzurgan, Amarah, north Buzurgan and Noor) respectively. The concentration of iron (2.016, 2.143, 3.212, 5.212 and 5.872 µg/mL) in crude oil samples in the following oil fields (south Buzurgan, north Buzurgan, Halfayah, Amarah and Noor) respectively. The concentration of cobalt (0.483, 0.561 , 0.572, 0.732 and 0.924 µg/mL) in crude oil samples in the following oil fields (south Buzurgan, Halfayah, north Buzurgan, Noor and Amarah) respectively. The concentration of nickel (20.143, 20.795, 21.763, 27.621 and 28.103 µg/mL) in crude oil samples in the following oil fields (Halfayah, south Buzurgan, north Buzurgan, Noor and Amarah) respectively. The concentration of copper (0.283, 0.389, 0.412, 0.592 and 0.871 µg/mL) in crude oil samples in the following oil fields (Halfayah, south Buzurgan, north Buzurgan, Noor and Amarah) respectively. The concentration of zinc (5.142, 5.535, 6.628, 6.895 and 8.723 µg/mL) in crude oil samples in the following oil fields (Halfayah, north Buzurgan, south Buzurgan, Noor and Amarah) respectively. The concentration of arsine (0.106, 0.132, 0.163, 0.181 and 0.252

µg/mL) in crude oil samples in the following oil fields (Amarah, Halfayah, north Buzurgan, south Buzurgan and Noor) respectively. The concentration of cadmium (0.187, 0.212, 0.212, 0.362 and 0.613 µg/mL) in crude oil samples in the following oil fields (north Buzurgan, Amarah, south Buzurgan, Noor and Halfayah) respectively. The concentration of tin (0.189, 0.206, 0.211, 0.287 and 0.312 µg/mL) in crude oil samples in the following oil fields (north Buzurgan, south Buzurgan, Noor, Halfayah and Amarah) respectively. The concentration of lead (2.836, 3.631, 4.474, 7.492 and 9.892 µg/mL) in crude oil samples in the following oil fields (Halfayah, south Buzurgan, north Buzurgan, Amarah and Noor) respectively. The concentration of lithium (2.175, 3.376, 4.553, 4.573 and 4.897 µg/mL) in crude oil samples in the following oil fields (Halfayah, Noor, north Buzurgan, Amarah and south Buzurgan) respectively. The concentration of magnesium (3.869, 4.351, 4.937, 7.182 and 9.724 µg/mL) in crude oil samples in the following oil fields (north Buzurgan, Halfayah, south Buzurgan, Noor, and Amarah) respectively. The concentration of potassium (4.122, 5.242, 5.811, 6.118 and 6.631 µg/mL) in crude oil samples in the following oil fields (Amarah, Noor, south Buzurgan, north Buzurgan and Halfayah) respectively. The concentration of calcium (4.441, 5.783, 6.629, 8.829 and 9.424 µg/mL) in crude oil samples in the following oil fields (Halfayah, Amarah, Noor, south Buzurgan and north Buzurgan) respectively. The concentration of barium (2.211, 2.513, 2.976, 3.377 and 3.792 µg/mL) in crude oil sample in the following oil fields (Halfayah, north Buzurgan, Amarah, Noor and south Buzurgan) respective.

CONCLUSIONS AND RECOMMENDATIONS

Conclusions

1- The NGO was synthesized by modified Hummer's method and characterized by FT-IR spectrophotometer, UV spectrophotometer, zeta potential analyzer, XRD, TEM, FESEM and EDX (attached with FESEM), obtain two dimension pure phase of synthesized NGO.

2- The abundant oxygen-containing functional groups (anionic nature) on NGO sheets, the analyte ions (cation nature) can be fast and efficiently adsorbed on the NGO surface at the optimum pH for each analyte ion.

3- The proposed method is cationic ion exchange chromatography where the NGO (anionic nature) acts a sorbent of stationary phase and the solution containing analyte (cationic nature) acts a mobile phase.

4- Using NGO in SPME method is an excellent alternative in adsorption process in comparison with the classical sorbent such as silica gel or activated carbon.

5- The proposed method is simple, fast, green chemistry and completely free organic reagent.

6- Using NaCl solution to aggregation the NGO after pre-concentration process, obtain high efficiency of adsorption.

7- The advantage of this method is cheap, time efficient and economic consumption of only 0.5mg NGO as sorbent.

8- A novel, method applied with cutting rock and crude oil samples, method is very suitable to separate of metal ions from the samples.

9- The conducted study reveals the great capable of NGO towards Mg(II), Co(II), Ni(II), Cd(II) and Pb(II) as excellent sorbent material in analytical chemistry, but low recovery of Cu(II) analyte.

Recommendations

1- Synthesis of derivative graphene oxide containing another anionic functional group as sulpher or nitrogen in addition to oxygen group and study the proposed SPME method with analytes.
2- Study the SPME method with trivalent analyte ions using NGO.
3- Study the SPME method, determination of analyte by low detection limit (LOD) of measurement such as inductively coupled plasma-optical emission spectroscopy (ICP-OES) or graphite furnace atomic absorption spectroscopy (GFAAS) .
4- Using the NGO as a treatment to reduce the heavy metal from crude oil samples, obtain light crude oil the high API (API : American petroleum institute is standard specification for crude oil quality) .
5- Study the proposed method for water samples, using the NGO as a treatment to reduce toxic ions in water sample.

REFERENCES

References

1. Kalinin EP. Geochemical Specificity of Oil and Its Nature. *Bull*. 2009;Vol. 1:6-12.

2. Mahjoubi M, Cappello S, Souissi Y, Jaouani A, Cherif A. Microbial Bioremediation of Petroleum Hydrocarbon– Contaminated Marine Environments. *Recent Insights Pet Sci Eng*. 2018;(325-350).

3. De Souza RM, Meliande ALS, Da Silveira CLP, Aucélio RQ. Determination of Mo, Zn, Cd, Ti, Ni, V, Fe, Mn, Cr and Co in crude oil using inductively coupled plasma optical emission spectrometry and sample introduction as detergentless microemulsions. *Microchem J*. 2006;82(2):137-141.

4. Altameemi AMH, Alzaidy A. Formation Evaluation by using Well Logging of Mishrif Formation in the Noor Oil Field, , Southeast Iraq. *Iraqi J Sci*. 2018;59(1A):144-155.

5. Al-Ameri TK, Al-Khafaji AJ, Zumberge J. Petroleum system analysis of the Mishrif reservoir in the Ratawi, Zubair, North and South Rumaila oil fields, southern Iraq. *GeoArabia*. 2009;14(4):91-108.

6. Dhannoun HY, Othman SM, Al-Dabbagh SM. The Relationship Between Chemical Index of Alteration and Some Major and Trace Elements Content in Rocks of Injana Formation of Northern Iraq. *Iraqi Natl J Earth Sci*. 2010;11(1):1-22.

7. Hazim AA-K, Zeki AA. Geochemistry of Marl Sediments within Fat'ha Formation at Selected Localities, Northern Iraq. *Iraqi Natl J Earth Sci*. 2008;8(2):27-46.

8. Mongenot T, Tribovillard N, Desprairies A, Lallier-verg E. Trace elements

as palaeoenvironmental markers in strongly mature hydrocarbon source rocks : the Cretaceous La Luna Formation of Venezuela b. *Sediment Geol*. 1996;103:23-37.

9. Jebour IK, Mohammed MY, Alheety MA. Synthesis and Characterization of Novel Nano Dithiocarbamate Complexes Derived From GO-benzimidazole. *Diyala J Pure Sci*. 2016;12(1):108-121.

10. Ibrahim F, Bakir ET, Ali SM. Synthesis of graphene-oxadiazole-2-thiol (RGS) / PVA composite and studying Its electric properties. *Tikrit J Pure Sci*. 2016;21(6):55-60.

11. Su S, Chen B, He M, Hu B, Xiao Z. Determination of trace/ultratrace rare earth elements in environmental samples by ICP-MS after magnetic solid phase extraction with Fe_3O_4@SiO_2@polyaniline–graphene oxide composite. *Talanta*. 2014;119:458-466.

12. Kudin KN, Ozbas B, Schniepp HC, Prud'homme RK, Aksay IA, Car R. Raman spectra of graphite oxide and functionalized graphene sheets. *Nano Lett*. 2008;8(1):36-41.

13. Zhao G, Ren X, Gao X, et al. Removal of Pb(ii) ions from aqueous solutions on few-layered graphene oxide nanosheets. *Dalt Trans*. 2011;40(41):10945-10952.

14. Muniraj VKA, Boukherroub R, Shelke MV. Flexible Energy Storage Device Based on Poly(N -phenylglycine), an Incentive-Energy Pseudocapacitive Conducting Polymer, and Electrochemically Exfoliated Graphite Sheets . *ACS Sustain Chem Eng*. 2020;8(16):6433-6441.

15. Chang H, Tang L, Wang Y, Jiang J, Li J. Graphene fluorescence resonance energy transfer aptasensor for the thrombin detection. *Anal Chem*. 2010;82(6):2341-2346.

16. Zhang K, Zhang LL, Zhao XS, Wu J. Graphene/polyaniline nanofiber composites as supercapacitor electrodes. *Chem Mater*. 2010;22(4):1392-1401.

17. Sitko R, Turek E, Zawisza B, et al. Adsorption of divalent metal ions from aqueous solutions using graphene oxide. *Dalt Trans*. 2013;42(16):5682-5689.

18. Zhao G, Li J, Ren X, Chen C, Wang X. Few-layered graphene oxide nanosheets as superior sorbents for heavy metal ion pollution management. *Environ Sci Technol*. 2011;45(24):10454-10462.

19. Shamsipur M, Farzin L, Amouzadeh Tabrizi M, Sheibani S. Functionalized Fe3O4/graphene oxide nanocomposites with hairpin aptamers for the separation and preconcentration of trace Pb2 + from biological samples prior to determination by ICP MS. *Mater Sci Eng C*. 2017;77:459-469.

20. Becerra-Paniagua DK, Sotelo-Lerma M, Hu H. Highly oxidized and exfoliated graphene using a modified Tour approach. *J Mater Sci Mater Electron*. 2019;30(4):3973-3983.

21. W.S. Hummers REO. preparation of graphene oxide by graphite oxidation. *J Am Chem Soc*. 1958;80(1339–1339).

22. Al-Gaashani R, Najjar A, Zakaria Y, Mansour S, Atieh MA. XPS and structural studies of high quality graphene oxide and reduced graphene oxide prepared by different chemical oxidation methods. *Ceram Int*. 2019;45(11):14439-14448.

23. Chen J, Yao B, Li C, Shi G. An improved Hummers method for eco-friendly synthesis of graphene oxide. *Carbon N Y*. 2013;64(1):225-229.

24. Liou YJ, Tsai B Da, Huang WJ. An economic route to mass production of graphene oxide solution for preparing graphene oxide papers. *Mater Sci*

Eng B Solid-State Mater Adv Technol. 2015;193(C):37-40.

25. Hu Y, Song S, Lopez-Valdivieso A. Effects of oxidation on the defect of reduced graphene oxides in graphene preparation. *J Colloid Interface Sci*. 2015;450:68-73.

26. Chen J, Li Y, Huang L, Li C, Shi G. High-yield preparation of graphene oxide from small graphite flakes via an improved Hummers method with a simple purification process. *Carbon N Y*. 2015;81(1):826-834.

27. Sun J, Yang N, Sun Z, et al. Fully Converting Graphite into Graphene Oxide Hydrogels by Preoxidation with Impure Manganese Dioxide. *ACS Appl Mater Interfaces*. 2015;7(38):21356-21363.

28. Peng L, Xu Z, Liu Z, et al. An iron-based green approach to 1-h production of single-layer graphene oxide. *Nat Commun*. 2015;6:1-9.

29. Yu H, Xin G, Ge X, et al. Porous graphene-polyaniline nanoarrays composite with enhanced interface bonding and electrochemical performance. *Compos Sci Technol*. 2018;154:76-84.

30. Cotet LC, Magyari K, Todea M, Dudescu MC, Danciu V, Baia L. Versatile self-assembled graphene oxide membranes obtained under ambient conditions by using a water-ethanol suspension. *J Mater Chem A*. 2017;5(5):2132-2142.

31. Jasim DA, Lozano N, Kostarelos K. Synthesis of few-layered, high-purity graphene oxide sheets from different graphite sources for biology. *2D Mater*. 2016;3(1):14006.

32. Dikin DA, Stankovich S, Zimney EJ, et al. Preparation and characterization of graphene oxide paper. *Nature*. 2007;448(7152):457-460.

33. Stobinski L, Lesiak B, Malolepszy A, et al. Graphene oxide and reduced graphene oxide studied by the XRD, TEM and electron spectroscopy methods. *J Electron Spectros Relat Phenomena*. 2014;195(March 2018):145-154.

34. Dimiev AM, Tour JM. Mechanism of graphene oxide formation. *ACS Nano*. 2014;8(3):3060-3068.

35. Zaaba NI, Foo KL, Hashim U, Tan SJ, Liu WW, Voon CH. Synthesis of Graphene Oxide using Modified Hummers Method: Solvent Influence. *Procedia Eng*. 2017;184:469-477.

36. Dreyer DR, Park S, Bielawski CW, Ruoff RS. The chemistry of graphene oxide. *Chem Soc Rev*. 2010;39(1):228-240.

37. Neklyudov V V., Khafizov NR, Sedov IA, Dimiev AM. New insights into the solubility of graphene oxide in water and alcohols. *Phys Chem Chem Phys*. 2017;19(26):17000-17008.

38. Gao W, Alemany LB, Ci L, Ajayan PM. New insights into the structure and reduction of graphite oxide. *Nat Chem*. 2009;1(5):403-408.

39. Schöche S, Hong N, Khorasaninejad M, et al. Optical properties of graphene oxide and reduced graphene oxide determined by spectroscopic ellipsometry. *Appl Surf Sci*. 2017;421:778-782.

40. Meng F, Zhang S, Oh Y, Zhou Z, Shin HS, Chae SR. Fouling in membrane bioreactors: An updated review. *Water Res*. 2017;114:151-180.

41. Ma F, Li Z, Zhao H, et al. Potential application of graphene oxide membranes for removal of Cs(I) and Sr(II) from high level-liquid waste. *Sep Purif Technol*. 2017;188(I):523-529.

42. Chen L, Shi G, Shen J, et al. Ion sieving in graphene oxide membranes via

cationic control of interlayer spacing. *Nature*. 2017;550(7676):380-383.

43. Wang S, Li X, Liu Y, et al. Nitrogen-containing amino compounds functionalized graphene oxide: Synthesis, characterization and application for the removal of pollutants from wastewater: A review. *J Hazard Mater*. 2018;342:177-191.

44. Peng W, Li H, Liu Y, Song S. A review on heavy metal ions adsorption from water by graphene oxide and its composites. *J Mol Liq*. 2017;230:496-504.

45. Sun Y, Wang X, Song W, Lu S, Chen C, Wang X. Mechanistic insights into the decontamination of Th(iv) on graphene oxide-based composites by EXAFS and modeling techniques. *Environ Sci Nano*. 2017;4(1):222-232.

46. Yu S, Wang J, Song S, et al. One-pot synthesis of graphene oxide and Ni-Al layered double hydroxides nanocomposites for the efficient removal of U(VI) from wastewater. *Sci China Chem*. 2017;60(3):415-422.

47. Wang J, Li Y, Chen W, et al. The rapid coagulation of graphene oxide on La-doped layered double hydroxides. *Chem Eng J*. 2017;309:445-453.

48. Qi Y, Yang M, Xu W, He S, Men Y. Natural polysaccharides-modified graphene oxide for adsorption of organic dyes from aqueous solutions. *J Colloid Interface Sci*. 2017;486:84-96.

49. Zhu Y, Murali S, Cai W, et al. Graphene and graphene oxide: Synthesis, properties, and applications. *Adv Mater*. 2010;22(35):3906-3924.

50. Dideikin AT, Vul' AY. Graphene oxide and derivatives: The place in graphene family. *Front Phys*. 2019;6(JAN).

51. Yadav S, Malik P, Khushboo, Jayoti D. Electro-optical, dielectric and optical properties of graphene oxide dispersed nematic liquid crystal

composites. *Liq Cryst*. 2020;47(7):984-993.

52. Jyoti J, Arya AK, Chockalingam S, et al. Mechanical, electrical and thermal properties of graphene oxide-carbon nanotube/ ABS hybrid polymer nanocomposites. *J Polym Res*. 2020;27(9).

53. Bai M jie, Liu J long, He J, et al. Heat transfer and mechanical friction reduction properties of graphene oxide nanofluids. *Diam Relat Mater*. 2020;108:107982.

54. Tian H, Chang X, Hu Z, et al. Activated carbon modified with 4-(8-hydroxyquinoline-azo)benzamidine for selective solid-phase extraction and preconcentration of trace lead from environmental samples. *Microchim Acta*. 2010;171(3):225-232.

55. Otero-Romaní J, Moreda-Piñeiro A, Bermejo-Barrera A, Bermejo-Barrera P. Evaluation of commercial C18 cartridges for trace elements solid phase extraction from seawater followed by inductively coupled plasma-optical emission spectrometry determination. *Anal Chim Acta*. 2005;536(1-2):213-218.

56. Deng J, Kang X, Chen L, Wang Y, Gu Z, Lu Z. A nanofiber functionalized with dithizone by co-electrospinning for lead (II) adsorption from aqueous media. *J Hazard Mater*. 2011;196:187-193.

57. Tokay F, Baıdat S. Simultaneous preconcentration of Cd(II) and Pb(II) with N,N'-bis(4-methoxysalicylidene) ethylenediamine coated silica gel prior to determination by flame atomic absorption spectrometry. *Water Air Soil Pollut*. 2015;226(3).

58. Saxena R, Meena PL. Flow injection online solid phase extraction system using Amberlite XAD-16 functionalized with 8-hydroxyquinoline for copper and zinc determination by flame atomic absorption spectrometry.

RSC Adv. 2014;4(39):20216-20225.

59. Ćwieląg-Piasecka I, Medyńska-Juraszek A, Jerzykiewicz M, et al. Humic acid and biochar as specific sorbents of pesticides. *J Soils Sediments*. 2018;18(8):2692-2702.

60. Faisal AAH, Abdul-Kareem MB, Mohammed AK, Naushad M, Ghfar AA, Ahamad T. Humic acid coated sand as a novel sorbent in permeable reactive barrier for environmental remediation of groundwater polluted with copper and cadmium ions. *J Water Process Eng*. 2020;36(June):101373.

61. Azeem SMA, Arafa WAA, El-Shahat MF. Synthesis and application of alizarin complexone functionalized polyurethane foam: Preconcentration/separation of metal ions from tap water and human urine. *J Hazard Mater*. 2010;182(1-3):286-294.

62. Zhang X Le, Niu HY, Zhang SX, Cai YQ. Preparation of a chitosan-coated C18-functionalized magnetite nanoparticle sorbent for extraction of phthalate ester compounds from environmental water samples. *Anal Bioanal Chem*. 2010;397(2):791-798.

63. Zawisza B, Baranik A, Malicka E, Talik E, Sitko R. Preconcentration of Fe(III), Co(II), Ni(II), Cu(II), Zn(II) and Pb(II) with ethylenediamine-modified graphene oxide. *Microchim Acta*. 2016;183(1):231-240.

64. Mcallister MJ, Li J, Adamson DH, et al. Expansion of Graphite. *Society*. 2007;19(4):4396-4404.

65. Islam A, Ahmad H, Zaidi N, Kumar S. Graphene oxide sheets immobilized polystyrene for column preconcentration and sensitive determination of lead by flame atomic absorption spectrometry. *ACS Appl Mater Interfaces*. 2014;6(15):13257-13265.

66. Ghanemi K, Nikpour Y, Omidvar O, Maryamabadi A. Sulfur-nanoparticle-based method for separation and preconcentration of some heavy metals in marine samples prior to flame atomic absorption spectrometry determination. *Talanta*. 2011;85(1):763-769.

67. Baytak S, Zereen F, Arslan Z. Preconcentration of trace elements from water samples on a minicolumn of yeast (Yamadazyma spartinae) immobilized TiO_2 nanoparticles for determination by ICP-AES. *Talanta*. 2011;84(2):319-323.

68. Zhang X, Kah M, Jonker MTO, Hofmann T. Dispersion State and Humic Acids Concentration-Dependent Sorption of Pyrene to Carbon Nanotubes. *Environ Sci Technol*. 2012;46:7166-7173.

69. Vallant RM, Szabo Z, Bachmann S, et al. Development and Application of C60-Fullerene Bound Silica for Solid-Phase Extraction of Biomolecules. *Anal Chem*. 2007;79(21):8144-8153.

70. Zhu S, Niu W, Li H, Han S, Xu G. Single-walled carbon nanohorn as new solid-phase extraction adsorbent for determination of 4-nitrophenol in water sample. *Talanta*. 2009;79:1441-1445.

71. He Q, Hu Z, Jiang Y, Chang X, Tu Z, Zhang L. Preconcentration of Cu(II), Fe(III) and Pb (II) with 2- ((2-aminoethylamino) methyl) phenol-functionalized activated carbon followed by ICP-OES determination. *Hazard Mater J*. 2010;175:710-714.

72. Ahmed KW. Competitive Adsorption of Furfural and Phenolic Compounds onto Activated Carbon in Fixed Bed Column. *Environ Sci Technol*. 2008;42(2):392-397.

73. Srogi K. *Developments in the Determination of Trace Elements by Atomic Spectroscopic Techniques*. Vol 41.; 2008.

74. Wang Y, Gao S, Zang X, Li J, Ma J. Graphene-based solid-phase extraction combined with flame atomic absorption spectrometry for a sensitive determination of trace amounts of lead in environmental water and vegetable samples. *Anal Chim Acta*. 2012;716:112-118.

75. Huang Z, Zheng X, Lv W, Wang M, Yang Q, Kang F. Adsorption of Lead(II) Ions from Aqueous Solution on Low-Temperature Exfoliated Graphene Nonosheets. *Langmuir*. 2011;(Ii):7558-7562.

76. Zhang L, Hu X, Zhu L, Jin X, Feng C. Water-dispersible ZnO/COFe2O4/graphene photocatalyst and their high-performance in water treatment. *Fullerenes Nanotub Carbon Nanostructures*. 2019;27(11):873-877.

77. Lin S, Shih CJ, Strano MS, Blankschtein D. Molecular insights into the surface morphology, layering structure, and aggregation kinetics of surfactant-stabilized graphene dispersions. *J Am Chem Soc*. 2011;133(32):12810-12823.

78. An X, Simmons T, Shah R, et al. Stable aqueous dispersions of noncovalently functionalized graphene from graphite and their multifunctional high-performance applications. *Nano Lett*. 2010;10(11):4295-4301.

79. Paquin F, Rivnay J, Salleo A, Stingelin N, Silva C. Multi-phase semicrystalline microstructures drive exciton dissociation in neat plastic semiconductors. *J Mater Chem C*. 2015;3(207890):10715-10722.

80. Deng D, Jiang X, Yang L, Hou X, Zheng C. Organic solvent-free cloud point extraction-like methodology using aggregation of graphene oxide. *Anal Chem*. 2014;86(1):758-765.

81. Arpa Ç, Arıdaşır I. Ultrasound assisted ion pair based surfactant-enhanced

liquid–liquid microextraction with solidification of floating organic drop combined with flame atomic absorption spectrometry for preconcentration and determination of nickel and cobalt ions in vegeta. *Food Chem*. 2019;284(January):16-22.

82. Cui L, Wu J, Ju H. Electrochemical sensing of heavy metal ions with inorganic, organic and bio-materials. *Biosens Bioelectron*. 2015;63:276-286.

83. Yao Y, Wu H, Ping J. Simultaneous determination of Cd(II) and Pb(II) ions in honey and milk samples using a single-walled carbon nanohorns modified screen-printed electrochemical sensor. *Food Chem*. 2019;274(Ii):8-15.

84. Banerjee P, Prasad B. Determination of concentration of total sodium and potassium in surface and ground water using a flame photometer. *Appl Water Sci*. 2020;10(5):1-7.

85. Ping J, Wu J, Ying Y, Wang M, Liu G, Zhang M. Evaluation of trace heavy metal levels in soil samples using an ionic liquid modified carbon paste electrode. *J Agric Food Chem*. 2011;59(9):4418-4423.

86. Ping JF, Wu J, Ying Y Bin. Determination of trace heavy metals in milk using an ionic liquid and bismuth oxide nanoparticles modified carbon paste electrode. *Chinese Sci Bull*. 2012;57(15):1781-1787.

87. Duarte K, Justino CIL, Freitas AC, Gomes AMP, Duarte AC, Rocha-Santos TAP. Disposable sensors for environmental monitoring of lead, cadmium and mercury. *TrAC - Trends Anal Chem*. 2015;64:183-190.

88. Gumpu MB, Sethuraman S, Krishnan UM, Rayappan JBB. A review on detection of heavy metal ions in water - An electrochemical approach. *Sensors Actuators, B Chem*. 2015;213:515-533.

89. Bilo F, Moscoso S, Borgese L, et al. Total reflection X-Ray fluorescence spectroscopy to study Pb and Zn accumulation in zebrafish embryos. *X-Ray Spectrom*. 2015;44(3):124-128.

90. Bilo F, Borgese L, Dalipi R, et al. Elemental analysis of tree leaves by total reflection X-ray fluorescence: New approaches for air quality monitoring. *Chemosphere*. 2017;178:504-512.

91. De La Calle I, Costas M, Cabaleiro N, Lavilla I, Bendicho C. Fast method for multielemental analysis of plants and discrimination according to the anatomical part by total reflection X-ray fluorescence spectrometry. *Food Chem*. 2013;138(1):234-241.

92. Ebrahimzadeh H, Moazzen E, Amini MM, Sadeghi O. Pyridine-2,6-diamine-functionalized Fe3O4 nanoparticles as a novel sorbent for determination of lead and cadmium ions in cosmetic samples. *Int J Cosmet Sci*. 2013;35(2):176-182.

93. Yi R, Yang X, Zhou R, et al. Determination of Trace Available Heavy Metals in Soil Using Laser-Induced Breakdown Spectroscopy Assisted with Phase Transformation Method. *Anal Chem*. 2018;90(11):7080-7085.

94. Habibiyan A, Ezoddin M, Lamei N, Abdi K, Amini M, Ghazi-khansari M. Ultrasonic assisted switchable solvent based on liquid phase microextraction combined with micro sample injection flame atomic absorption spectrometry for determination of some heavy metals in water, urine and tea infusion samples. *J Mol Liq*. 2017;242:492-496.

95. Ghaedi M, Ahmadi F, Soylak M. Preconcentration and separation of nickel, copper and cobalt using solid phase extraction and their determination in some real samples. *J Hazard Mater*. 2007;147(1-2):226-231.

96. Pehlivan E, Altun T. Ion-exchange of Pb2+, Cu2+, Zn2+, Cd2+, and Ni2+ ions from aqueous solution by Lewatit CNP 80. *J Hazard Mater*. 2007;140(1-2):299-307.

97. Anthemidis AN, Zachariadis GA, Farastelis CG, Stratis JA. On-line liquid-liquid extraction system using a new phase separator for flame atomic absorption spectrometric determination of ultra-trace cadmium in natural waters. *Talanta*. 2004;62(3):437-443.

98. Yildiz E, Saçmaci Ş, Kartal Ş, Saçmaci M. A new chelating reagent and application for coprecipitation of some metals in food samples by FAAS. *Food Chem*. 2016;194:143-148.

99. Lemos VA, da França RS, Moreira BO. Cloud point extraction for Co and Ni determination in water samples by flame atomic absorption spectrometry. *Sep Purif Technol*. 2007;54(3):349-354.

100. Lemos VA, Santos MS, David GT, Maciel MV, Bezerra M de A. Development of a cloud-point extraction method for copper and nickel determination in food samples. *J Hazard Mater*. 2008;159(2-3):245-251.

101. Manzoori JL, Karim-Nezhad G. Development of a cloud point extraction and preconcentration method for Cd and Ni prior to flame atomic absorption spectrometric determination. *Anal Chim Acta*. 2004;521(2):173-177.

102. Sakata M, Kitano Y, Matsumoto E. Diagenetie Behavior of Manganese in Tokyo Bay Sediment *. *Oceanogr Soc Japan*. 1981;37:212-217.

103. Chen J, Teo KC. Determination of cobalt and nickel in water samples by flame atomic absorption spectrometry after cloud point extraction. *Anal Chim Acta*. 2001;434(2):325-330.

104. Safavi A, Abdollahi H, Nezhad MRH, Kamali R. Cloud point extraction,

preconcentration and simultaneous spectrophotometric determination of nickel and cobalt in water samples. *Spectrochim Acta - Part A Mol Biomol Spectrosc*. 2004;60(12):2897-2901.

105. Zhu X, Hu B, Jiang Z, Li M. Cloud point extraction for speciation of chromium in water samples by electrothermal atomic absorption spectrometry. *Water Res*. 2005;39(4):589-595.

106. Journal C, Geochemistry OF, Enfeng LIU, et al. Geochemical features of heavy metals in core sediments of northwestern Taihu Lake , China *. *CHINESE J GEOCHEMISTRY*. 2005;24(1).

107. Gaudino S, Galas C, Belli M, et al. The role of different soil sample digestion methods on trace elements analysis: A comparison of ICP-MS and INAA measurement results. *Accredit Qual Assur*. 2007;12(2):84-93.

108. Harikumar PS, Nasir UP, Rahman MPM. Distribution of heavy metals in the core sediments of a tropical wetland system. *spring*. 2009;6(2):225-232.

109. Seshan BRR, Natesan U, Deepthi K. Geochemical and statistical approach for evaluation of heavy metal pollution in core sediments in southeast coast of India. *Environ Sci Tech*. 2010;7(2):291-306.

110. Carreiro MM. Forest soils adjacent to urban interstates : Soil physical and chemical properties , heavy metals , disturbance legacies , and relationships with woody vegetation. *Urban Ecosyst*. 2011;(14):525-552.

111. Gayatri SR, Venkateswarlu B, Jakkula VS, et al. Heavy metals concentration in soils under rainfed agro-ecosystems and their relationship with soil properties and management practices. *Environ Sci Technol*. Published online 2013.

112. Liang Y, Cao X, Zhao L, Arellano E. Biochar- and phosphate-induced

immobilization of heavy metals in contaminated soil and water : implication on simultaneous remediation of contaminated soil and groundwater. *Env Sci Pollut Res*. Published online 2013.

113. Zhang Y, Gao X, Arthur Chen CT. Rare earth elements in intertidal sediments of Bohai Bay, China: Concentration, fractionation and the influence of sediment texture. *Ecotoxicol Environ Saf*. 2014;105(1):72-79.

114. Adhikari G, Bhattacharyya KG. Ecotoxicological risk assessment of trace metals in humid subtropical soil. *Ecotoxicology*. Published online 2015.

115. Kharnoob HH, Mahmood AR. Determination of Heavy Metals (Zn , Cd , Pb , Cu) by Atomic Absorption Spectrophotometer (AAS) Technique Absorption . *Diyala J pure Sci*. 2015;(3):51-67.

116. Li JX, Zhu ZW, Yin XF, et al. Analysis of contents and distribution patterns of rare earth elements in the surface sediments of the South Mid-Atlantic Ridge. *Chinese J Anal Chem*. 2015;43(1):21-26.

117. G. M. Balak, A. N. Privalenko, A. V. Oreshenkov, L. V. Krasnaya, V. D. Zueva and IAS. Determination of elemental composition of precipitates formed during use of petroleum products by flame atomic absorption spectroscopy. *Chem Technol Fuels Oils*. 2016;52(2):51-56.

118. Makombe M, Horst C van der, Silwana B, Iwuoha E, Somerset V. Optimisation of Parameters for Spectroscopic Analysis of Rare Earth Elements in Sediment Samples. *Rare Earth Elem*. Published online 2017.

119. Vieira LV, Marchezi TTB, de Castro EVR, Brandão GP, Carneiro MTWD. Metals determination in crude oil by inductively coupled plasma optical emission spectrometry using nanoemulsification as sample preparation. *Fuel*. 2019;244(October 2018):352-358.

120. Gab-Allah MA, Goda ES, Shehata AB, Gamal H. Critical Review on the

Analytical Methods for the Determination of Sulfur and Trace Elements in Crude Oil. *Crit Rev Anal Chem*. 2020;50(2):161-178.

121. Chukwuneke CE, Madu JO, Agboola BO. Determining Ash Content and Trace Metal Concentration in Crude Oil Samples to Teach Students Sample Preparation and Instrumental Analysis. *J Chem Educ*. 2021;98(2):633-638.

122. Tsolakidou A, Buxeda I Garrigós J, Kilikoglou V. Assessment of dissolution techniques for the analysis of ceramic samples by plasma spectrometry. *Anal Chim Acta*. 2002;474(1-2):177-188.

123. Hu Z, Qi L. Sample Digestion Methods. *Treatise Geochemistry Second Ed*. 2013;15(January 2014):87-109.

124. Drews A. Standard Test Methods for Determination of Nickel, Vanadium, Iron, and Sodium in Crude Oils and Residual Fuels by Flame Atomic Absorption Spectrometry. *Man Hydrocarb Anal 6th Ed*. 2008;(Reapproved 2016):1000-1000-1005.

125. Beata Zawisza, Rafal Sitko EM and ET. Graphene oxide as a solid sorbent for the preconcentration of cobalt, nickel, copper, zinc and lead prior to determination by energydispersive X-ray fluorescence spectrometry. *Anal Methods*. 2013;3(1):2-6.

126. Crouch S, Skoog D, Holler FJ. *Principles of Instrumental Analysis Seventh Edition*. Vol 88.; 2016.

127. Paredes JI, Villar-Rodil S, Martínez-Alonso A, Tascón JMD. Graphene oxide dispersions in organic solvents. *Langmuir*. 2008;24(19):10560-10564.

128. Varenne F, Coty JB, Botton J, et al. Evaluation of zeta potential of nanomaterials by electrophoretic light scattering: Fast field reversal versus

Slow field reversal modes. *Talanta*. 2019;205(June):120062.

129. Atkins, P. W.; de Paula J. Physical Chemistry (8th ed.). *Oxford Univ Press*. Published online 2006:764.

130. Krishnamoorthy K, Veerapandian M, Yun K, Kim SJ. The chemical and structural analysis of graphene oxide with different degrees of oxidation. *Carbon N Y*. 2013;53:38-49.

131. Ain QT, Haq SH, Alshammari A, Al-Mutlaq MA, Anjum MN. The systemic effect of PEG-nGO-induced oxidative stress in vivo in a rodent model. *Beilstein J Nanotechnol*. 2019;10(April):901-911.

132. Monshi A, Foroughi MR, Monshi MR. Modified Scherrer Equation to Estimate More Accurately Nano-Crystallite Size Using XRD. *World J Nano Sci Eng*. 2012;02(03):154-160.

133. Liou TH, Lin MH. Characterization of graphene oxide supported porous silica for effectively enhancing adsorption of dyes. *Sep Sci Technol*. 2020;55(3):431-443.

134. Drewniak S, Muzyka R, Stolarczyk A, Pustelny T, Kotyczka-Morańska M, Setkiewicz M. Studies of reduced graphene oxide and graphite oxide in the aspect of their possible application in gas sensors. *Sensors (Switzerland)*. 2016;16(1).

135. Xu Y, Nguyen Q, Malekahmadi O, et al. Synthesis and characterization of additive graphene oxide nanoparticles dispersed in water: Experimental and theoretical viscosity prediction of non-Newtonian nanofluid. *Math Methods Appl Sci*. 2020;(February):1-20.

136. Li D, Müller MB, Gilje S, Kaner RB, Wallace GG. Processable aqueous dispersions of graphene nanosheets. *Nat Nanotechnol*. 2008;3(2):101-105.

137. Li D, Kaner RB. Processable stabilizer-free polyaniline nanofiber aqueous colloids. *Chem Commun*. 2005;(26):3286-3288.

138. Lingamdinne LP, Kim IS, Ha JH, Chang YY, Koduru JR, Yang JK. Enhanced adsorption removal of Pb(II) and Cr(III) by using nickel ferrite-reduced graphene oxide nanocomposite. *Metals (Basel)*. 2017;7(6).

139. Wu W, Yang Y, Zhou H, et al. Highly efficient removal of Cu(II) from aqueous solution by using graphene oxide. *Water Air Soil Pollut*. 2013;224(1).

140. Gary D.Christian PKD and KAS. *Analytical Chemistry*. (Seventh, ed.).; 2014.

141. West, Skoog FJH and SRC. Fundamentals of analytical chemistry 9E. Published online 2013:62-128.

الخلاصة

تتضمن الرسالة ثلاث فصول، الفصل الاول مقدمة عامة عن النفط الخام والصخور النفطية و اوكسيد الكرافين النانوي و طرق تركيز وتقدير العناصر النزرة.

الفصل الثاني يصف الجزء العملي والذي يتضمن تخليق اوكسيد الكرافين النانوي وهضم نماذج الفتات الصخري والنفط الخام وتحضير المحاليل القياسية من الايونات المراد تحليلها (analytes) .

الفصل الاخير يوضح النتائج والمناقشة والتي تتضمن تشخيص اوكسيد الكرافين النانوي ودراسة الظروف المثلى لعملية الامتزاز واستخدام طريقة استخلاص الطور الصلب المايكروية لفصل العناصر (المغنيسيوم والكوبالت و النيكل والنحاس والكادميوم والرصاص) من النماذج باستخدام اوكسيد الكرافين النانوي كمادة مازة عند الظروف المثلى التي كانت: (pH=5.5, 6.0, 6.5, 7.0, 7.5, 8.0) للـ (Ni, Mg, Cd, Co, Cu and Pb) لكل ايون فلزي (analyte) غلى التوالي، ووزن اوكسيد الجرافين النانوي كان 0.5 mg وحجم النموذج 20 mL وزمن التحريك لإجراء عملية الامتزاز كان 5 دقائق وزمن الصوتنة Sonicating time كان دقيقتين ودرجة الحرارة هي درجة حرارة الغرفة (30 ºC) مع اضافة 6.5 mg/mL من محلول كلوريد الصوديوم NaCl، وتمت دراسة تأثير الايونات المتداخلة (الكروم (III) والمنغنيز (IV) والحديد (II) والحديد (III) والخارصين (II) الزرنيخ (III) والقصدير(II) والليثيوم (I) والبوتاسيوم (I) والكالسيوم (II) والباريوم (II)) لإيجاد حد السماح لتعايش الايونات المتداخلة مع العنصر المراد تحليله (analyte) الذي ممكن أن تقلل أو تزيد الاستعادية (Recovery) بمقدار ±5 . تم حساب سعة الامتزاز للعناصر المراد تقديرها (analytes) كما في النتائج :- المغنيسيوم (34.04 µg/mg)، الكوبالت (34.04 µg/mg)، النيكل (32.88 µg/mg)، النحاس (28.76 µg/mg)، الكادميوم (33.32 µg/mg) والرصاص (33.96 µg/mg). ووجد ان معدل تراكيز العناصر في عينات الفتات الصخري : المغنسيوم ، الكوبالت، النيكل، النحاس، الكادميوم والرصاص (9.72 µg/mL) ،(1.318 µg/mL)، (5.646 µg/mL)، (0.616 µg/mL) ، (0.567 µg/mL) و (9.296 µg/mL) على التوالي. ومعدل تراكيز العناصر في عينات النفط الخام، المغنسيوم ، الكوبالت، النيكل، النحاس، الكادميوم والرصاص (6.013µg/mL)، (0.654 µg/mL)، (23.685 µg/mL)، (0.509 µg/mL)، (0.317 µg/mL) و (5.665 µg/mL) على التوالي. معدل تراكيز العناصر في عينات الفتات الصخري قد قلت بعد استخدام طريقة استخلاص الطور الصلب المايكروية لفصل الايونات بواسطة اوكسيد الكرافين النانوي كما في النتائج: المغنيسيوم (2.082 µg/mL) والكوبالت (0.24 µg/mL) والنيكل (1.066 µg/mL) والنحاس (0.162 µg/mL) والكادميوم (0.055 µg/mL) والرصاص (2.153 µg/mL) على التوالي.

وفي عينات النفط الخام المغنيسيوم (1.044 µg/mL) والكوبالت (0.078 µg/mL) والنيكل (5.266 µg/mL) والنحاس (0.091 µg/mL) والكادميوم (0.038 µg/mL) والرصاص (1.042 µg/mL) على التوالي.

جمهورية العراق
وزارة التعليم العالي و البحث العلمي
جامعة ميسان
كلية العلوم
قسم الكيمياء

إزالة بعض العناصر الثقيلة من نماذج الصخور والنفط الخام باستخدام اوكسيد الكرافين النانوي

رسالة مقدمة الى

كلية العلوم / جامعة ميسان جزء من متطلبات نيل

شهادة الماجستير في علوم الكيمياء

من الطالب

أحمد عبد الواحد محمد الزبيدي

بكالوريوس علوم كيمياء/ جامعة ميسان (2012)

بإشراف

الأستاذ المساعد

صفاء صبري نجم

مدرس دكتور

حوراء حميد راضي

آب (2021)